Wind Tunnel Testing of an Airfoil with a Moving Surface Boundary-Layer Control

by

Abdullah Mohammed Al-Garni

A Thesis Presented to the

FACULTY OF THE COLLEGE OF GRADUATE STUDIES

KING FAHD UNIVERSITY OF PETROLEUM & MINERALS

DHAHRAN, SAUDI ARABIA

In Partial Fulfillment of the
Requirements for the Degree of

MASTER OF SCIENCE

In

MECHANICAL ENGINEERING

May, 1999

INFORMATION TO USERS

This manuscript has been reproduced from the microfilm master. UMI films the text directly from the original or copy submitted. Thus, some thesis and dissertation copies are in typewriter face, while others may be from any type of computer printer.

The quality of this reproduction is dependent upon the quality of the copy submitted. Broken or indistinct print, colored or poor quality illustrations and photographs, print bleedthrough, substandard margins, and improper alignment can adversely affect reproduction.

In the unlikely event that the author did not send UMI a complete manuscript and there are missing pages, these will be noted. Also, if unauthorized copyright material had to be removed, a note will indicate the deletion.

Oversize materials (e.g., maps, drawings, charts) are reproduced by sectioning the original, beginning at the upper left-hand corner and continuing from left to right in equal sections with small overlaps. Each original is also photographed in one exposure and is included in reduced form at the back of the book.

Photographs included in the original manuscript have been reproduced xerographically in this copy. Higher quality 6" x 9" black and white photographic prints are available for any photographs or illustrations appearing in this copy for an additional charge. Contact UMI directly to order.

UMI®

Bell & Howell Information and Learning
300 North Zeeb Road, Ann Arbor, MI 48106-1346 USA
800-521-0600

WIND TUNNEL TESTING OF AN AIRFOIL WITH A MOVING SURFACE BOUNDARY-LAYER CONTROL

BY

ABDULLAH MOHAMMED AL-GARNI

A Thesis Presented to the
DEANSHIP OF GRADUATE STUDIES

KING FAHD UNIVERSITY OF PETROLEUM & MINERALS
DHAHRAN, SAUDI ARABIA

In Partial Fulfillment of the
Requirements for the Degree of

MASTER OF SCIENCE

In

MECHANICAL ENGINEERING

MUHARAM, 1420 H
MAY, 1999

KING FAHD UNIVERISTY OF PETROLEUM & MINERALS

DHAHRAN, SAUDI ARABIA

DEANSHIP OF GRADUATE STUDIES

This thesis, written by **Abdullah Mohammed Al-Garni** under the direction of his Thesis Advisor and approved by his Thesis Committee, has been presented to and accepted by the Dean of Graduate Studies, in partial fulfillment of the requirements for the degree of **Master of Science in Mechanical Engineering**.

THESIS COMMITTEE

Dr. Ahmed Z. Al-Garni, **Chairman**

Dr. Saad A. Ahmed, **Co-Chairman**

Dr. Ahmet Z. Sahin, **Member**

Dr. Ibrahim Dincer, **Member**

Dr. Abdul-Ghani Al-Farayedhi
Chairman, Department of Mechanical Engineering

Dr. Abdullah M. Al-Shehri
Dean of Graduate Studies
Date: 22/6/99

عمادة الدراسات العليا
DEANSHIP OF GRADUATE STUDIES

Dedicated to

My mother, brothers, sisters,

and to

My wife

ACKNOWLEDGMENT

"In the name of Allah (God), the Most Gracious, the Most Merciful. Read! In the name of your Lord Who has created (all that exist). He has created man from a clot (a piece of thick coagulated blood). Read! And your Lord is the Most Generous. Who has taught (the writing) by the pen. Nay! Verily, man does transgress (in disbelief and evil deed). Because he considers himself self-sufficient. Surely, unto your Lord is the return." (The Noble Qur'an, Sûrah No. 96)

First and above all, all praise to Allah, Who made every difficult thing easy. Who guided and protected me throughout my life and gave me the opportunity and patience to carry out this work. I am happy to have had a chance to glorify His name, in the sincerest way, through this accomplishment, and I ask Him, with hope only Him, to accept my efforts. And second, prayers and peace upon His Prophet, Mohammed.

The support provided by the King Fahd University of Petroleum & Minerals is highly acknowledged.

I am indebted to my thesis advisor, Dr. Ahmed Z. Al-Garni, for his help and advice. Also, his valuable time, encouragement and guidance are sincerely appreciated. Working with him was indeed an experience. I wish to offer sincere

thanks to my thesis co-advisor, Dr. Saad A. Ahmed, for his keen interest in the experimental program.

Many thanks are also due to my thesis committee members, Dr. Ahmet Z. Sahin and Dr. Ibrahim Dincer for their help and advice.

I also want to thank all the faculty in the Mechanical Engineering Department for their help and my friends and fellow graduate students for their support.

Finally, Thanks are due to the members of my family for their patience, encouragement, understanding and moral support. No such work could ever been accomplished without their continuous support.

CONTENTS

LIST OF TABLES

LIST OF FIGURES

NOMENCLATURE

c	= airfoil's chord
C_D	= drag coefficient
C_L	= lift coefficient
C_P	= pressure coefficient
D	= drag
L	= lift
N	= number of samples
L/D	= lift-to-drag ratio
P	= static pressure
P_∞	= freestream pressure
S	= airfoil's area
u	= streamwise velocity, m/s
u'	= root mean square values of velocity fluctuations along x, m/s
U	= freestream velocity, m/s
U_c	= cylinder tangential velocity, m/s
$\frac{u'}{U}$	= turbulence intensity
U_c/U	= cylinder surface velocity ratio

x = distance along the chord

y = distance normal to the chord

α = angle of attack, deg.

δ = flap deflection angle, deg.

ρ = freestream density, kg/m^3

σ_u = standard deviation

Subscripts

c = cylinder

l = lower

max = maximum

R = required for flow reattachment

u = upper

THESIS ABSTRACT

NAME OF STUDENT: AL-GARNI, ABDULLAH MOHAMMED

TITLE OF STUDY: WIND TUNNEL TESTING OF AN AIRFOIL WITH A MOVING SURFACE BOUNDARY-LAYER CONTROL

MAJOR FIELD: MECHANICAL ENGINEERING

DATE OF DEGREE: MAY, 1999

The control of boundary layer is very important in the field of aerodynamics and hydrodynamics and becomes essential for current wing design technology to increase lift, stalling angle of attack and lift-to-drag ratio. Therefore, an experimental investigation has been conducted on a two-dimensional airfoil, NACA 0024, equipped with a moving surface to control the boundary layer. The moving surface, which is the surface of a rotating cylinder, is located at the leading edge of the airfoil. The airfoil was tested for different values of U_c/U and δ. This investigation includes the effects of α, U_c/U, and δ on lift and drag coefficients, the size of the separated flow region and the stalling angle of attack. In addition to these, the study shows the effect of U_c/U on the boundary layer growth and turbulence intensity. Experimental results showed that the leading-edge rotating cylinder increases the lift coefficient of the NACA 0024 airfoil from 0.85 for U_c/U = 0 to 1.63 for U_c/U =4 and delays the stalling angle of attack by about 160%. The smoke-wire flow visualization results were used to demonstrate the tremendous effect of the leading-edge rotating cylinder on the size of the recirculation region.

MASTER OF SCIENCE DEGREE
KING FAHD UNIVERSITY OF PETROLEUM & MINERALS
Dhahran, Saudi Arabia
May, 1999

خلاصة الرسالة

الاسم : عبدالله محمد القرني

عنوان الرسالة: اختبار بالنفق الهوائي لجناح ذو سطح متحرك للتحكم في الطبقة المتاخمة

التخصص: هندسة ميكانيكية

تاريخ الشهادة: محرم ١٤٢٠هـ (مايو ١٩٩٩ م)

التحكم في الطبقة المتاخمة لسطوح الأجنحة أصبح مهما في مجال ديناميكا الهواء والديناميكا المائية وأصبح أيضا ضروريا لتصميم الأجنحة لزيادة قوة الرفع، زاوية الانهيار وقوة الرفع إلى قوة مقاومة الهواء. لذا، تم القيام بدراسة تجريبية على جناح ذو بعدين، ناكا ٠٠٢٤، ذو سطح متحرك للتحكم في الطبقة المتاخمة، والسطح المتحرك هو عبارة عن اسطوانة تقع في مقدمة الجناح. لقد تم اختبار الجناح لقيم مختلفة من سرعة الاسطوانة إلى سرعة الهواء في النفق الهوائي، زوايا مختلفة للجنيح الإضافي المتحرك. هذه الدراسة تشتمل على تأثير زاوية الهجوم (α)، سرعة الاسطوانة إلى سرعة الهواء في النفق الهوائي، و زاوية الجنيح الإضافي المتحرك (δ) على معاملي الرفع ومقاومة الهواء، حجم المنطقة ذات الهواء المنفصل و على زاوية الانهيار. بالإضافة إلى ذلك، هذه الدراسة تظهر تأثير السطح المتحرك على تطور الطبقة المتاخمة وقوة الاضطراب. وقد أظهرت نتائج هذه الدراسة أن السطح المتحرك زاد قيمة معامل الرفع للجناح من ٠,٨٥ عندما تكون الاسطوانة ساكنة إلى ١,٦٣ عندما تكون الاسطوانة تدور بسرعة ٤ أضعاف سرعة الهواء في النفق الهوائي. أيضا، تم زيادة زاوية الانهيار بنسبة ١٦٠%. وقد تم تظهير الهواء حول الجناح باستخدام سلك الدخان لإظهار تأثير السطح المتحرك على حجم المنطقة ذات الهواء المنفصل.

ماجستير في العلوم

جامعة الملك فهد للبترول والمعادن

الظهران- المملكة العربية السعودية

محرم ١٤٢٠هـ (مايو ١٩٩٩م)

CHAPTER 1

INTRODUCTION

1.1 Boundary Layer

The influence of viscosity at high Reynolds numbers is confined to a very thin layer in the immediate neighborhood of the solid wall. This layer is called the *boundary layer*, and was first introduced by L. Prandtl. The subject of boundary layer is of great practical interest because nearly all flows occurring in practice are viscous flows.

The effect of viscosity, within the boundary layer, is such that the velocity parallel to the wall changes along the distance perpendicular to the surface, i.e. the velocity gradient $\partial u / \partial y$ exists (u is the streamwise velocity and y is the distance normal to the surface). Flow velocity at the wall is zero; however, with increasing the distance y, u gradually increases and finally reaches U, the inviscid flow velocity at the outer edge of the boundary layer. Compared to the main stream,

the retarded flow in the boundary layer suffers a relatively greater deceleration; hence the momentum of the flow near the wall is small and the ability of the fluid to move forward against any pressure rise is also limited. This small amount of momentum and energy along the body surface is eventually used to overcome the pressure rise and friction. Hence, the fluid particles are finally brought to rest. Thus, the surface streamline reaches the point on the wall where $\partial u / \partial y|_{y=0} = 0$ and begins to break away from the wall and separates the flow from the surface. This is called *boundary layer separation*.

The boundary layer separation is always associated with the formation of vortices and with large energy losses in the wake of the body. It occurs primarily near blunt bodies, such as circular cylinders and spheres. Behind such a body there exists a region of strongly decelerated flow (so-called *wake*), in which pressure distribution deviates considerably from that in a frictionless region. As a result of decelerated flow, the lift decreases, the drag increases, and reverse flow and stalling occur. The term *stall* is used to express the unfavorable aspect of flow separation. Since stall usually occurs near peak operating performance. The control of stall is concerned with preventing or reducing boundary layer separation in the interest of efficient operation. It is evident that the boundary layer separation may be prevented or delayed if the momentum of the flow near the wall is increased. Thus, one means of boundary layer control (BLC) is to inject, blow and/or increase the level of mixing by vortex generator in the shear layer.

Boundary layer control technology has undergone tremendous progress in recent years due to the focused research efforts in the areas of aerodynamics, structures, and materials. Experimental effort has been made in aerodynamics not only because it has been experimentally convenient, but more importantly because of the very strong influence of the boundary layer separation and transition on many aerodynamic characteristics. For example, attached laminar flow over major portions of an aircraft wing has long been known to have favorable effects in terms of aerodynamics performance and fuel economy. On the other hand, it has been observed experimentally that, at high angles of attack (e.g., during takeoff or while performing a sharp maneuver), the flow tends to separate from the upper surface of the wing and this results in significant reduction in the attainable lift and a considerable increase in the total drag. Since the maximum usable lift is very important in high angle of attack maneuvering for combat aircraft and in determining the maximum payloads for commercial and rotary wing aircraft, different methods of BLC and lift augmentation devices have been a focus of extensive experimental research over the past 40 years.

1.2 Methods of Boundary Layer Control

Several methods, which have been developed for the purpose of artificially controlling the behavior of the boundary layer, have been investigated at length

and employed in practice with varying degree of success. These methods can be classified as follows:

1. Suction
2. Blowing
3. Vortex generator
4. Delay of transition by the use of suitable shaped (Laminar airfoils)
5. Cooling of the wall
6. Moving surfaces

Methods 1 to 5 will be discussed briefly in this section. Method 6 will be described in Sec. 1.3. Regardless of the boundary-layer control method used, the main objective of a control method is to delay or perhaps prevent separation of the boundary layer from the surface.

1.2.1 Suction

Among the various methods of the BLC, the suction of boundary layer from a slit is the most widely applied. The decelerated flow particles in the boundary layer are removed before they are given a chance to cause separation, in order that the newly formed boundary layer is capable of overcoming a certain adverse pressure gradient. This newly formed boundary layer is allowed to form behind the slit. However, an auxiliary power is required to achieve this goal.

Suction may be provided continuously or discontinuously. For the prevention of boundary layer separation by suction, it appears more effective to provide the suction mainly in the region of adverse pressure gradient [1]. Effective suction could improve the performance of the airfoil in terms of lift and drag.

The suction reduces the pressure drag, hence decrease the total drag. With suitable arrangements of suction slits it is possible to increase lift and shift the point of separation downstream. The effect of the delay in separation caused by suction is to reduce the boundary-layer thickness, which becomes less prone to turning turbulent. Furthermore, the velocity profiles in a boundary layer with suction have forms, which are less likely to induce turbulence compared to those in boundary layers without suction and of equal thickness [2].

1.2.2 Blowing

In blowing, an additional energy is supplied to the fluid particles which are being retarded in the boundary layer. This can be achieved by injecting a foreign fluid in the neighborhood of a wall with the aid of special blower or by deriving the required energy directly from the main stream. This later effect can be produced by connecting the retarded region to a region of higher pressure through a slot in the wing (slotted wing). If the fluid is injected parallel to the wall, the momentum of the shear layer is augmented whereas if it is injected normal to the

wall, the mixing rate is increased. The former term is called tangential blowing while the later is called normal blowing. Both effects are advantageous.

Lift and position of transition are influenced by blowing. In the case of slotted wing, it is possible to relegate separation to considerably larger angles of incidence, and to achieve much larger lifts. The phenomena in the slot formed by the flap near the trailing edge are, in principle, the same as those at the forward slat. The gain in lift is seen to be considerable.

1.2.3 Vortex Generator

The vortex generator transports energy into the boundary layer from the outer flow, and is used mainly for control of already separated flow rather than for the prevention of separation on wings, diffusers, or bends in channels at subsonic and supersonic speeds. Wall length is saved by using a vortex generator for a given pressure recovery. For example, the wall length can be saved by about 60 percent for a pressure recovery coefficient of 0.67 at subsonic speed.

There are many different kinds of vortex generators, such as simple blow, shielded plow, triangular plow, scoop, twist interchanger, ramp, tapered fin, dom, shielded sink, wedge, vane, wing, fence, leading edge fairing, dorsa fin, etc. The mixing on a coarse scale by relatively large widely spaced devices is far more effective than fine scale mixing. Thus multiple rows are less effective than a

single row of devices properly spaced and stationed. The successful application of the vortex generator to inhibit the development of the separation of the boundary layer profile is independent more critically on the strength and disposition of the individual vortices in the precise region of adverse pressure gradient than on the boundary layer profile just downstream. The vortex generators increase the lift of a wing. The wedge is useful for turbulence mixing, boundary layer attenuation between wedges, and discharge of the rest of the boundary layer into the general flow [3].

1.2.4 Delay of Transition by the Use of Suitable Shapes. Laminar Airfoil.

Transition from laminar to turbulent flow can also be delayed by the use of suitably shaped bodies. The objective, as in the case of suction, is to reduce frictional drag by causing the point of transition to move downstream. The location of the point of transition in the boundary layer is strongly influenced by the pressure gradient in the external stream. With a decrease in pressure, transition occurs at much higher Reynolds numbers than with an increase of pressure. A decrease in pressure has a highly stabilizing effect on the boundary layer, and the opposite is true of an increase in pressure along the stream. This circumstance is utilized in modern low-drag airfoils. The desired result is

achieved by displacing the section of maximum thickness far rearwards. In this manner a large portion of the airfoil remains under the influence of a pressure which decreases downstream and a laminar boundary layer is maintained.

1.2.5 Cooling of the Wall

In a certain range of supersonic Mach numbers it is completely possible to stabilize the boundary layer by cooling the wall. Cooling can also be applied in order to reduce the thickness of the boundary layer. This possibility may become important, e. g. when gases of very low density are made to flow through the nozzles of wind tunnels, because otherwise the very thick boundary layers would unacceptably reduce the useful area of the test section.

At subsonic Mach numbers, the position of the separation and the extent of the separated region are affected by heat transfer. By cooling the wall of the body the pressure gradient deepens and the extent of the separated region is delayed, and vice versa. At hypersonic speeds, by cooling the model of a flare-cylinder combination, the extent of laminar separation is reduced and the pressure gradient is increased similar to lower speed cases; also the flare pressure level (control effectiveness) is sometimes increased [3].

1.3 Moving Surfaces

Since the boundary layer owes its existence to the difference between the velocity of the fluid and that of the solid wall, it is possible to eliminate the formation of the boundary layer by reducing that difference, i.e. by causing the solid wall to move with the stream. This energizes the low momentum boundary layer flow by the dynamic motion of the wall and thus prevents separation. The simplest way of achieving such a result involves the rotation of a circular cylinder. If the cylinder is rotated with a sufficient speed and in such a direction that the tangential velocity of the cylinder surface is the same or greater than the freestream, then flow separation may be prevented. A rotating cylinder in a fluid is capable of producing strong effects on the boundary layer and in the flow fields in its vicinity.

The nature of these effects for a rotating cylinder in a water channel at various cylinder peripheral speeds was investigated at Goettingen by Prandtl [3]. The rotating cylinder is capable of producing a force normal to the cylinder angular velocity vector, as shown in Fig. 1.1. This aerodynamic force, which is due to air circulation around a cylinder is called *Magnus effect*.

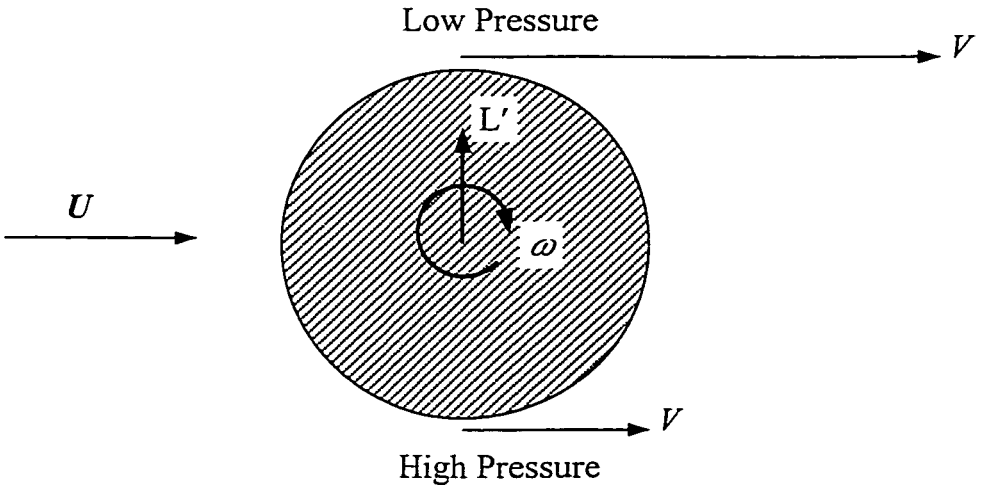

Figure 1.1 Magnus effect on a spinning cylinder

1.3.1 Applications of Moving Surfaces to Airfoil

The application of a rotating cylinder to control flow separation and to improve aerodynamics performance is versatile because it can be combined with flap, a droop nose, or leading edge slats. Fig. 1.2 shows the airfoil with the rotating cylinder located at the leading edge of the airfoil. The moving surface of the cylinder energizes the low-energy boundary-layer flow impinging on the cylinder from the airfoil upstream of the cylinder and formed a new boundary layer downstream on the surface of the airfoil. Since the level of energy in this new boundary layer is high, it is possible to overcome the large adverse pressure gradient on the airfoil at high angles of attack and thus prevents or delays separation. This reenergizing process depends on the cylinder peripheral speed and the location of the cylinder.

1.4 Airfoil Nomenclature

The cross-sectional shape obtained by the intersection of the wing with the perpendicular is an *airfoil*. Fig.1.3 shows the airfoil with some basic terminology. The major design feature of an airfoil is the *mean camber line*, which is the locus of points halfway between the upper and lower surfaces as

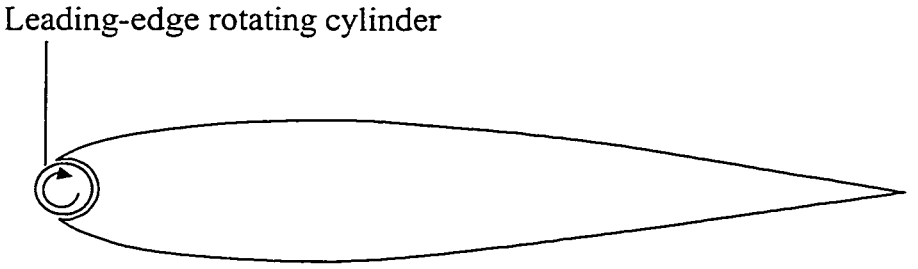

Figure 1.2 Airfoil with a leading-edge Rotating cylinder

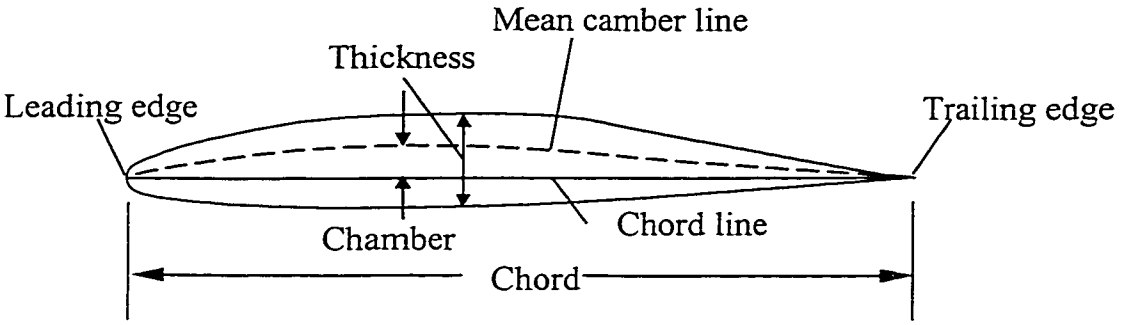

Figure 1.3 Airfoil nomenclature.

measured perpendicular to the mean camber line itself. The most forward and rearward points of the mean camber line are the *leading* and *trailing edges*, respectively. The straight line connecting the leading edge and trailing edge of the airfoil is called the *chord line* of the airfoil. The distance from the leading edge to the trailing edge measured along the chord line is simply designated by the *chord* of the airfoil, given by the symbol c. The camber is the maximum distance between the mean camber line and the chord line, measured perpendicular to the chord line. The thickness is the distance between the upper and lower surface, perpendicular to the chord line. The shape of the airfoil at the leading edge is usually circular, with the leading edge radius of approximately $0.02c$. An airfoil with no camber, i.e., with the camber line and chord line coincident, is called a symmetric airfoil.

1.5 Aerodynamic Forces

Fig. 1.4 shows an airfoil inclined to a stream of air. The freestream velocity U is the velocity of the air far upstream of the airfoil. The *direction* of U is defined as the *relative wind*. The angle between the freestream velocity and the chord line is the *angle of attack* α of the airfoil. The resultant aerodynamic force created by the pressure and shear stress distributions over the airfoil is shown by the vector R. This aerodynamic force can be resolved into two forces, parallel and

perpendicular to the relative wind. The *drag, D,* is always defined as the component of the aerodynamic force parallel to the *relative wind* and the *lift, L,* is always defined as the component of the aerodynamic force perpendicular to the *relative wind.*

The dimensionless force are defined as follows:

Lift coefficient $$C_L = \frac{L}{\frac{1}{2}\rho U^2 S}$$

Drag coefficient $$C_D = \frac{D}{\frac{1}{2}\rho U^2 S}$$

another dimensionless quantity is

Pressure coefficient $$C_P = \frac{P - P_\infty}{\frac{1}{2}\rho U^2}$$

The lift and drag coefficients can be obtained by integrating pressure coefficient from the leading edge (*LE*) to the trailing edge (*TE*) as follows:

$$C_l = \frac{1}{c}\left[\int_0^c (C_{p,l} - C_{p,u})dx\cos\alpha + \int_{LE}^{TE} (C_{p,u} - C_{p,l})dy\sin\alpha\right] \qquad (1.3)$$

$$C_d = \frac{1}{c}\left[\int_0^c (C_{p,l} - C_{p,u})dx\sin\alpha + \int_{LE}^{TE} (C_{p,u} - C_{p,l})dy\cos\alpha\right] \qquad (1.4)$$

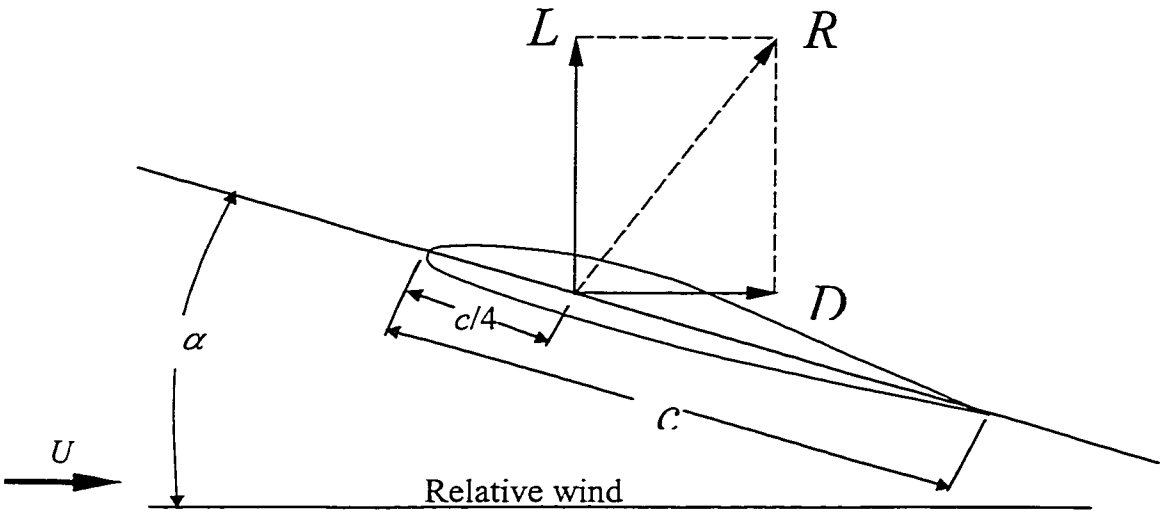

Figure 1.4 Definition of lift, drag, angle of attack and relative wind

CHAPTER 2

LITERATURE REVIEW

2.1 Previous Work

Johnson et al. [4] have conducted tests with a wedge-shaped flap having a rotating cylinder as the leading edge. Flap deflection was limited to 15°, and the critical cylinder velocity necessary to suppress separation was determined. The study includes the effect of the gap between the rotating and fixed surfaces on the boundary-layer control. It also showed that a rotating cylinder at the leading edge of a lifting body could effectively control boundary-layer separation. The gap between the rotating and fixed surfaces should be kept at its minimum in order to minimize the cylinder speed required for effective boundary-layer control. No efforts were made to observe the influence of the increase in U_c/U beyond 1.2.

Sayers [5] presented lift coefficients and stalling angles of a rudder with a leading-edge rotating cylinder. Tufts of wool were also mounted on the surface of the rudder to indicate flow direction. Results of the study showed that the leading-

edge rotating cylinder increases the lift coefficient and stalling angle, thus increases the maneuverability of a vessel fitted with such a rudder.

Modi et al. [6] studied the effectiveness of the moving surface boundary-layer control (MSBLC) on a NACA 63-218 (modified) two-dimensional wing used in the canadair CL-84, a twin-propeller V/STOL design. Three models were tested: 1) an airfoil with its leading edge formed by a rotating cylinder, 2) an airfoil with its leading edge formed by a rotating cylinder and provided with a plain unslotted flap, 3) an airfoil with slotted flap, leading edges of both formed by a rotating cylinders. A significant effect on the maximum lift, stall characteristics, and lift/drag ratio was observed. It appeared that a rotating cylinder at the leading edge of an airfoil is likely to provide the maximum benefit.

Hassan and Sankar [7] conducted a numerical study to investigate the effects of forebody boundary-induced vorticity on the development of the laminar/turbulent boundary layers over the modified NACA 0012, NACA 63-218 airfoils having leading-edge rotation. They utilize an implicit finite-difference procedure to solve the two-dimensional compressible full Reynolds-averaged Navier-Stokes equations on a body-fitted curvilinear coordinate system. The study presented the effect of varying the circumferential speed on the location of point(s) of the laminar and/or turbulent separation, the size of the separated flow region above the airfoil, the strength and location of shock waves, and the

computed sectional lift coefficients. Qualitative comparisons with smoke wire flow visualization results were presented.

Modi et al. [8] presented an experimental program complemented by a flow visualization study to investigate of the concept of MSBLC as applied to a Joukowsky airfoil. The moving surface was provided by rotating cylinders located at the leading edge and upper surface of the airfoil. Results suggested that the leading-edge rotating cylinder effectively extends the lift curve without substantially affecting its slope, thus increasing the maximum lift and delaying stall. The maximum coefficient of lift realized was about 2.73, approximately three times that of the base airfoil. The maximum delay in stall was around 48° The study showed that an increase in the ratio of the cylinder surface speed to the freestream speed to greater than 4 does not yield any additional benefit. It also showed that the optimum location for the cylinder is at the upper side of the leading edge.

Tennant and Yang [9] relied on an artifice to model the region of transition from a fixed wall to a moving wall, and ignored the physical gap between the walls by assuming all of the acceleration effect of the wall occurred in a fixed streamwise span, λ. By allowing the numerical calculation procedure to make a step length λ, they found that satisfactory calculations could proceed streamwise; this method was verified by a small amount of experimental data. In particular,

their results showed that the value of λ for adequate calculations was equal to the boundary-layer thickness.

Tennant at al. [10] analyzed a moving wall as a boundary-layer control device. The moving wall normally the surface of a rotating cylinder, is located in a region of high adverse pressure gradient and energizes the boundary layer in an effort to delay or prevent flow separation. A numerical method based on the method of Cebeci and Smith was presented for the region of flow from the fixed wall, through the transition region, and onto the moving surface. Comparison between numerical results and experimental results showed excellent agreement.

Modi at al. [11] assessed effectiveness of a rotating cylinder in reducing the drag of bluff bodies, such as a two-dimensional flat plate at large angles of attack, rectangular prisms, and three-dimensional models of trucks, through an extensive wind-tunnel test program. Results suggested that injection of momentum through the rotating cylinder could significantly delay separation of the boundary layer and reduce the pressure drag. For the flat plate at $\alpha = 90°$, it reduced the drag coefficient by 75% and for square prism, the maximum reduction varied from 40% ($L/H = 2$) to 54% ($L/H = 1$) while the drag coefficient of the truck reduced by around 13% at $U_c/U = 1.5$. A flow visualization study, conducted in closed-circuit water tunnel using polyvinylchloride tracer particles, showed effectiveness of the rotating cylinder.

Moktarian and Modi [12] conducted a numerical simulation of a Joukowsky airfoil modified, with a leading-edge rotating cylinder, using surface singularity approach with viscous corrections. Results showed that the predicted pressure distributions are in good agreement with the experimental one almost up to the point of complete separation except in the separation region, where the prediction of separated boundary layers with flow reversal would require the solution of the full Navier-Stokes equations. The cylinder rotation increased the maximum lift coefficient by more than 150% and delayed the stall angle to 48°.

Kubo et al. [13] presented an active suppression of vortex resonance and galloping type of wind induced instabilities associated with two-dimensional square prisms by using MSBLC method. Two rotating cylinders at the leading edge of a two-dimensional prism were installed. The experiments were conducted under three different conditions of the rotating cylinder, during which both surface pressure and dynamic response were studied: 1) the upper and lower cylinders rotating at the same speed; 2) the upper and lower cylinders have different speeds; and 3) the upper cylinder is at rest and only the lower cylinder rotates. Flow visualization study was also presented. Results showed that the rotating cylinder effectively renders a bluff body more streamlined, reduces drag coefficient of a square prism by 30% and leads to a significant reduction in fluctuating loading on both top and bottom surfaces of a two-dimensional prism.

In addition, the rotating cylinder successfully alters the associated aerodynamics to suppress both vortex resonance and galloping.

Tennant et al. [14] have reported circulation control for a symmetrical airfoil with a rotating cylinder forming its trailing edge. For zero angle of attack, the lift coefficient of 1.2 was attained with $U_c/U = 3$. The lift coefficient and the stagnation point location were found to be a linear function of U_c/U. A comparison was made by examining the lifting performance of a lone rotating cylinder in crossflow and that of the same cylinder with an attached body.

Kubo et al. [15] used boundary-layer control by means of rotating cylinders at the leading edges of super-tall structures, like pylons of super-long bridges and super-tall buildings for suppressing the aerodynamic vibrations. It was shown that the rotating cylinder eliminated the drag force and aerodynamic response amplitude of a tall building.

Modi et al. [16] studied the effect of MSBLC in increasing lift and/or reducing drag of a two-dimensional wedge shaped airfoil, a flat plat at high angles of attack, and a two-dimensional prism through an extensive wind tunnel test-program and flow visualization study. Result showed that the MSBLC could significantly delay separation of the boundary layer. The wedge airfoil showed an increase in C_L/C_D from 2 to 80 while the flat plate at 90° experienced a reduction in drag coefficient by around 75%. For the two-dimensional prism, the reduction in drag was observed to be as high as 54%.

Mokhtarian et al. [17] studied the effect of a rotating cylinder, located at the leading edge of a symmetrical Joukowsky airfoil, on boundary layer using three different cylinder configurations: 1) a solid circular cylinder, 2) a scooped cylinder, and 3) a reversed scooped cylinder. The rotating scooped cylinder appeared to redirect more air over the upper surface. However, at high rates of rotation, the solid rotating cylinder appeared to be more effective than the other two.

Kubo et al. [18] studied the effect of MSBLC on very high two- and three-dimensional buildings with a square cross-section using different rotor arrangements and different directions of rotation. It was found that the momentum injection was more effective in the three-dimensional condition. The MSBLC was also successful in suppressing wind-induced oscillations and torsional instability.

Modi et al. [19] have reported an extensive wind tunnel test-program followed by a flow visualization study. The test program investigated: 1) a two-dimensional flat plat with a rotating cylinder at each edge, 2) a family of a two-dimensional rectangular prisms with rotating cylinder at two edges, 3)a 1/12 scale tractor-trailer configuration of the truck with the MSBLC applied at the top leading edge and a downstream location on the trailer.

Modi et al. [20] presented a study focusing on:1) numerical simulation of the MSBLC as applied to both streamlined geometry (airfoil) as well as bluff geometry (D-section) multi-element systems, 2) effects of the angle of attack and

U_e/U on the surface pressure distribution and aerodynamic coefficients, 3) Validation of the numerical results through extensive wind tunnel tests, and 4) flow visualization study to gain better appreciation of the complex flow.

Alvarez-Calderon and Arnold [21] carried out tests on a rotating cylinder flap to evolve a high-lift airfoil for STOL-type aircraft. The system was flight-tested on a single-engine high-wing research aircraft designed by the Aeronautics division of the Universidad Nacional de Ingenieria in Lima, Peru.

Of same interest is the North American Rockwell designed OV-10A aircraft, which was flight tested by the NASA Ames Research Center [22 & 23]. Cylinders, located at the leading edges of the flaps, are made to rotate at high speed with the flaps in lowered position. The main objective of the test program was to assess handling qualities of the propeller-powered STOL-type aircraft at higher lift coefficients. The aircraft was flown at speeds of 29-31 m/s along approaches up to – 8° (i.e., glide path with respect to the horizontal), that corresponded to a lift coefficient of about 4.3. In the pilot's opinion, any farther reductions in approach speed were limited by the lateral-directional stability and control characteristics.

Modi et al. [24] presented a numerical simulation using a multi-element panel method in addition to wind tunnel program to investigate the effect of MSBLC. Three different types of surfaces were used in the test program: smooth cylinder, rough cylinder, and splined cylinder. The panel method is used for

modeling the flow separation using free vortex lines. Results showed that panel method predicts the overall aerodynamics of airfoil with MSBC quite accurately.

Tennant [25] presented an interesting analysis for the two-dimensional, moving-wall diffuser with a step change in area. The diffuser incorporated rotating cylinders to form a part of its wall at the station of the area change. Preliminary experiments were also conducted for rotations up to 40% of the diffuser inlet velocity. Results showed no separation for the appropriate ratio of the moving surface to the diffuser inlet velocity.

2.2 Objective of the Study

The brief discussions above point out to the need for detailed experimental data. So far no efforts have been mad to investigate the effect of moving surface on the velocity and turbulence intensity profiles over the surface of an airfoil. In this investigation, the blockage ratio is 100% smaller than that reported by Modi [8]. The small blockage ratio reduces the need for boundary corrections [26]. Also, thick airfoils with MSBLC have not been investigated. This investigation should help to evaluate the lift and drag coefficients, and the turbulence quantities in the boundary layer as affected by the moving surface. The freestream velocity at which measurements were taken was 5 m/s corresponding to a Reynolds number of 6.5×10^4 based on the model chord. Pressure measurements were carried out

on pressure and suction sides of the airfoil at different α, different values of U_c/U, and different δ. Lift and drag were determined by the integration of measured pressures over the portion in which pressure measurements were taken. Boundary layer measurements were investigated using miniature single hot-wire probes. The data were collected using a data acquisition system and stored on the computer. Turbulence quantities, such as the mean and turbulence intensity, were computed using TSI Data Analysis Package (DAP software). In order to get better understanding of the flow pattern around the airfoil, a flow visualization using smoke wire technique was conducted.

More specifically, the objective of this investigation is to addresse the effects of α, U_c/U and δ on the following:

1. pressure distribution on the upper and lower surfaces of the airfoil,
2. lift and drag coefficients and stalling characteristics of the airfoil,
3. the size of the separated flow region,
4. velocity profiles of the upper surface of the airfoil, and
5. turbulence intensity profiles of the upper surface of the airfoil.

CHAPTER 3

EXPERIMENTAL SETUP AND TECHNIQUES

3.1 Testing Equipment

The following testing facility was used for the experimental investigation of the airfoil with leading-edge rotating cylinder.

3.1.1 Wind Tunnel

The experiments were conducted in the low-speed, low turbulence wind tunnel of the Wind Tunnel Laboratory at the King Fahd University of Petroleum & Minerals (KFUPM), shown in Fig. 3.1. The tunnel test section of 800×600×2600 mm is a closed, horizontal and designed with a large plexiglas window in the top and sides to provide adequate illumination and viewing for visualization study. The contraction ratio of the nozzle is about 6.5 and the return circuit is partially

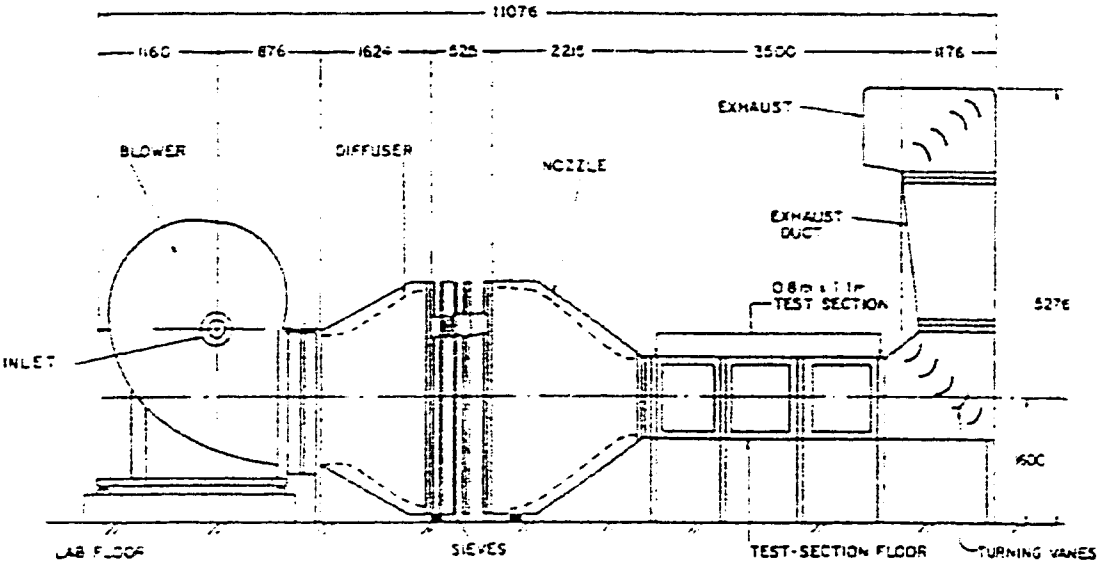

(a)

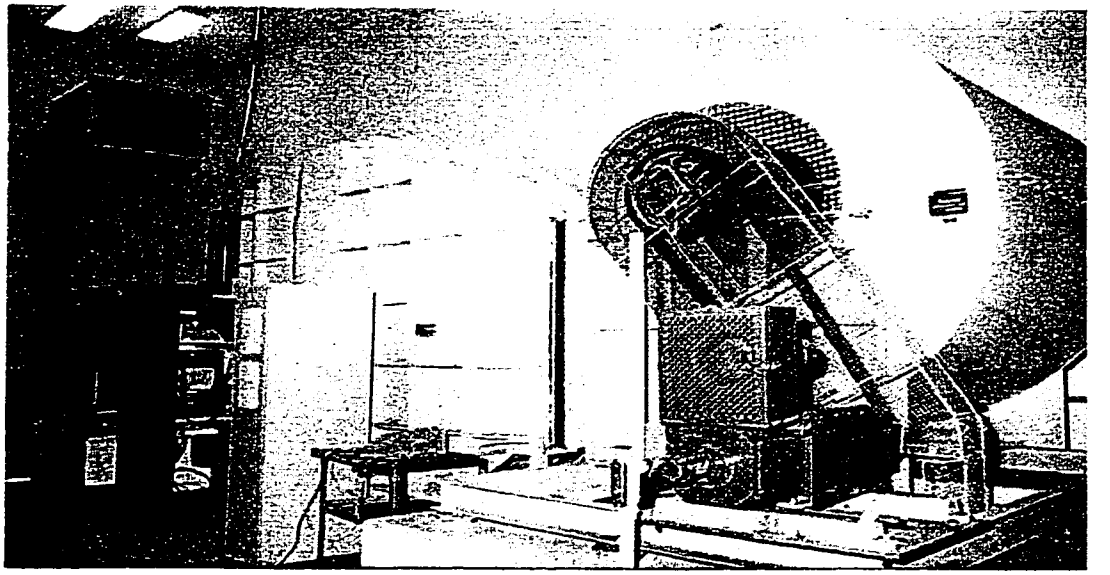

(b)

Figure 3.1 Schematic diagram and photographic view of the KFUPM wind tunnel.

open. The tunnel is powered by a 5.8 kW motor operating a centrifugal fan. The airspeed in the test section can be varied from 1- 40 m/s with a turbulence intensity of less than 0.2%.

3.1.2 Pressure Measurement Equipment

Manometers: Two Betz micromanometer (model 5585 series, manufactured by T.E.M Engineering Limited, new name Eleven Precision Limited) with an accuracy of 0.2 mm of water were used to measure surface pressure over the surface of the airfoil and other pressures like dynamic and static pressures in the wind tunnel.

Pitot-Static Tube: The static and dynamic pressures in the wind tunnel were measured using a pitot-static (Prandtl) tube. The tube was fixed to the roof of the test section and placed at the entrance of the test section.

3.1.3 Boundary-Layer Measurement Equipment

The velocity measurement equipment used in this investigation are hot-wire probe, anemometer, A/D converter and traverse mechanism. Fig. 3.2 shows a photographic view of the anemometer, A/D converter and computer.

Hot-Wire Probe: The velocity fluctuations were investigated using miniature single probe. The probe (DISA 55P15) is made of platinum-coated tungsten of nominal diameter 0.005 mm and a sensing length of 1.25 mm.

Anemometer: The probe was connected to a constant temperature anemometer (IFA 100) which has low-pass filter and a signal-conditioning unit. The analog outputs from the anemometer are conditioned (offset, gain and filter).

A/D Converter: The signal was digitized using A/D converter (TSI Model IFA 200 and Model 6260 DMA interface board). The DMA interface board was connected to the computer. IFA 200 was connected to the DMA interface board using 50-pin connector. The input voltage of A/D converter is typically 0-10 V or ±5 V with a resolution of 2.442 millivolts.

Traverse Mechanism: Fig. 3.3 shows the two-dimensional traverse mechanism used to survey the velocity fluctuations in the vicinity of the airfoil. The traverse mechanism moves in steps and each step is 0.025 mm. It can move in the vertical and horizontal direction as shown in the figure.

3.1.4 Flow Visualization Equipment

Smoke-Wire: To visualize the flow around the model, a 0.1 mm-diameter Nichrome wire was placed vertically and 400 mm ahead of the model's leading edge at midspan point.

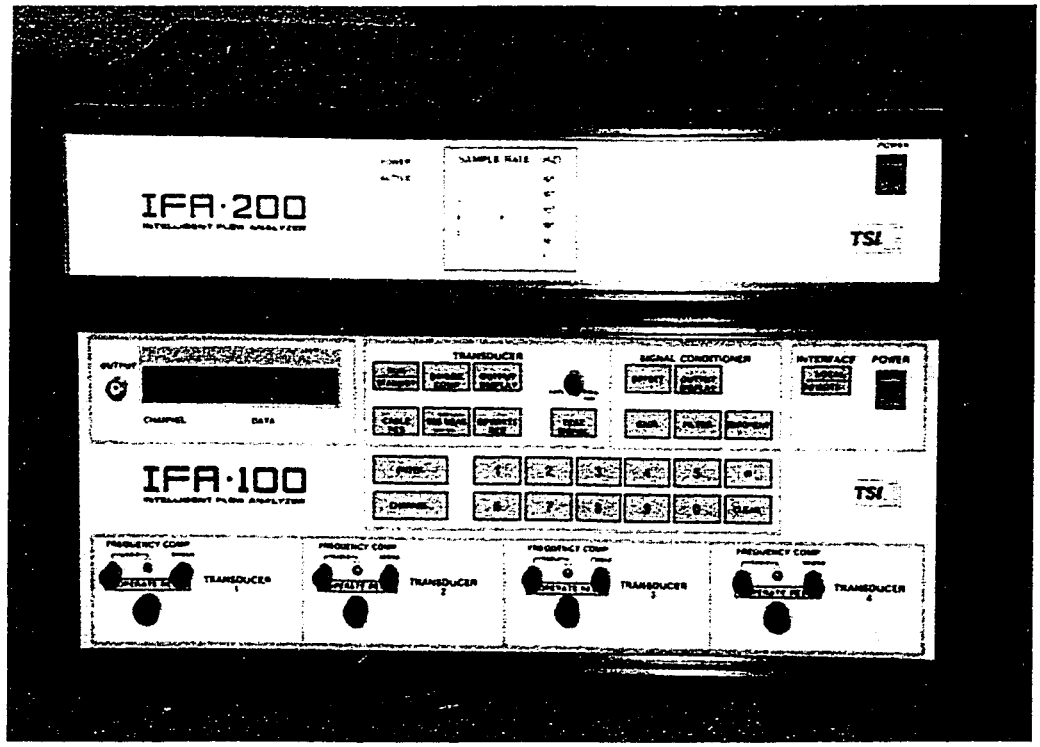

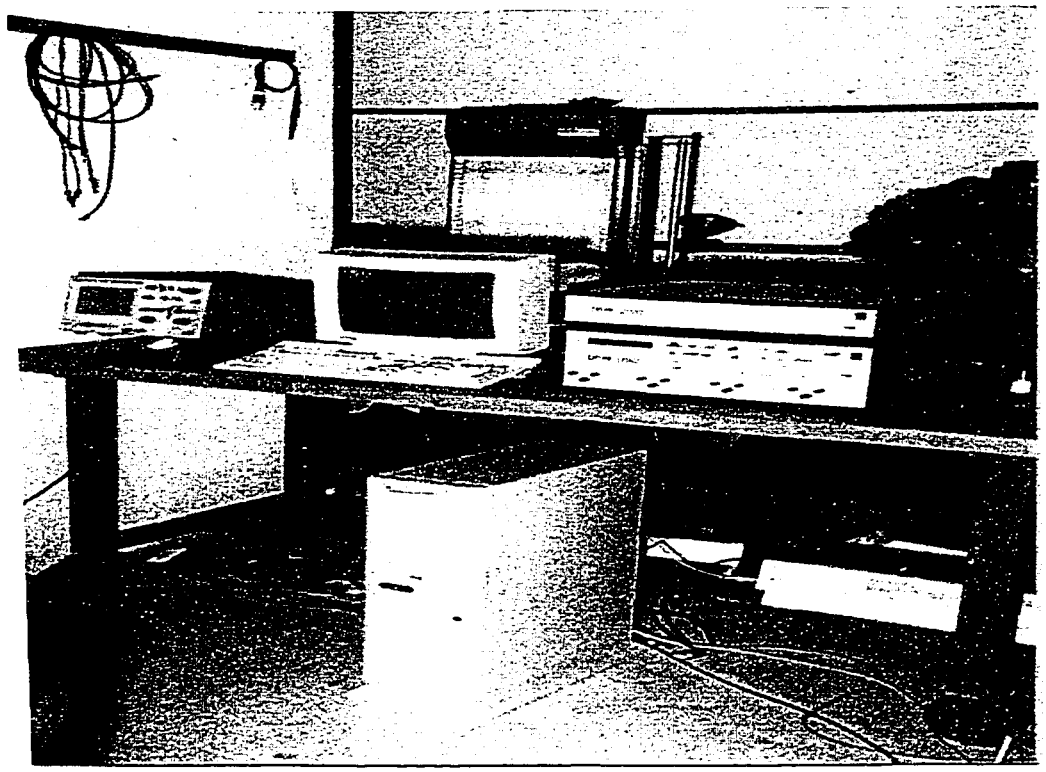

Figure 3.2 Boundary layer measurement equipment.

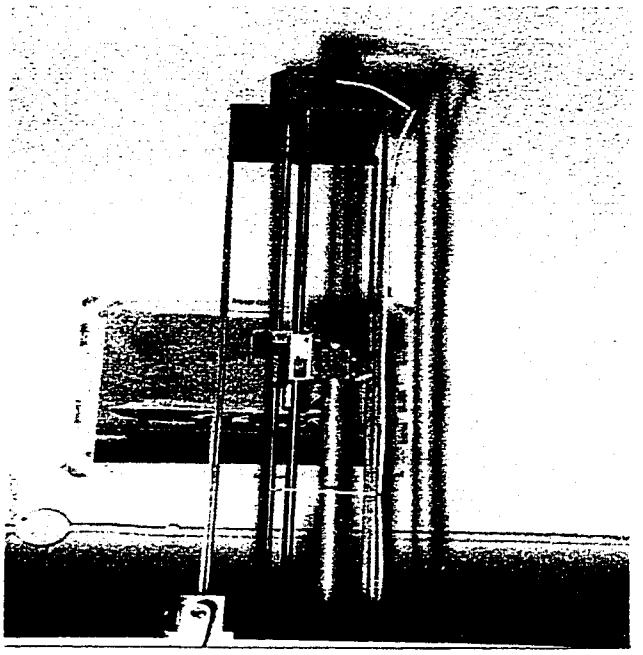

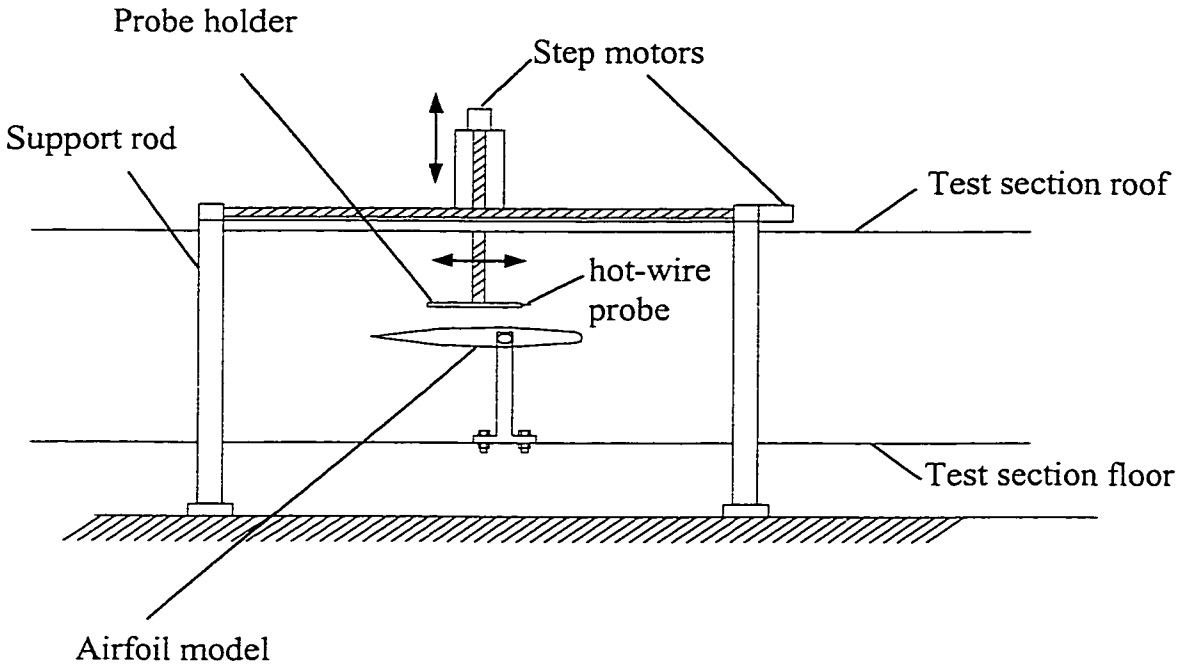

Figure 3.3 Two-dimensional traverse mechanism (a) photograph of the system (b) schematic of the mechanism, model and wind tunnel.

Coating Material: A number of different liquids were initially used to coat the smoke-wire to produce smoke filaments. These include several types of lubricating and mineral oils such as machine oil, commercial grad mineral oil. The best coating material was found to be a paste of mineral oil and blue dye.

Photographic Camera and Film: Still photography of the flow around the airfoil were taken using Nikon F3. The focal length of the camera can be varied from 80-200 mm. Pictures were taken with a shutter speed of one eighth of a second and at an aperture opening of f:11. The flow pattern were recorded on Kodak *Tri-X* 400, black and white Films. The model was illuminated by a single 1000 W studio light from above.

3.2 Airfoil Model

The airfoil, NACA 0024, with the leading-edge rotating cylinder is shown in Fig. 3.4. The model has 200 mm chord and 48 mm maximum thickness spanned the tunnel test section, 600 mm, to create essentially two-dimensional conditions. The aspect ratio of the airfoil is 3. A circular cylinder with a diameter of 25 mm and a plain flap with a chord of 40 mm were placed at the leading edge and trailing edge of the airfoil, respectively. The airfoil was made of wood and was hollow at the midspan where the pressure tabs were located in order to

connect plastic tubes of 1.0 mm inner diameter to the pressure tabs. The plastic tubes were then connected to the manometer outside the tunnel.

The rotating cylinder was mounted between high-speed bearings housed in the brackets at both ends of the model. It was driven by 1.0 hp, 15 A. variable speed motor (model No. 2M191 and made by Dayton). The motor was located outside the tunnel through standard couplings. The speed of the motor can be varied from 0 to 14,400 RPM and was measured using optical-digital tachometer.

The gap between the rotating cylinder and the remaining stationary part of the airfoil was about 0.5 mm. A total of 24 static pressure taps, with inner diameter of 1 mm were distributed chordwise along the suction and pressure sides at the midspan point of the airfoil except, of course, on the rotating cylinder and a plain flap. The model was painted black to minimize light reflections from its surface.

The whole assembly was supported on a frame that is outside the test section, as shown in Fig. 3.5. With this frame, the airfoil angle of attack could be changed by rotating the whole assembly while the motor remained in fixed position on the support.

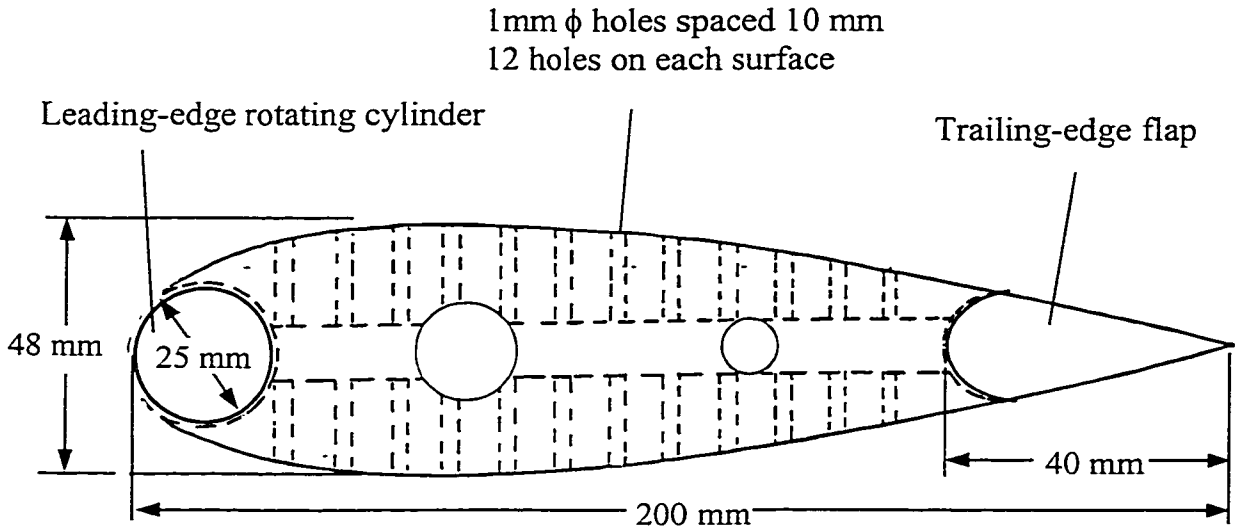

(a) schematic diagram

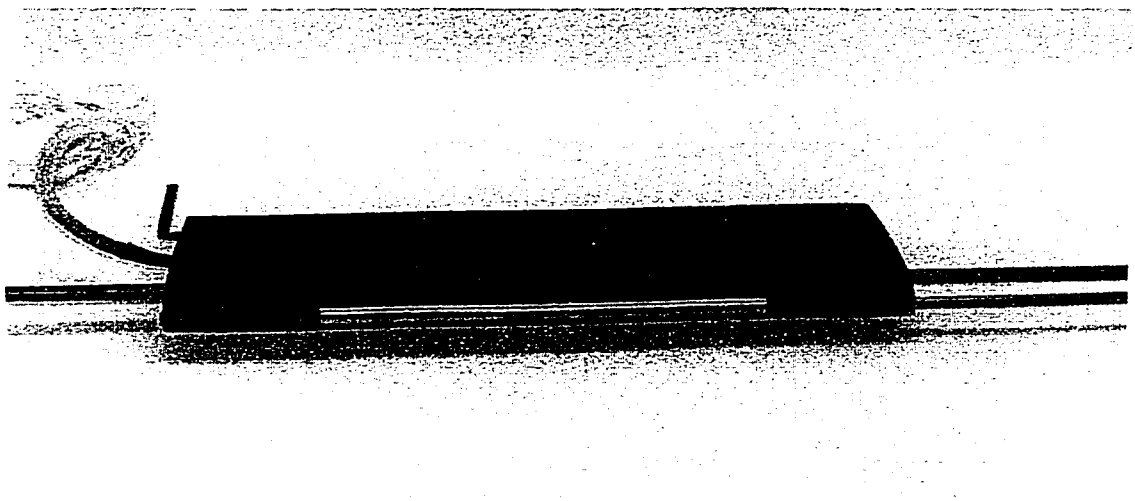

(b) Photographic view

Figure 3.4 The NACA 0024 airfoil with the leading-edge rotating cylinder.

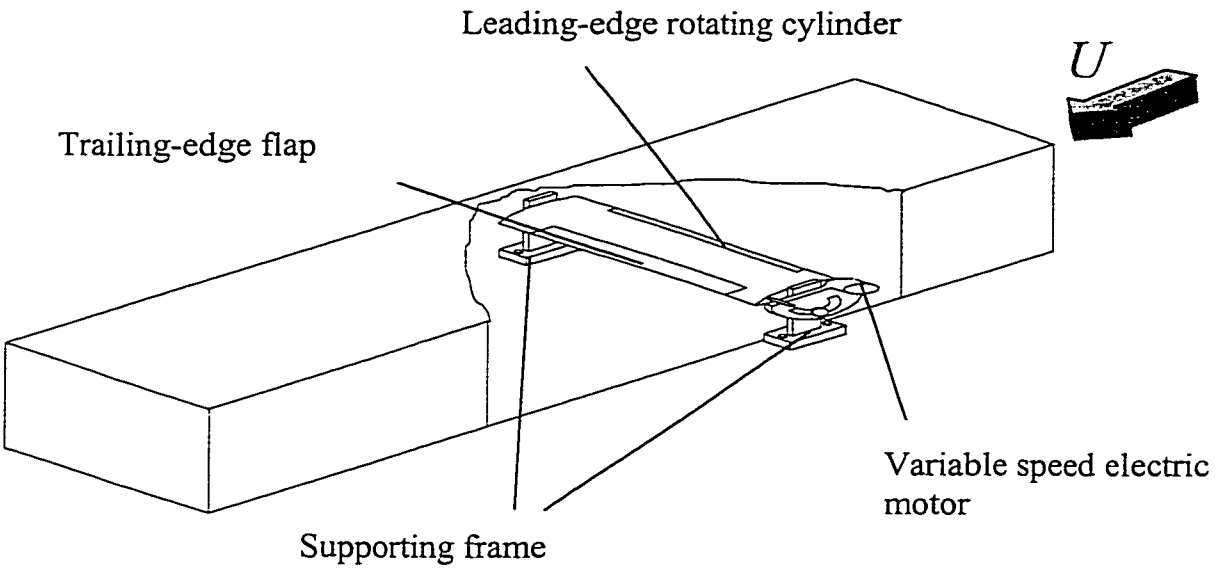

(a) Schematic of the airfoil mounted in the wind tunnel

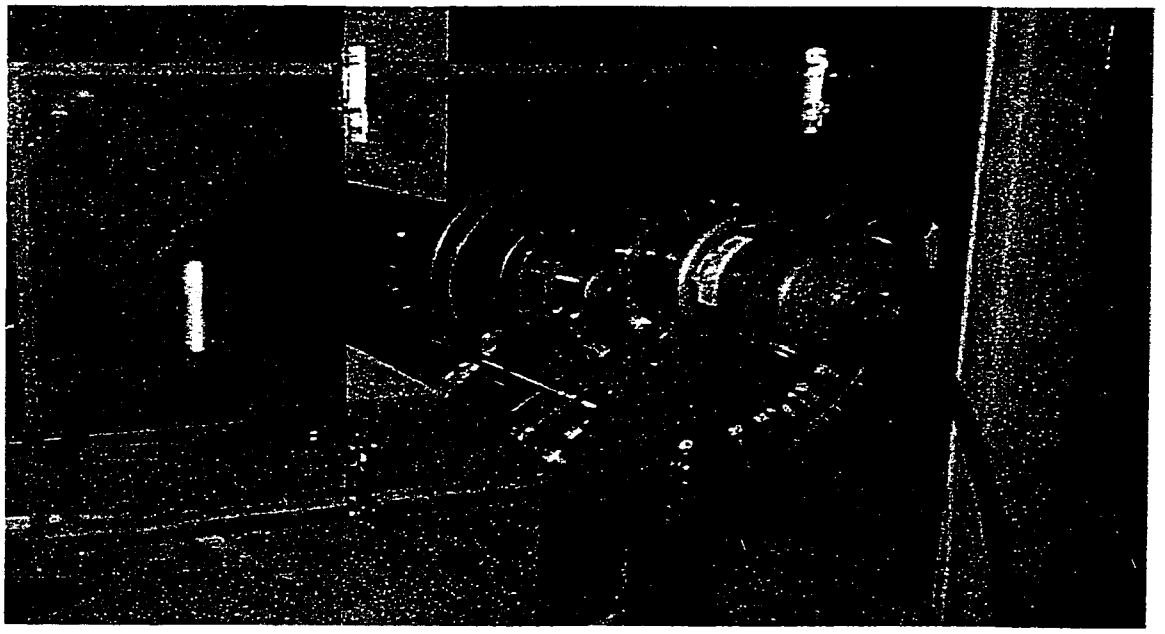

(b)Photograph of the airfoil mounted in the wind tunnel

Figure 3.5 Airfoil installation in the wind tunnel

3.3 Experimental Technique and Testing Conditions

Pressure and velocity fluctuation measurements, and flow visualization were conducted as described below:

3.3.1 Pressure Measurements

To get the forces acting on the model, surface pressure distributions were measured on the upper and lower surfaces of the airfoil at various α raging from 0 to 40°. The freestream velocity at which pressure measurements were taken was 5 m/s corresponding to a Reynolds number of 6.5×10^4 based on the model chord. Different angular speeds of 0 to 14,400 RPM corresponding to $U_c/U = 0,1,2,3$ and 4, were directly imparted to the leading-edge cylinder. Also, δ were varied from 0 to 30°. Test conditions are shown in table 3.1. For each case studied, 24 pressure tubes were connected to the manometer in turn and the pressures were recorded.

Angle of attack (α)	Flap deflection angle (δ)	U_c/U varies
0°, 10°, 20°, 30° and 40°	0°, 10°, 20°, 30° for each α	0, 1, 2, 3, 4 for each δ

Table 3.1 Test conditions.

3.3.2 Boundary-Layer Measurements

The velocity fluctuations were investigated using miniature single hot-wire probe (DISA 55P15) made of platinum-coated tungsten of nominal diameter 0.005 mm and a sensing length of 1.25 mm. Before taking measurements of the velocity fluctuations, the hot-wire probe was mounted at the center of the tunnel test section for calibration. The velocity inside the test section was varied from 0 to approximately 10 m/s. The Pitot tube was used to measure the velocity. Fig. 3.6 shows the calibration curve for the hot-wire probe (DISA 55P15). A two-dimensional traverse mechanism with step of 0.025 mm was used to survey the velocity fluctuations in the vicinity of the airfoil. The units contained in the digital velocity measurement system is illustrated in Fig. 3.7. The probe was connected to a constant temperature anemometer (TSI Model IFA 100). The analog outputs from the anemometer are conditioned (offset, gain and filter), simultaneously digitized and sent to a computer using A/D Converter (TSI Model IFA 200 and Model 6260). The digitized data is then deconditioned, corrected for temperature, and converted into velocity data using 4^{th} order polynomial calibration. The data were stored on the computer and turbulence quantities such as the mean and turbulence intensity were computed using TSI Data Analysis Package (DAP Software).

The freestream velocity at which velocity measurements were taken was 5 m/s corresponding to a Reynolds number of 6.5×10^4 based on the model chord.

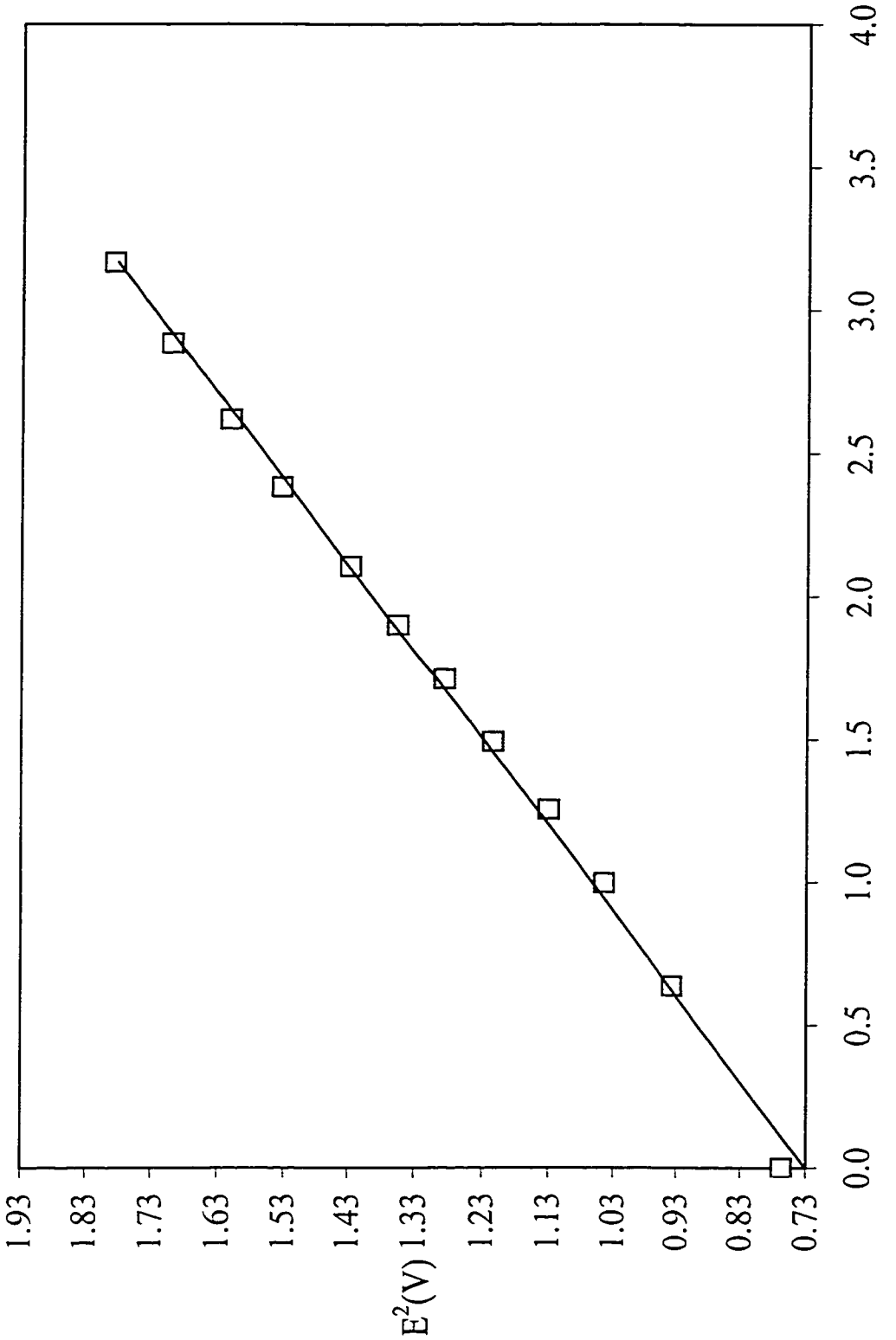

Figure 3.6 Calibration curve of the hot-wire (DISA 55P15)

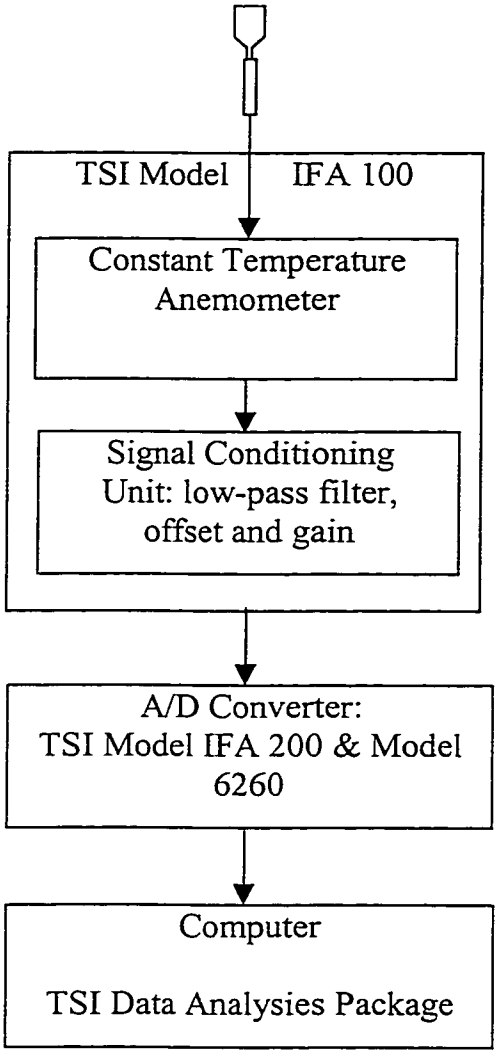

Figure 3.7 Flow chart of velocity measurement system

The airfoil was placed at $\alpha = 0°$ and 10°and U_c/U were varied between 0 and 4. The measurements were taken at five streamwise stations, x/c = 0.2, 0.4, 0.6, 0.8 and 1.0. Values of effective cooling velocity at each position were ensemble for a number of sweeps large enough to ensure that the calculated velocity values were determined with a minimum uncertainty.

3.3.3 Flow Visualization

The Smoke wire technique was used to visualize the flow around the model. A 0.1 mm-diameter Nichrome smoke wire was placed vertically and 40 cm ahead of the model's leading edge at midspan point [27]. The smoke wire was coated manually using cotton-tipped applicator soaked with a paste of mineral oil and blue dye and heated using a power supply of 65 V. This provided a uniform coating with no model fouling.

Positions of light, photographic camera and the smoke wire are shown in Fig. 3.8. Still photography were taken using **Nikon F3 (f:11)** with a shutter speed of one eighth of a second and **Kodak *Tri-X* 400** black-white Films. The camera was positioned along the spanwise axis of the model. The model was illuminated from the top, normal to the model, through 25.0 mm slit in the top of the test section. Lighting was accomplished by using a continuous single 1000 W lamp.

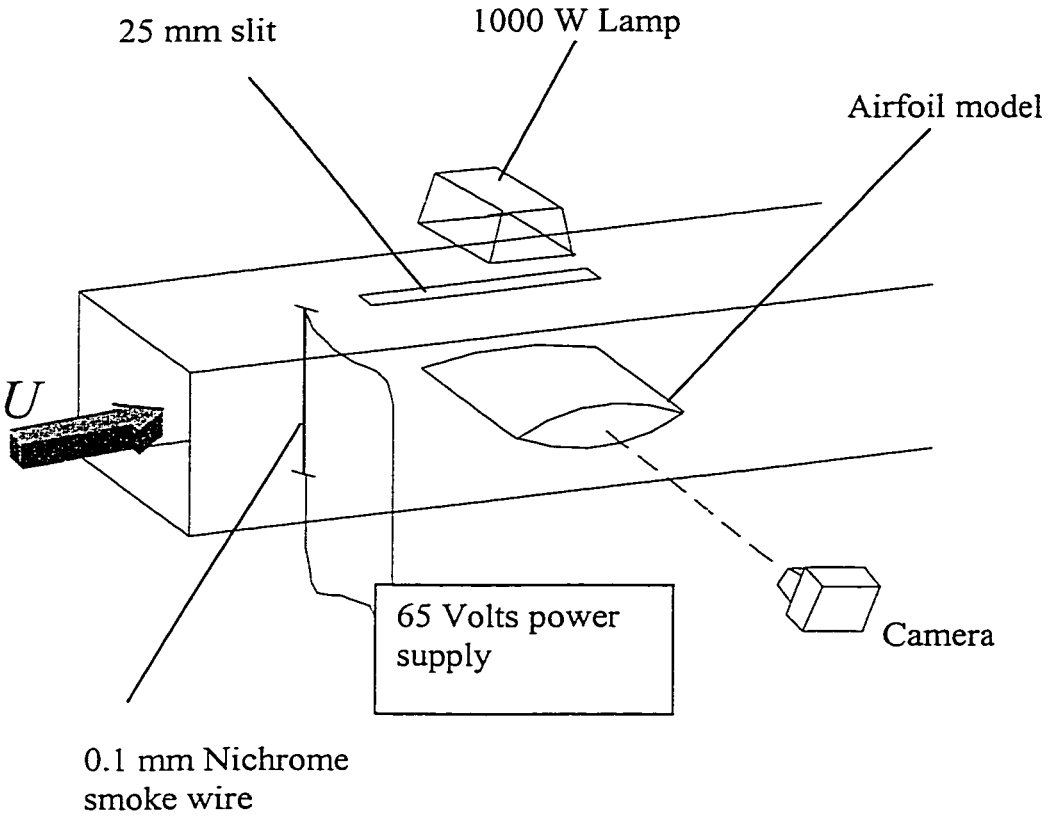

Figure 3.8 Schematic of the flow visualization setup.

CHAPTER 4

RESULTS AND DISCUSSIONS

The NACA 0024 airfoil with leading-edge rotating cylinder was tested at a chord Reynolds number of 6.5×10^4 to obtain pressure distributions on the upper and lower surfaces, lift and drag characteristics of the airfoil, boundary layer measurements and flow pattern around the airfoil. Different angular speeds of 0 to 14,400 rpm corresponding to U_c/U = 0,1,2,3 and 4, were directly imparted to the leading-edge cylinder. The α and δ were varied from 0 to 40° and 0 to 30°, respectively. It should be noted that model produced wind-tunnel blockage of around 15%. The U_c/U is the parameter of prime importance in the present investigation and the case of U_c/U = 0 serves as a reference. The pressure distributions were integrated over the portion, where the pressure measurements were taken, to obtain lift and drag forces acting on the airfoil.

4.1 Flow Visualization Results

Smoke wire technique was used to visualize the flow around the model. The results show the effect of the leading-edge rotating cylinder and trailing-edge flap on the size of the separated region.

4.1.1 Effect of the Leading-Edge Rotating Cylinder

The flow visualization photographs, shown in Figs. 4.1 to 4.6, give an indication of the flow conditions existing on the upper surface of the airfoil at various angles of attack for different cylinder rotations.

I. At $\alpha = 0°$:

The leading-edge rotating cylinder airfoil is shown in Fig. 4.1 at $\alpha = 0°$. In the absence of the cylinder rotation, trailing edge separation is noted at about x/c = 0.9 and the flow is everywhere laminar as shown in Fig. 4.1a. Increasing the cylinder speed to $U_c/U = 1$, shown in Fig. 4.1b, does not have much influence on the boundary layer separation.

II. At $\alpha = 10°$:

Figures 4.2a-b show the airfoil at $\alpha = 10°$ for $U_c/U = 0, 1, 2$. The wake behind the airfoil, shown in Fig. 4.2a, is formed when the laminar boundary layer separates from the surface as a result of adverse pressure gradient downstream the

point of separation. The separation is followed by turbulent boundary layer reattachment at the trailing edge. Since the angle of attack is low, the size of the wake is small. With the cylinder rotating at $U_c/U = 1$, the flow is completely attached to the surface of the airfoil. Again, increasing the speed of the cylinder to $U_c/U = 2$ is seen to have no effect on the flow over the upper surface.

III. At $\alpha = 20°$:

The flow pattern over the airfoil at $\alpha = 20°$ is illustrated in Figs. 4.3a-e. At $U_c/U = 0$, the strong adverse pressure cause the flow over the upper surface of the airfoil to separate. Increasing the cylinder rotation to $U_c/U = 1$ delays the separation but does not bring back complete re-attachment of the flow. As the cylinder rotates at $U_c/U = 2$, the size of the wake behind the airfoil diminishes until the flow becomes completely attached to the upper surface of the airfoil at $U_c/U =$ 3-4, Fig. 4.3e-f.

IV. At $\alpha = 30°$:

Figures 4.4a-e show the effect of the leading-edge rotating cylinder on the flow around the airfoil at $\alpha = 30°$. In the absence of any rotation, the wake behind the airfoil is very large compared to that at $\alpha = 20°$. There is no much difference between the flow pattern at $U_c/U = 1$ and 2. It is noted that rotating the cylinder at $U_c/U = 3$ does not suppress the separation. However, increasing the speed of the cylinder to higher value of U_c/U such as 4 reduces the size of the wake but

separation is still present at the trailing edge of the airfoil. This is because the adverse pressure gradient at high angle of attack such as 30° is very large.

V. At $\alpha = 40°$:

Similar trends persist at $\alpha = 40°$ as shown in Figs. 4.5a-d. The size of the wake reduces as the cylinder rotation increased. It should be noted that the complete reattachment of the boundary layer was not achieved for $\alpha = 40°$ (Fig. 4.5d). Considering the changes in Figs. 4.1-5 suggests that the required rotations of the leading-edge cylinder $(U_c/U)_R$ to reattach the flow are as shown in table 4.1.

Angle of Attack	$(U_c/U)_R$
10	1
20	3
30	≥ 4
40	> 4

Table 4.1 Velocity ratio, U_c/U required for reattachment of the flow.

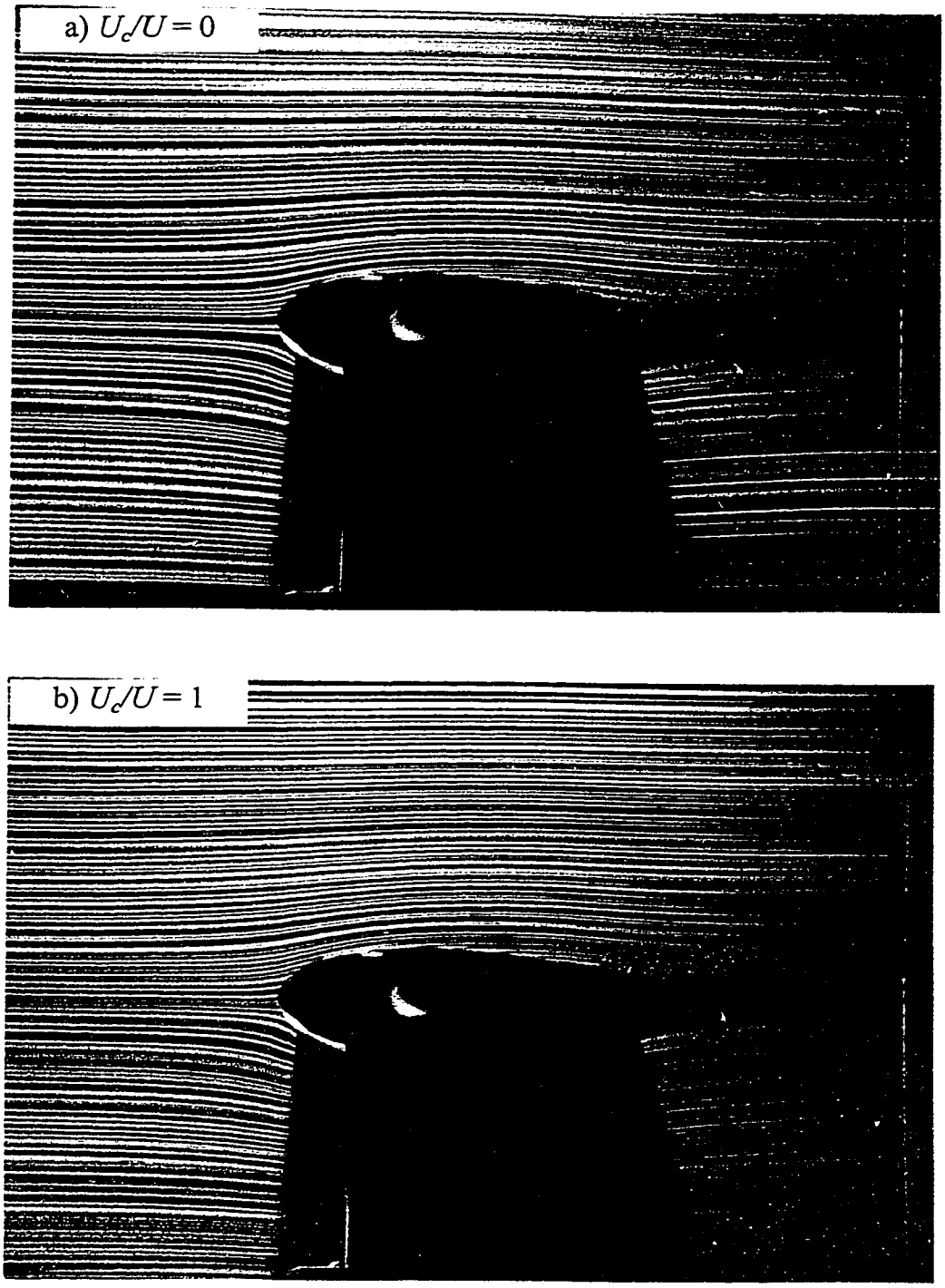

Figure 4.1 Flow visualization photographs at $\alpha = 0°$.

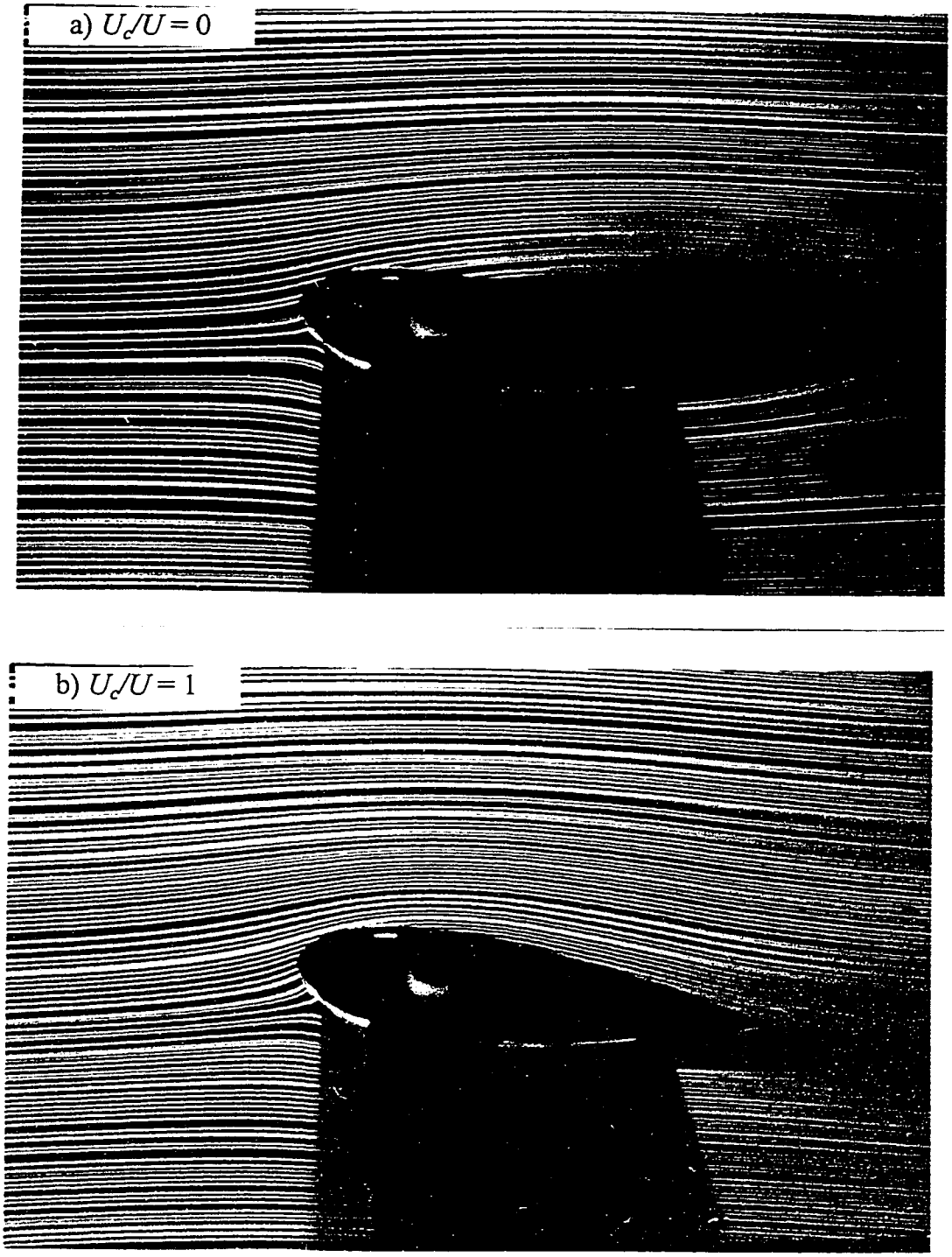

Figure 4.2 Flow visualization photographs at $\alpha = 10°$.

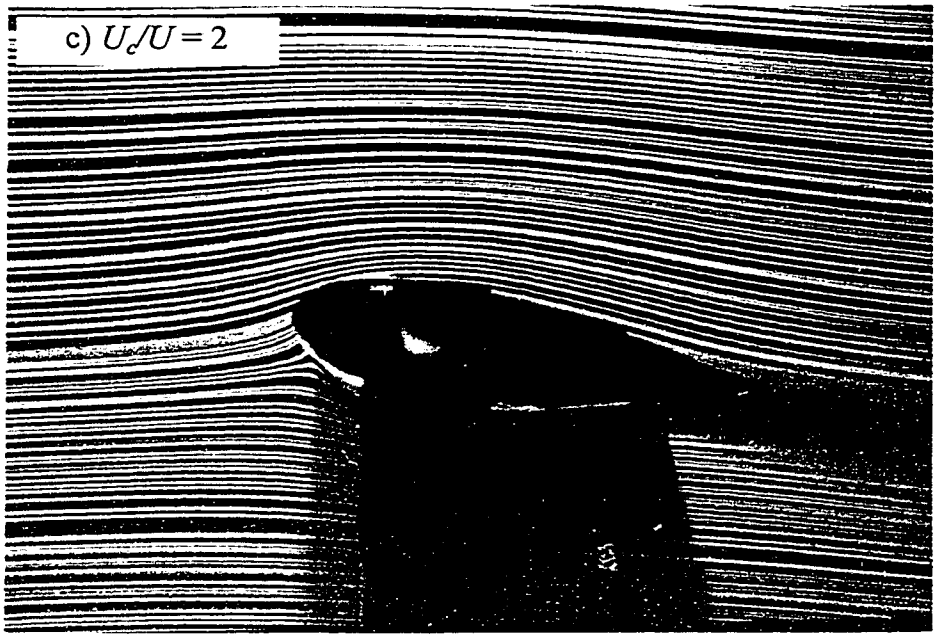

Figure 4.2 Continued.

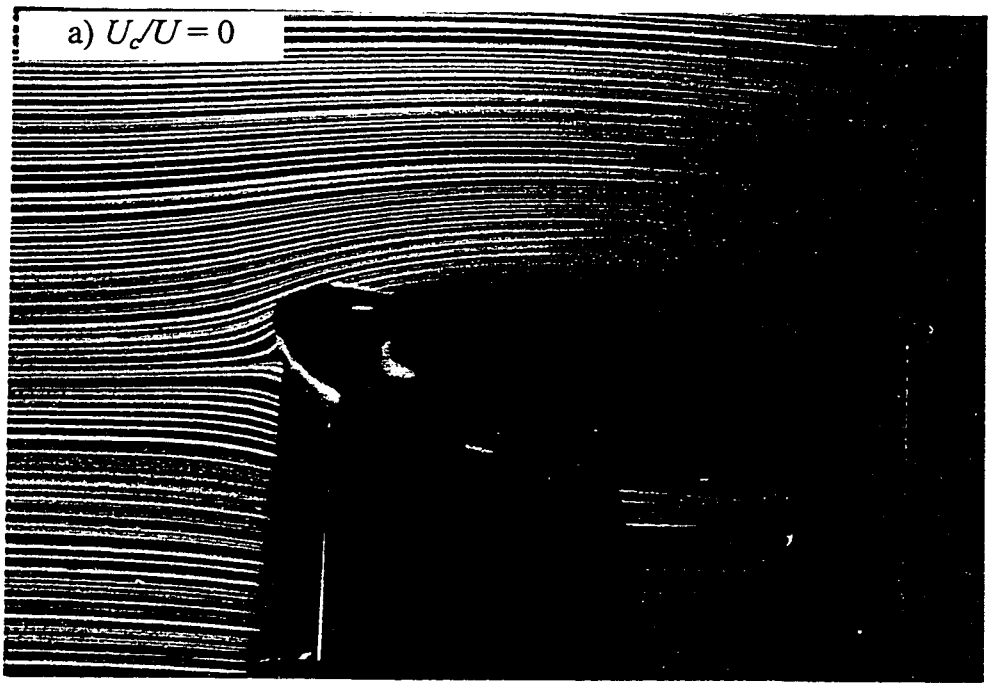

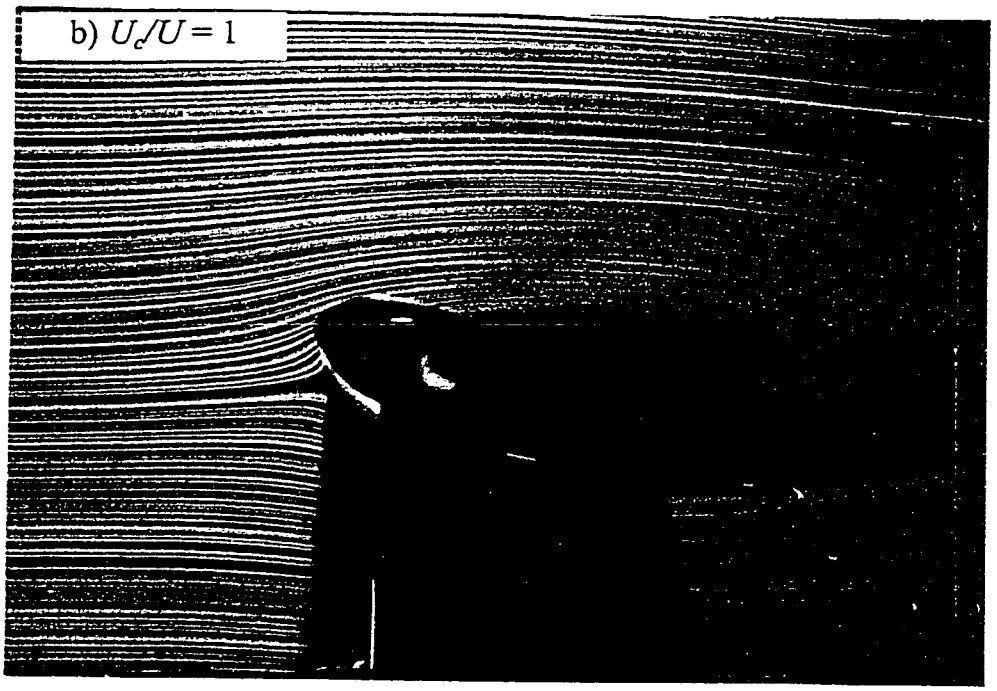

Figure 4.3 Flow visualization photographs at $\alpha = 20°$

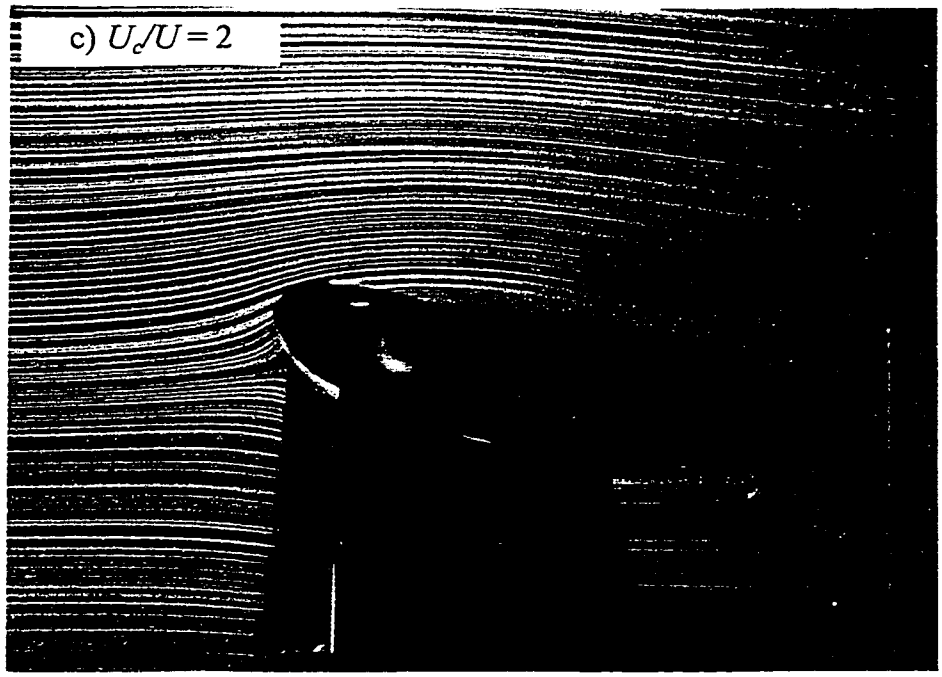

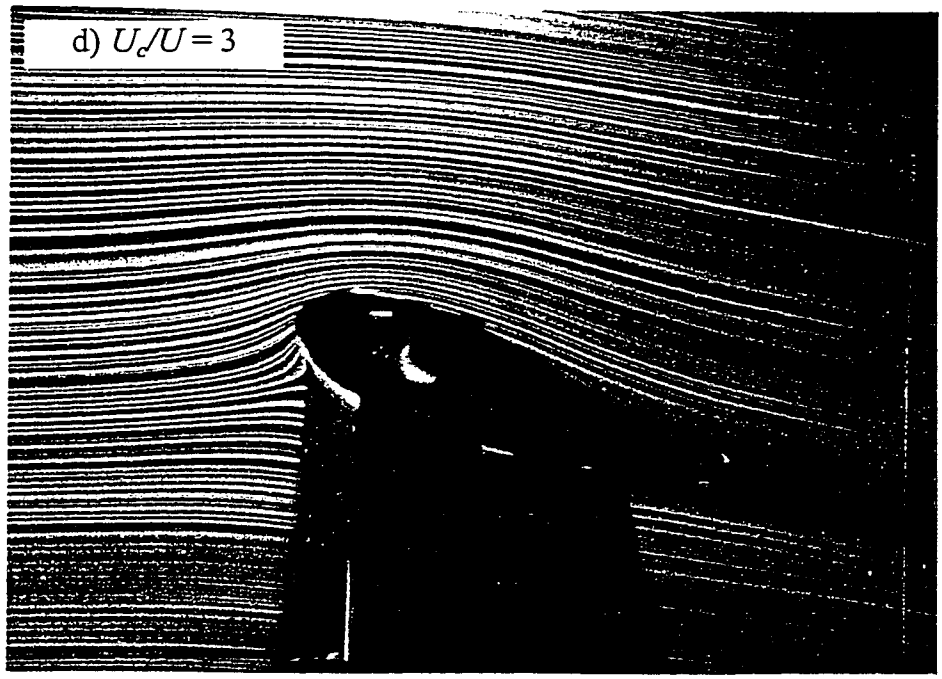

Figure 4.3 Continued

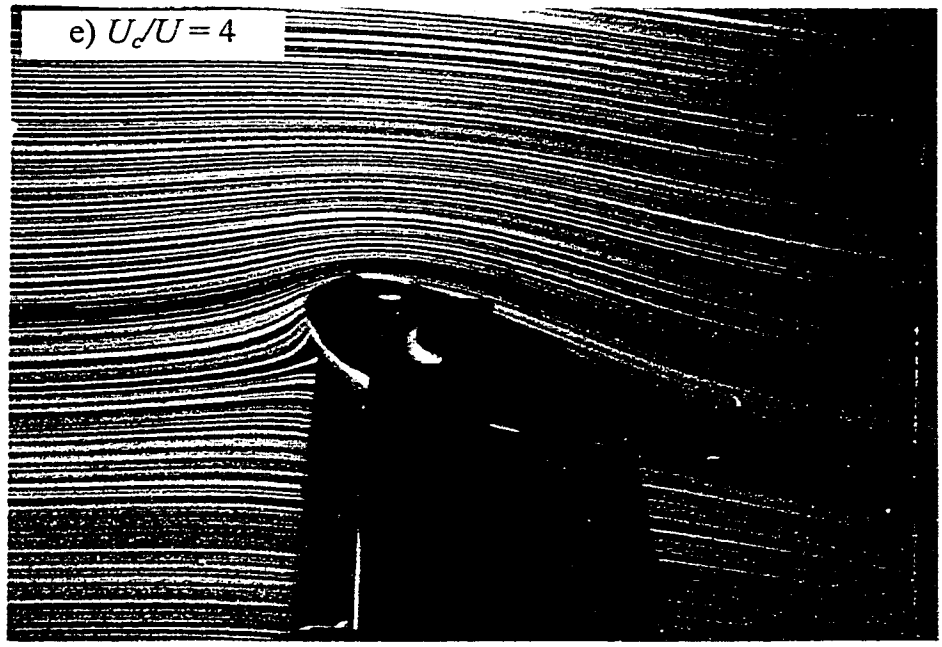

Figure 4.3 Continued.

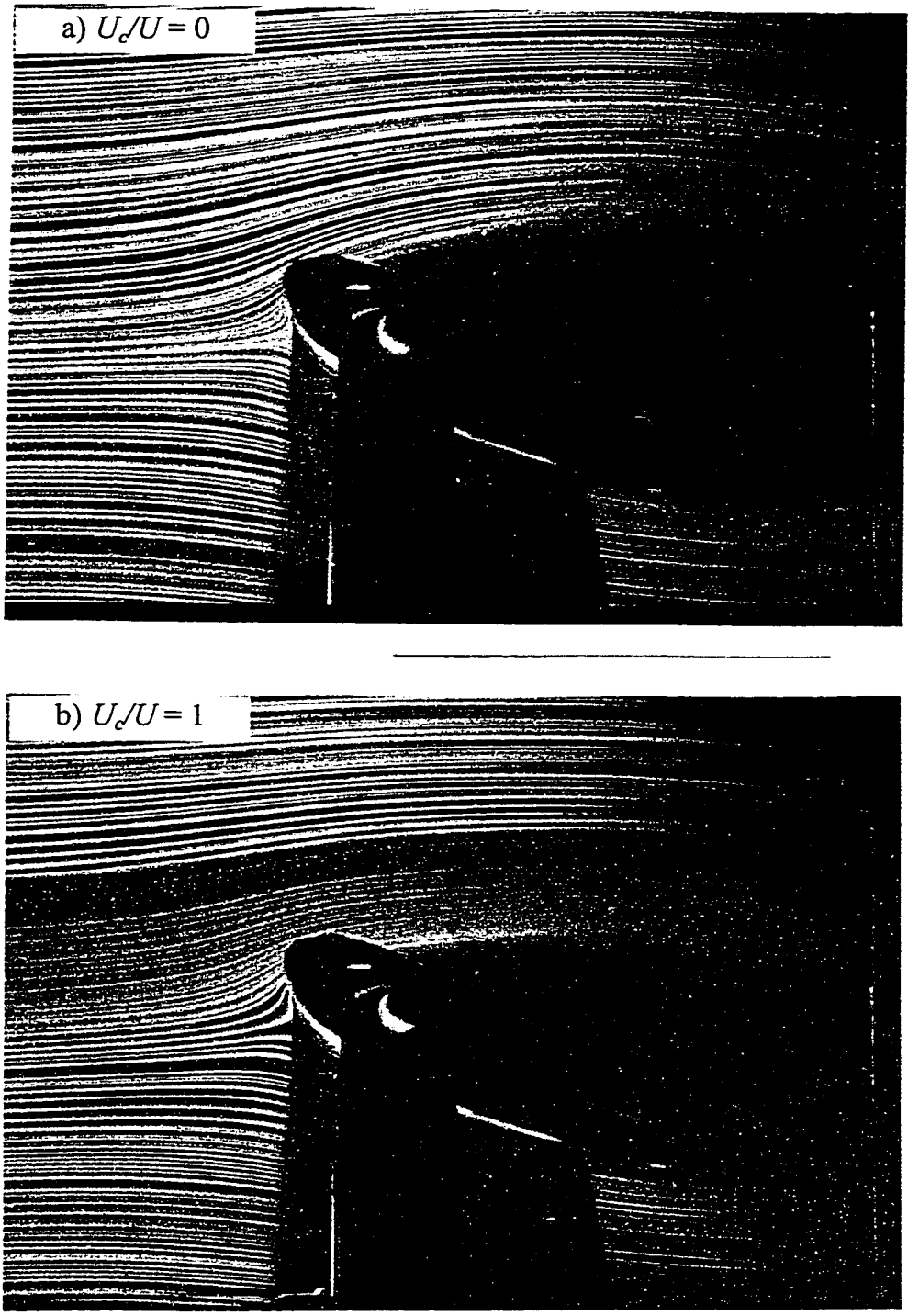

Figure 4.4 Flow visualization photographs at $\alpha = 30°$.

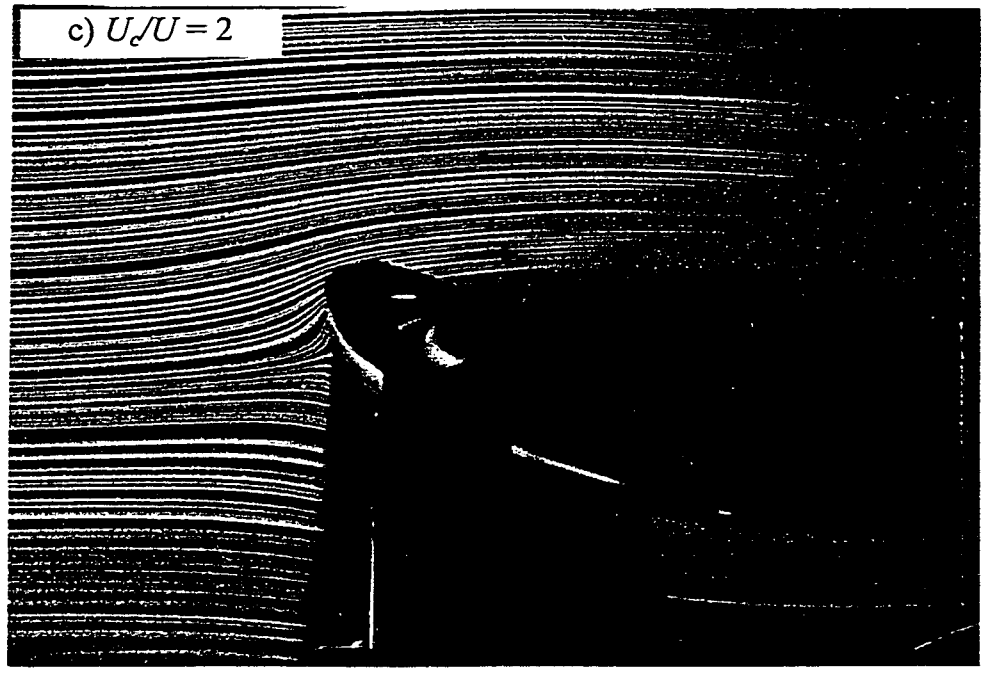

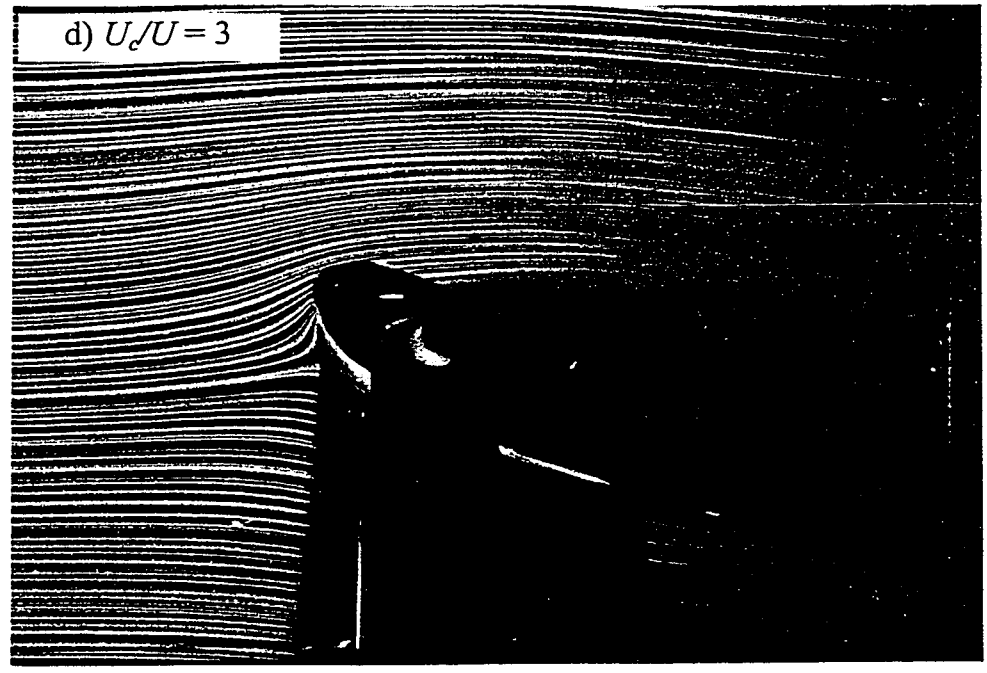

Figure 4.4 Continued.

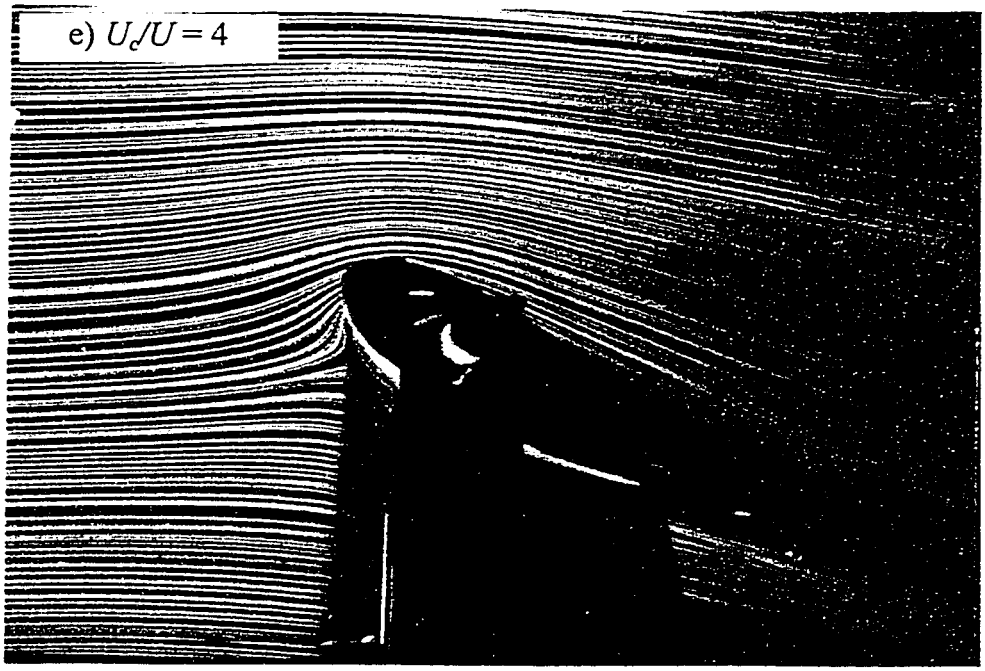

Figure 4.4 Continued.

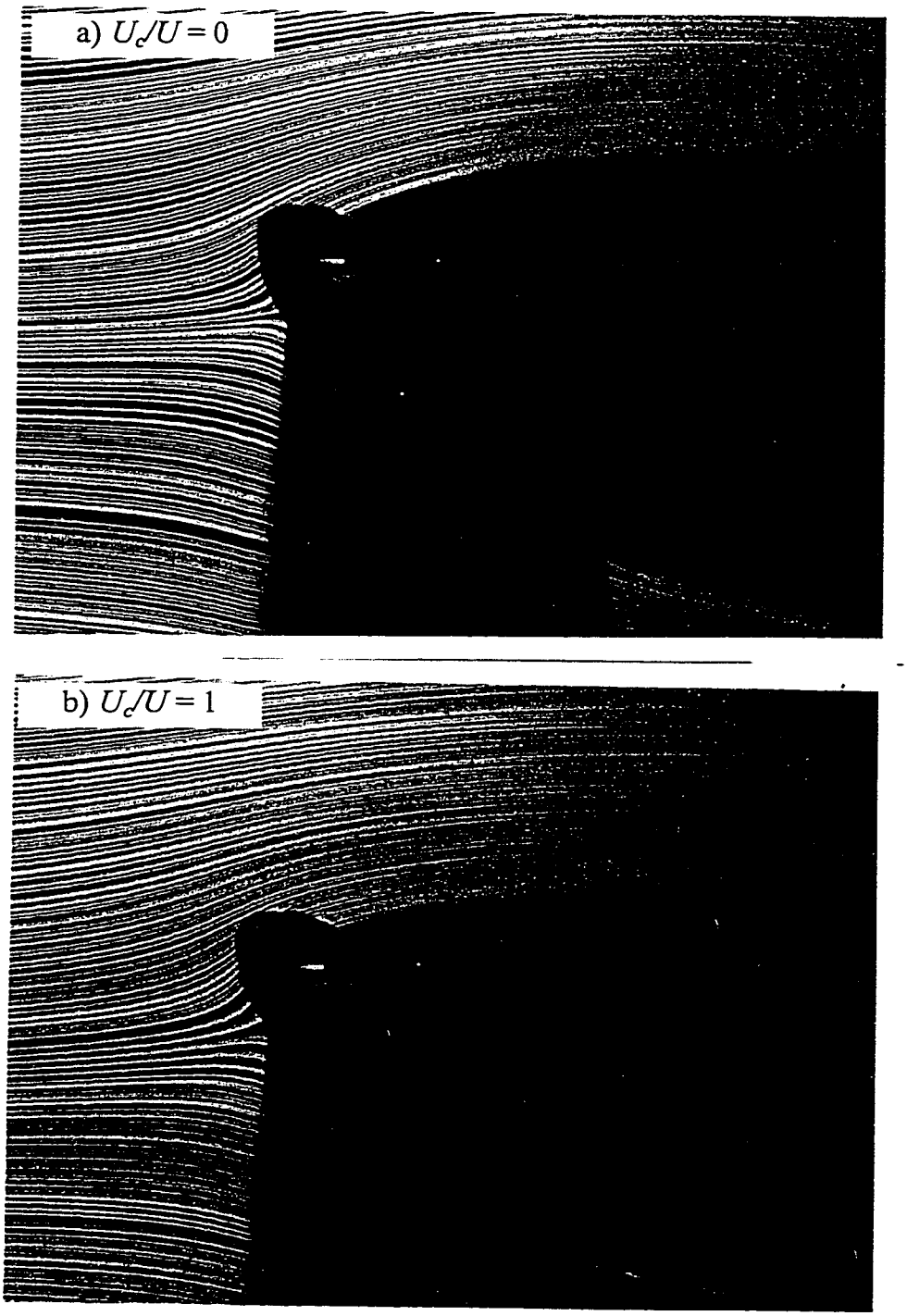

Figure 4.5 Flow visualization photographs at $\alpha = 40°$.

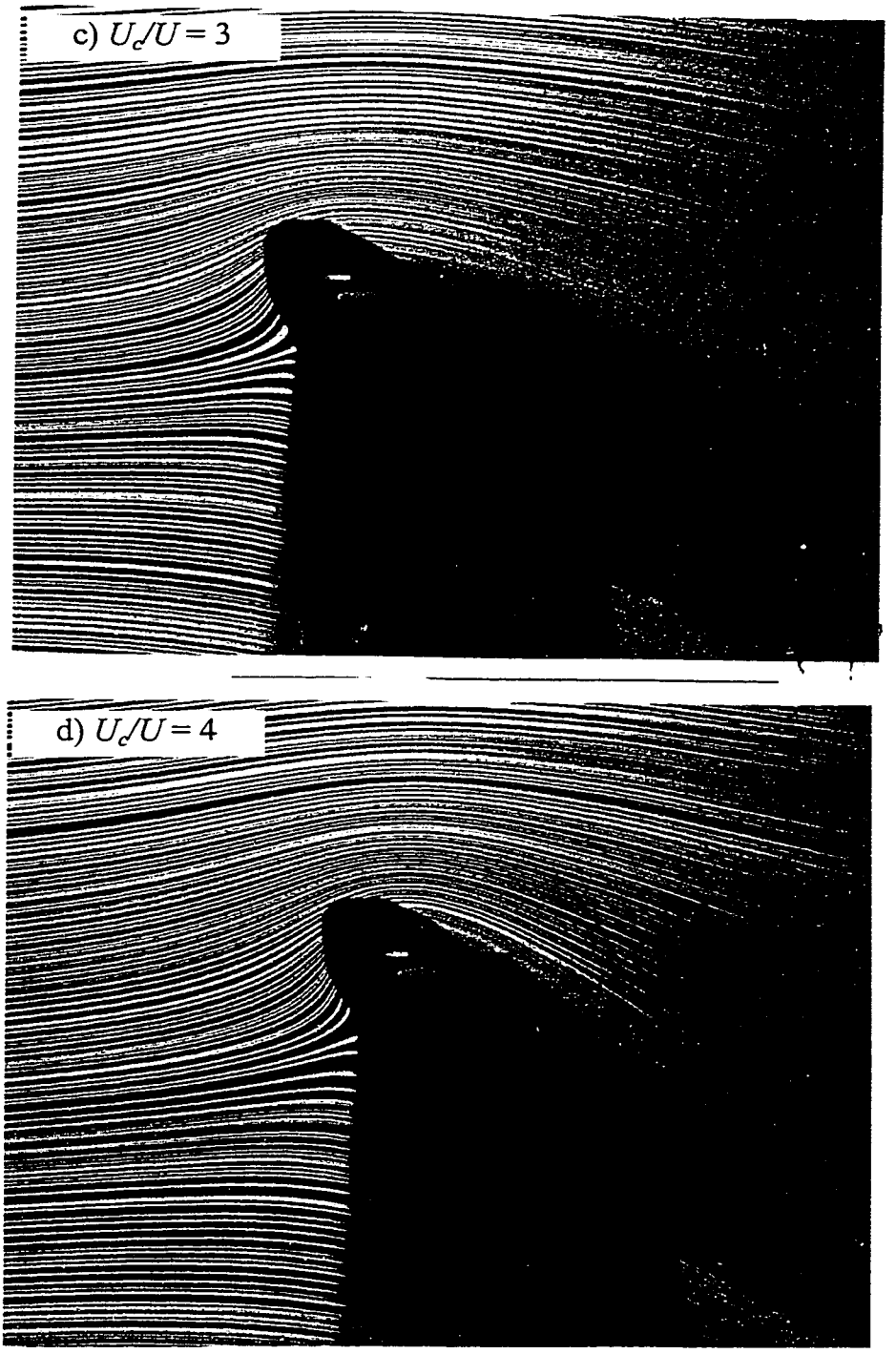

Figure 4.5 Continued.

4.1.2 Effect of Plain Flap

The effect of the flap on the flow pattern over the upper surface of the airfoil is illustrated in Fig. 4.6. The rotation of the cylinder was kept constant at $U_c/U = 4$ and δ was changed. It is noted that deflection of the flap moves the separation point toward the leading edge airfoil. As a result, the size of the wake is increased and hence large drag force will produce. These also verified the pressure measurement and lift and drag characteristics, which is presented in section 4.2 and 4.3. In general, the flap affected the flow over the upper surface of the airfoil adversely.

4.2 Pressure Measurements Results

Figures 4.7 to 4.26 show the effect of the cylinder rotation on the surface pressure distribution on the upper and lower surfaces of the NACA 0024 airfoil at several angles of attack and flap deflection angles. The discontinuity in the pressure distribution is due to the difficulty in locating pressure taps close to and on the surface of the cylinder and in the cusp region. Although, the missing data are important for accurate calculation of the lift and drag coefficients, this does not obscure the effect of the leading-edge rotating cylinder discussed presently. The maximum uncertainty in pressure measurement was about 4%.

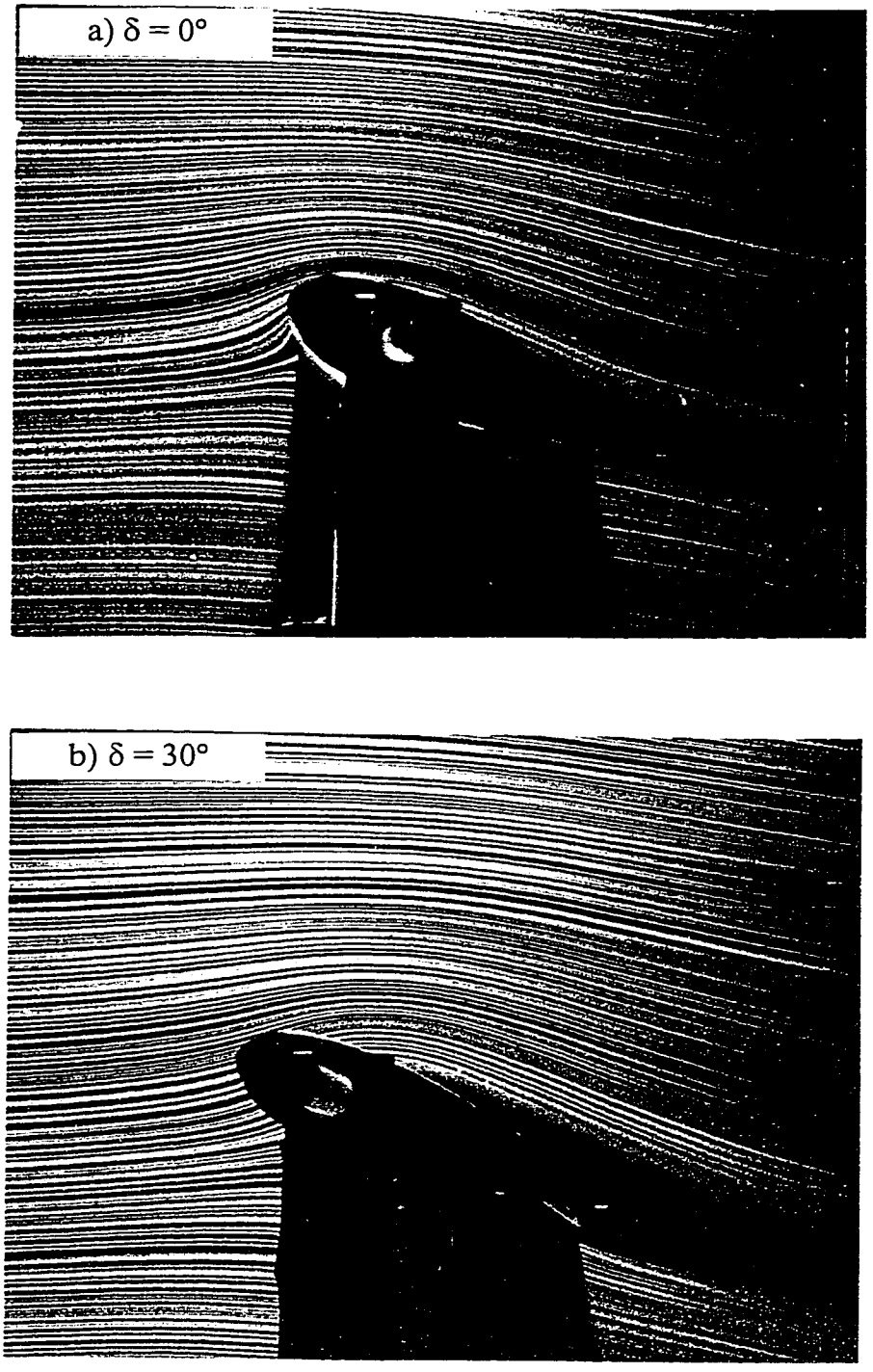

Figure 4.6 Flow visualization photographs for $U_c/U = 4$ and $\alpha = 20°$.

I. At $\alpha = 0°$:

Figure 4.7 shows the airfoil at zero angle of attack and zero flap deflection angle for different U_c/U. In the absence of any rotation and since the airfoil is symmetric, the pressure distributions in the upper and lower surfaces of the airfoil are the same. This means that the lift force is zero as we will see in section 4.3. However, with the increasing of U_c/U, it is noted that the pressure difference between the lower and upper surfaces of the airfoil increases. As a result, there is some finite lift on the airfoil.

The effect of cylinder rotation in the presence of plain flap deflected to 10° is summarized in Fig. 4.8. At $U_c/U = 0$, the effect of the flap on the surface pressure distribution near the leading edge of the upper surface is quite small. However, at the trailing edge, the pressure difference between the lower and upper surfaces is higher. The peak negative pressure for the case of $U_c/U = 4$ and $\delta = 0°$ is about -1.23 while it is -1.43 for $U_c/U = 4$ and $\delta = 30°$. When the cylinder rotates at higher U_c/U, the difference gets bigger. Therefore, the leading-edge rotating cylinder adds more lift to the lift generated by the flap.

II. At $\alpha = 10°$:

Figures 4.11 to 4.14 present the effect of the cylinder rotation on the pressure distributions at $\alpha = 10°$. Note that in the absence of any rotation the flow over the upper surface separates near the trailing edge. At higher U_c/U, however, the flow is completely attached. Considering the changes in Figs. 4.11 to 4.14

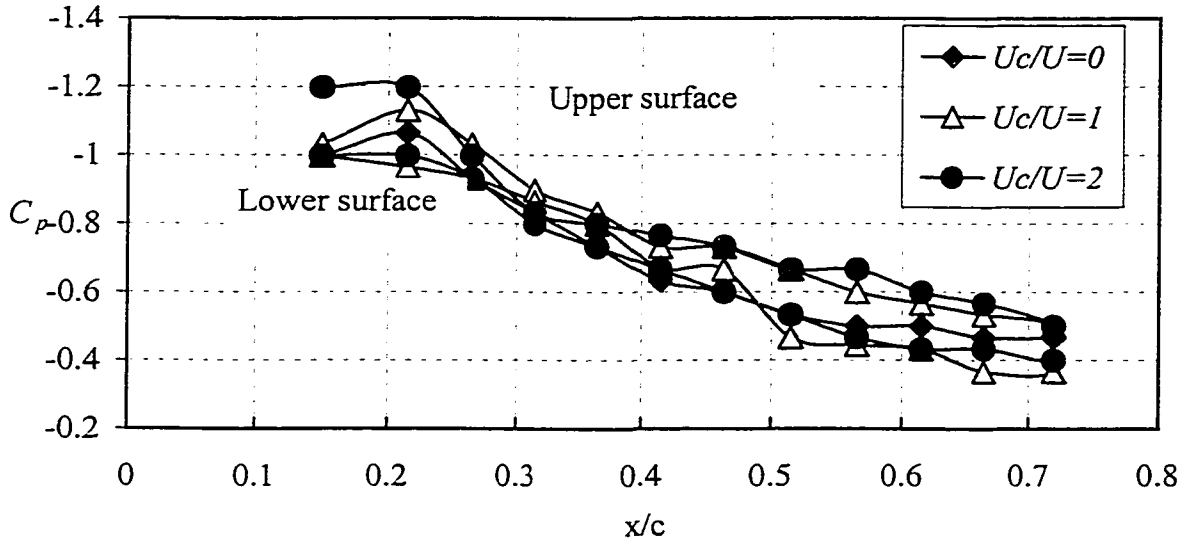

(a)

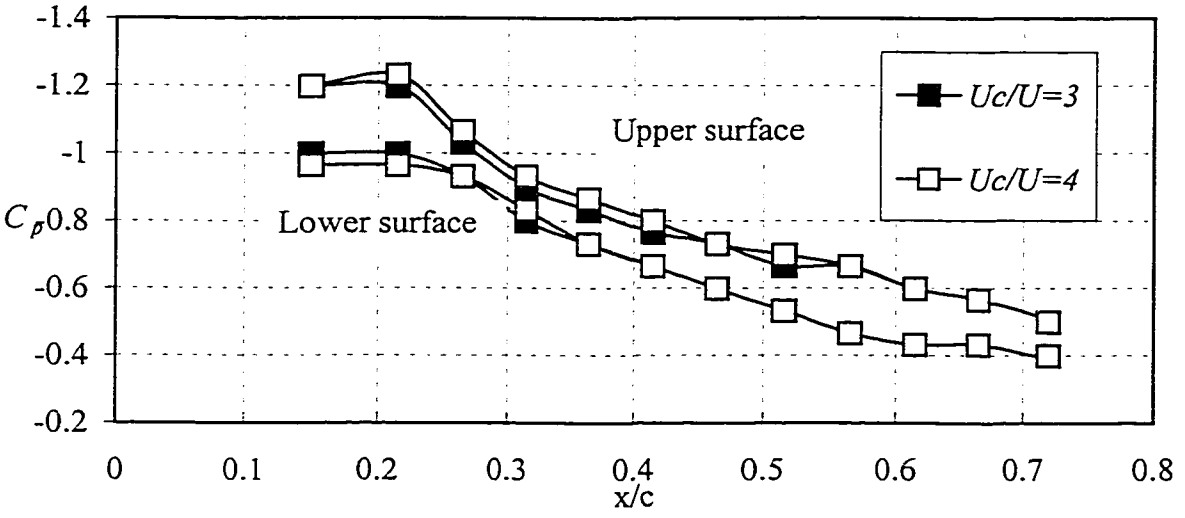

(b)

Figure 4.7 Effect of cylinder rotation on the surface pressure distribution for $\alpha = 0^\circ$ and $\delta = 0^\circ$: (a) low values of *Uc/U* (b) high values of *Uc/U*.

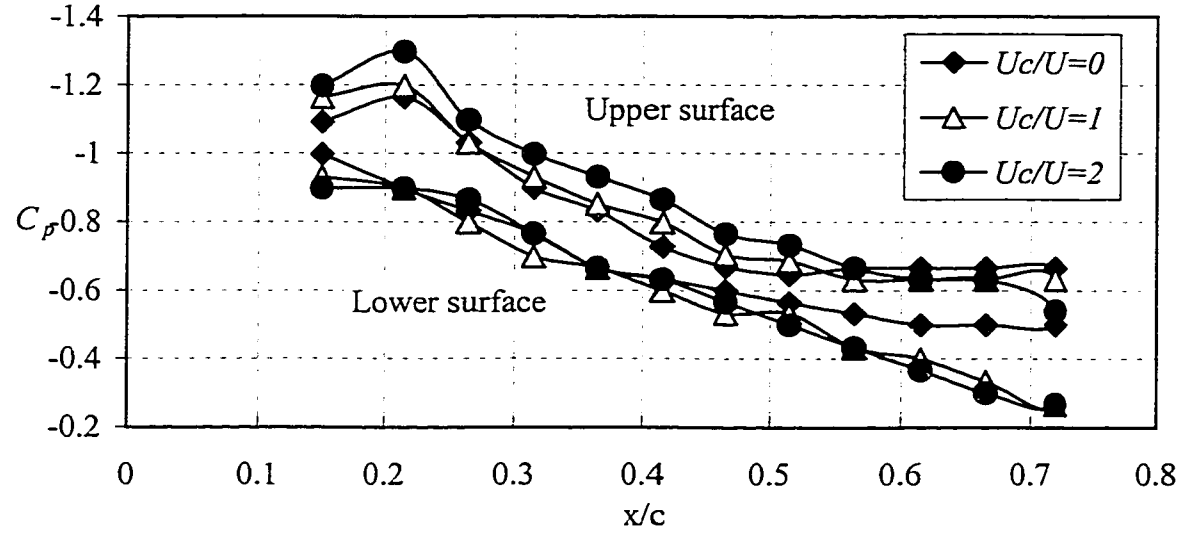

(a)

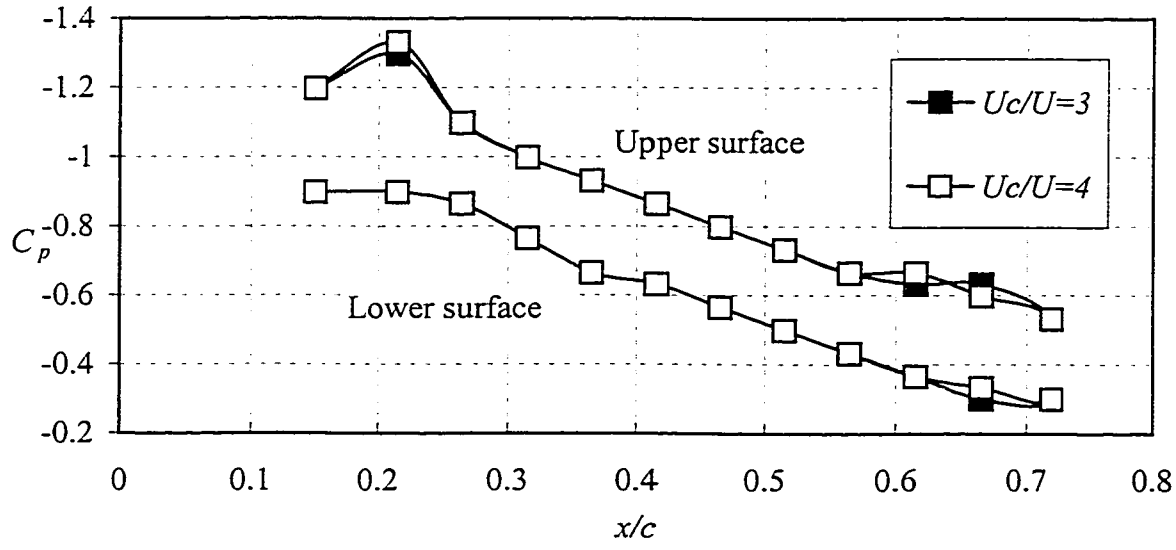

(b)

Figure 4.8 Effect of cylinder rotation on the surface pressure distribution for $\alpha = 0^{o}$ and $\delta = 10^{o}$: (a) low values of *Uc/U* (b) high values of *Uc/U*.

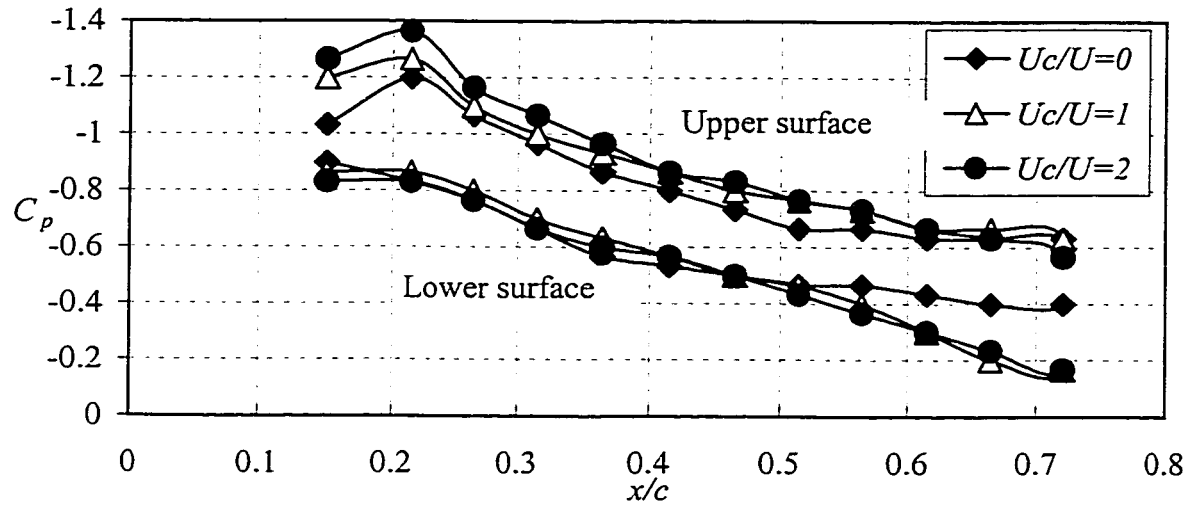

(a)

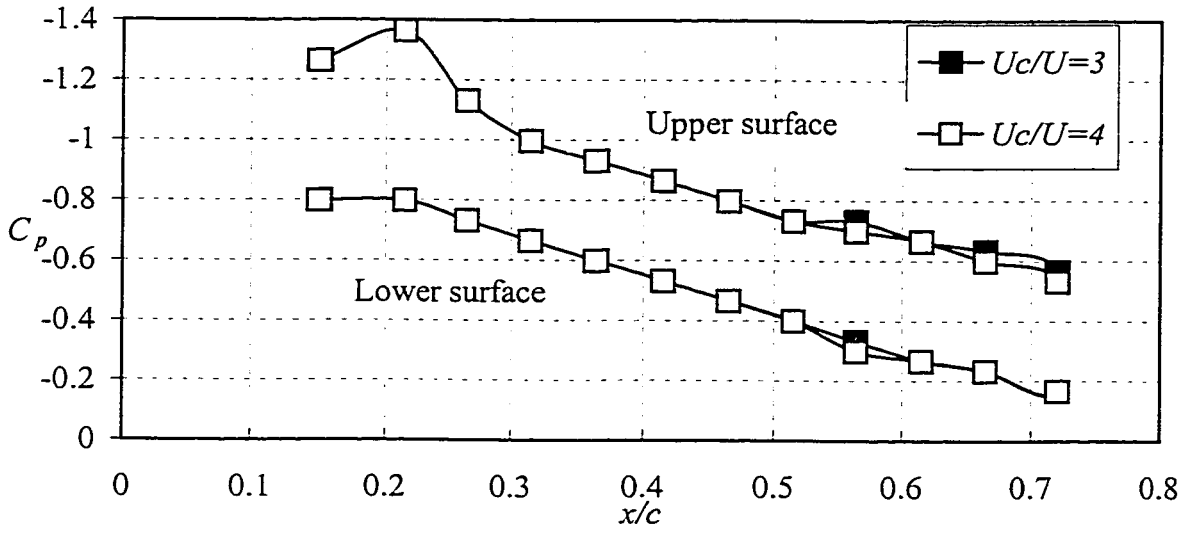

(b)

Figure 4.9 Effect of cylinder rotation on the surface pressure distribution for $\alpha = 0^{\circ}$ and $\delta = 20^{\circ}$: (a) low values of *Uc/U* (b) high values of *Uc/U*.

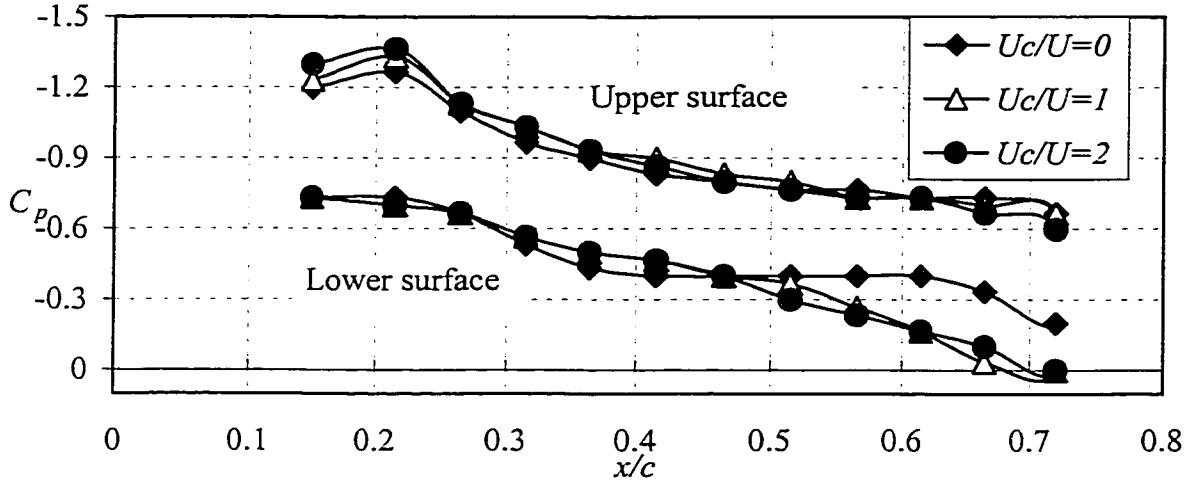

(a)

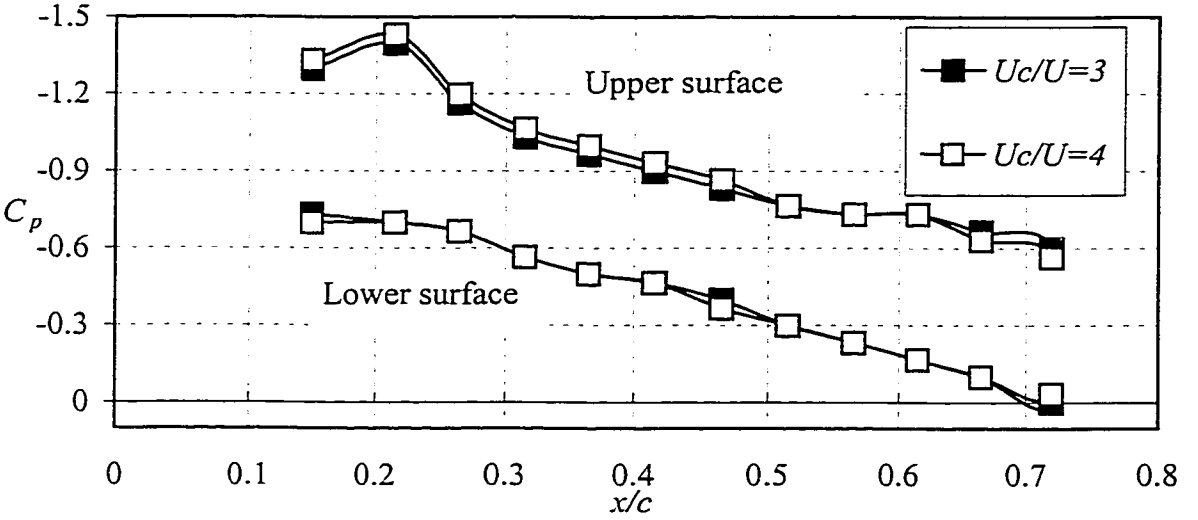

(b)

Figure 4.10 Effect of cylinder rotation on the surface pressure distribution for $\alpha = 0^{\circ}$ and $\delta = 30^{\circ}$: (a) low values of *Uc/U* (b) high values of *Uc/U*.

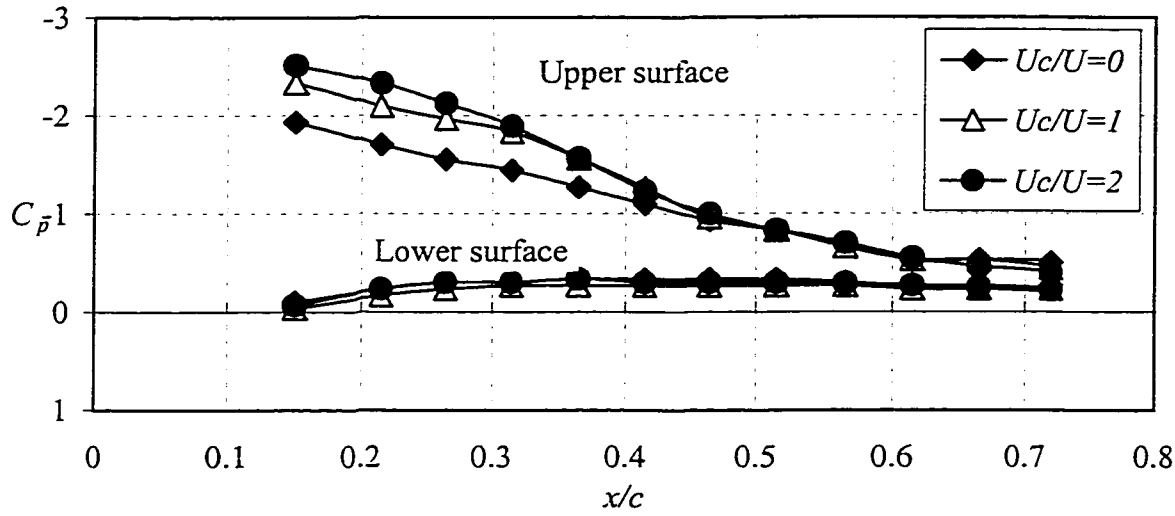

(a)

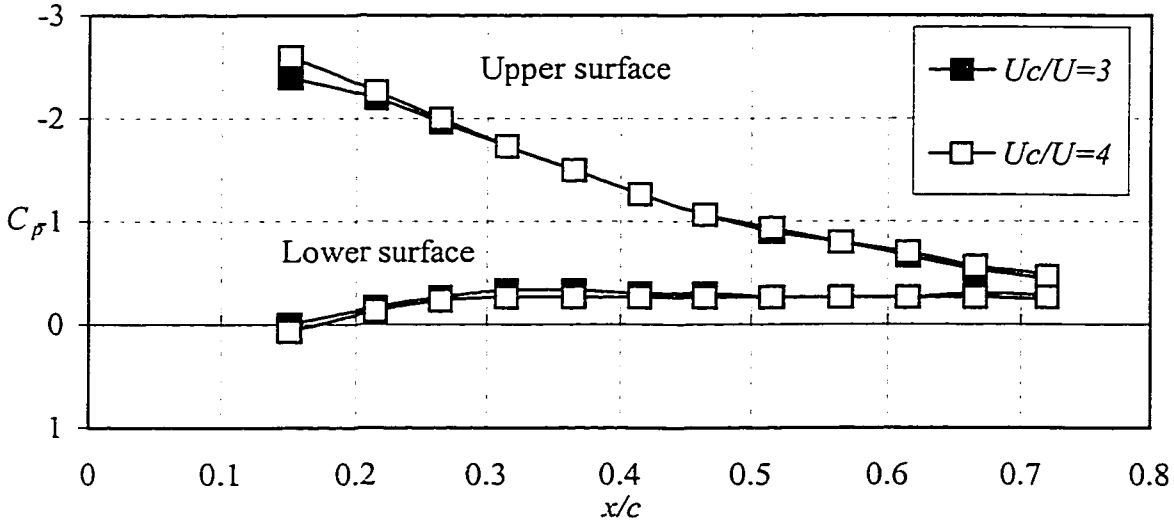

(b)

Figure 4.11 Effect of cylinder rotation on the surface pressure distribution for $\alpha = 10^{\circ}$ and $\delta = 0^{\circ}$: (a) low values of Uc/U (b) high values of Uc/U.

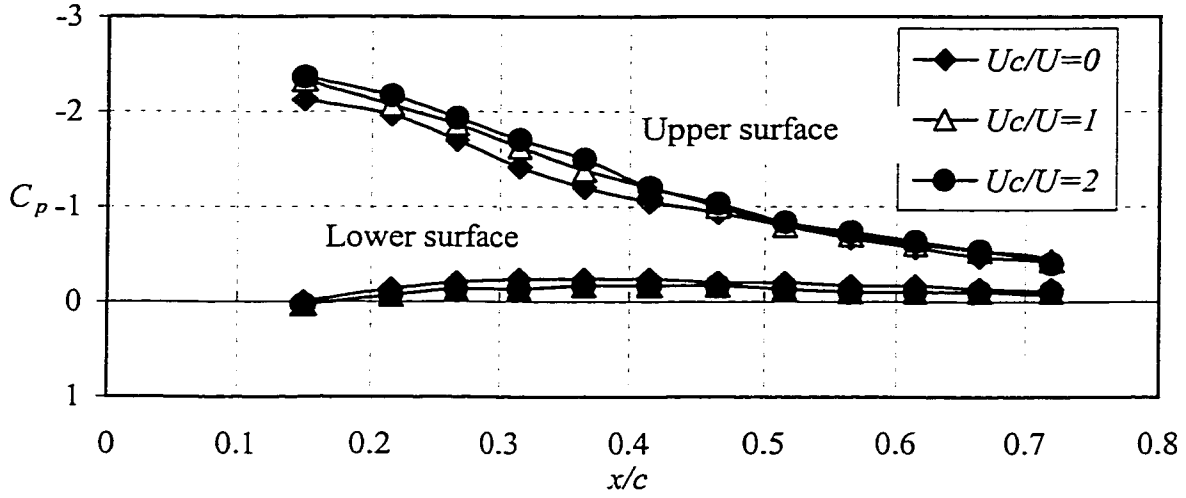

(a)

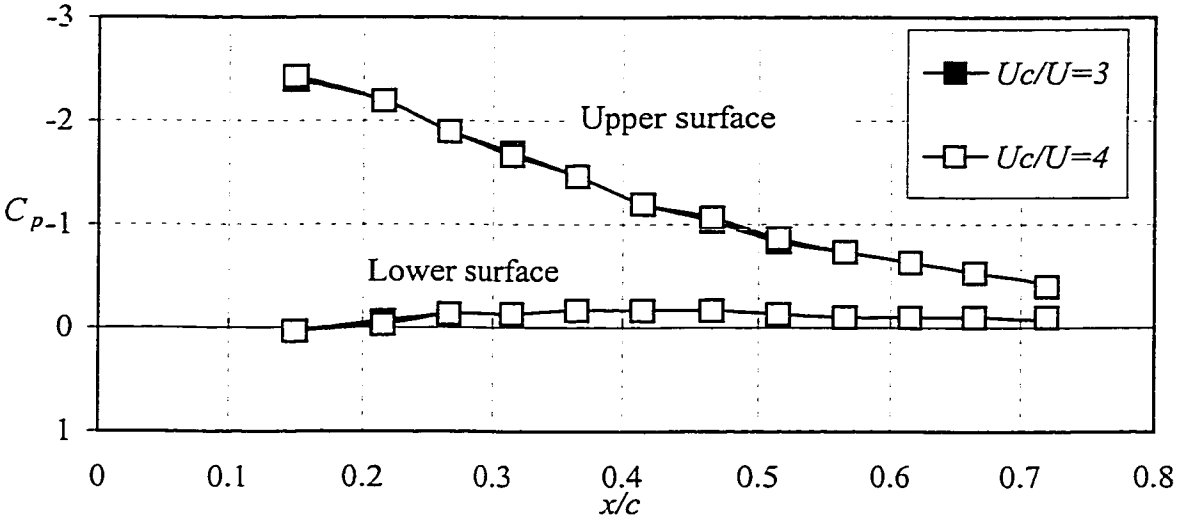

(b)

Figure 4.12 Effect of cylinder rotation on the surface pressure distribution for $\alpha = 10^{\circ}$ and $\delta = 10^{\circ}$: (a) low values of *Uc/U* (b) high values of *Uc/U*.

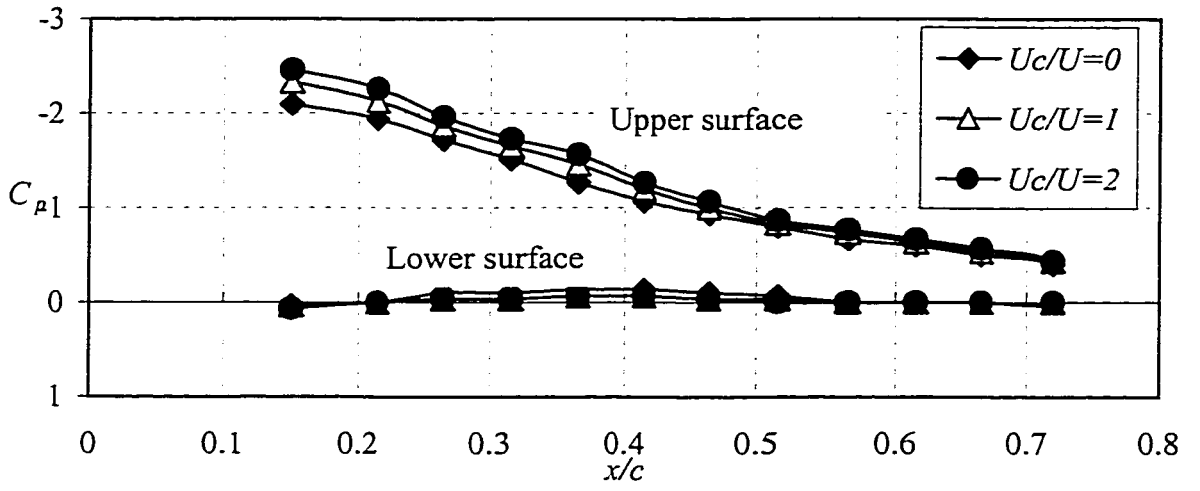

(a)

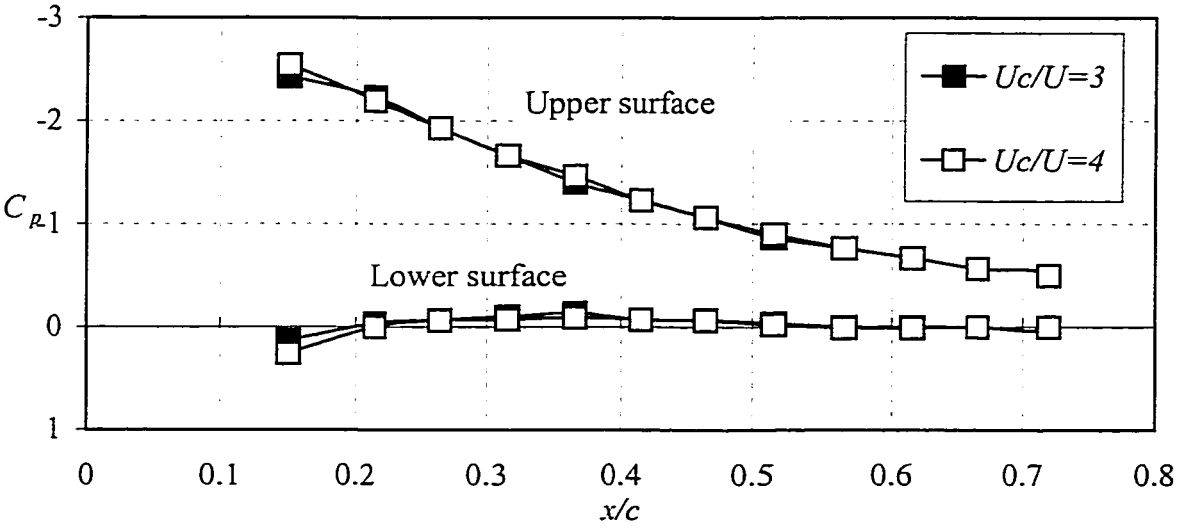

(b)

Figure 4.13 Effect of cylinder rotation on the surface pressure distribution for $\alpha = 10^{\circ}$ and $\delta = 20^{\circ}$: (a) low values of Uc/U (b) high values of Uc/U.

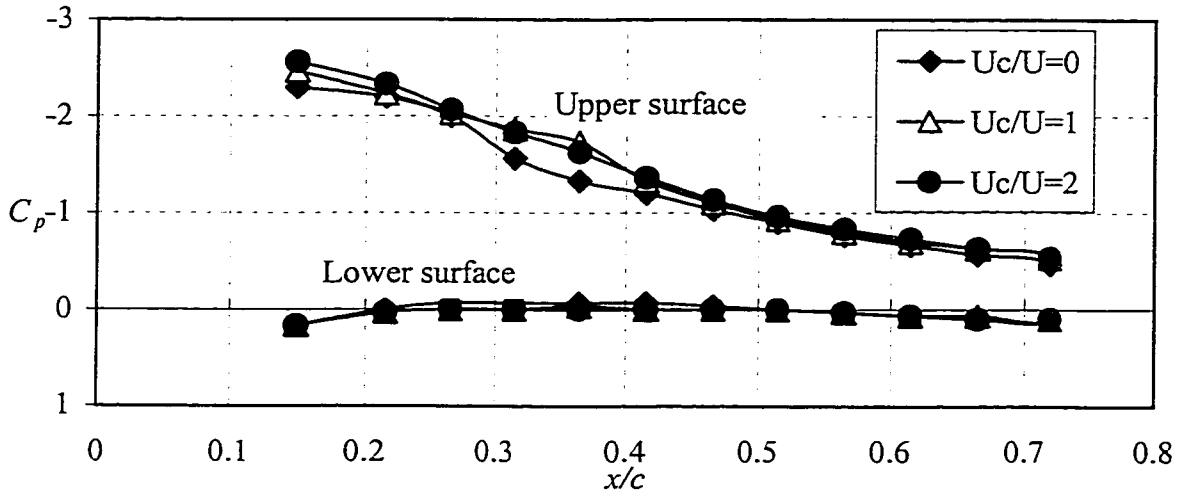

(a)

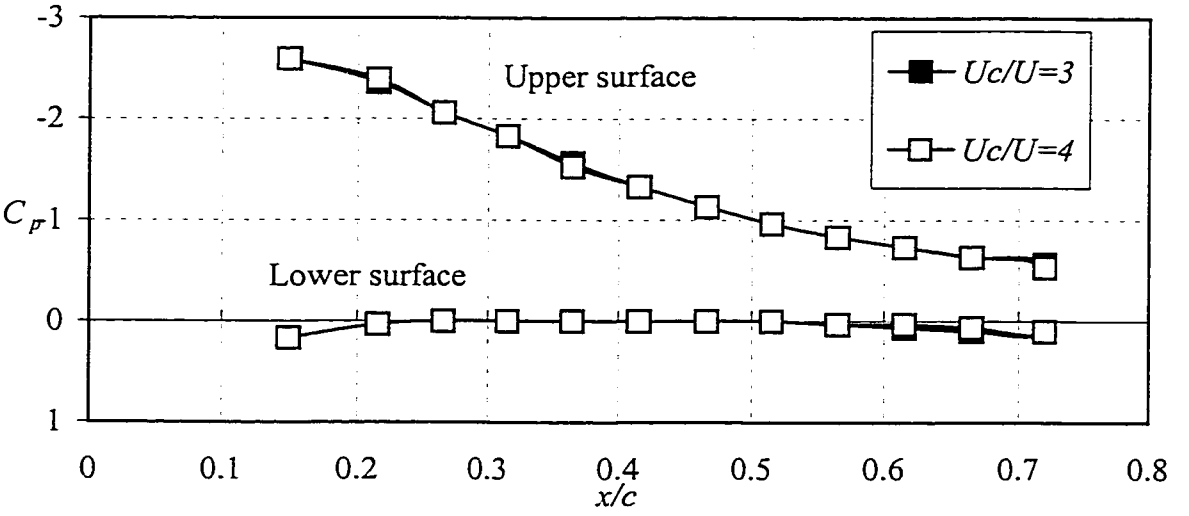

(b)

Figure 4.14 Effect of cylinder rotation on the surface pressure distribution for α = 10°and δ = 30°: (a) low values of *Uc/U* (b) high values of *Uc/U*.

suggests that the pressure difference between the upper and lower surfaces can be increased by using the leading-edge rotating cylinder in conjunction with trailing-edge flap.

At $\delta = 0°$, the peak negative pressure increases from –1.9 at $U_c/U = 0$ to –2.6 at $U_c/U = 4$. At $\delta = 30°$, However, the peak negative pressure increases from –2.3 at $U_c/U = 0$ to –2.6 at $U_c/U = 4$. Clearly the percentage increase due to the rotating cylinder alone is higher than that in the presence of the flap. In general, the leading-edge rotating cylinder increases the peak negative pressure. The effect of the cylinder is felt downstream near the trailing edge. The pressure in the lower surface of the airfoil at $\alpha = 10°$ is negative and this is likely due to the effect of the gap between the rotating cylinder and the remaining part of the airfoil. But Since the angle of attack is very low and the flow is almost attached, the effect of U_c/U is seen to be very small.

III. At $\alpha = 20°$:

The surface pressure distributions at $\alpha = 20°$ are presented in Figs. 4.15 to 4.18. When the cylinder is stationary, the flow over the upper surface is under separation. However, as the cylinder rotation increases from $U_c/U = 0$ to 4, reattachment of the flow over the upper surface occurs. In Fig. 4.15, The separation point moves from about $x/c \approx 15\%$ at $U_c/U = 0$ to $x/c \approx 55\%$ at $U_c/U = 1$. As the cylinder rotates at speed of $U_c/U = 2$, the separation point moves to about $x/c \approx 65\%$ and with $U_c/U = 3$ and 4, the separation takes place at the trailing

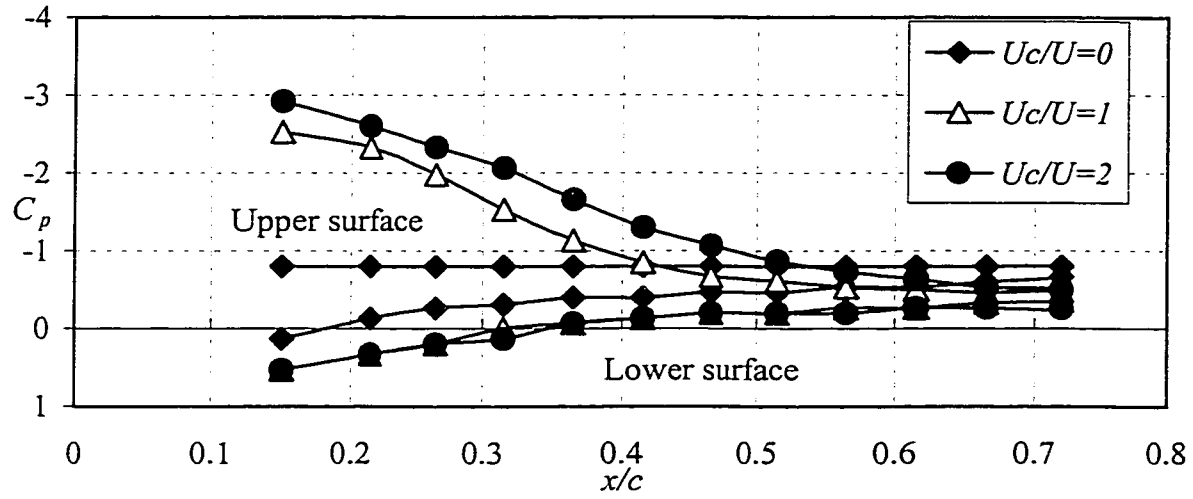

(a)

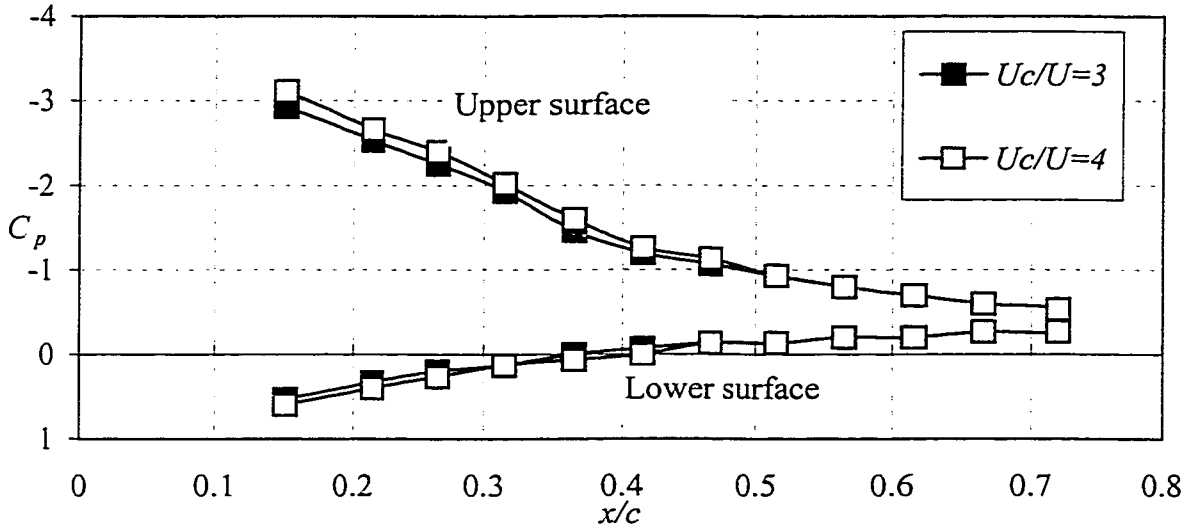

(b)

Figure 4.15 Effect of cylinder rotation on the surface pressure distribution for $\alpha = 20^{\circ}$ and $\delta = 0^{\circ}$: (a) low values of *Uc/U* (b) high values of *Uc/U*.

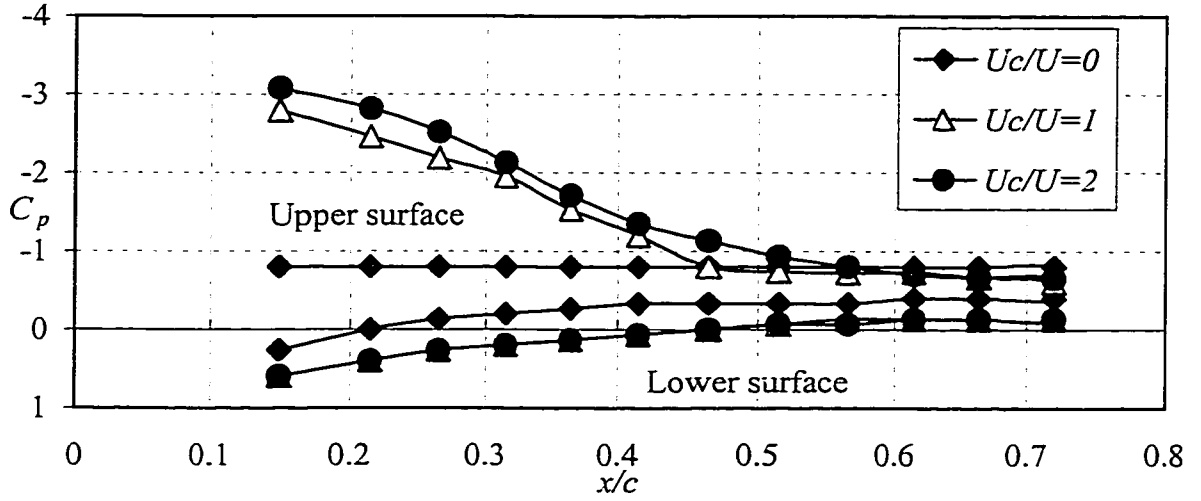

(a)

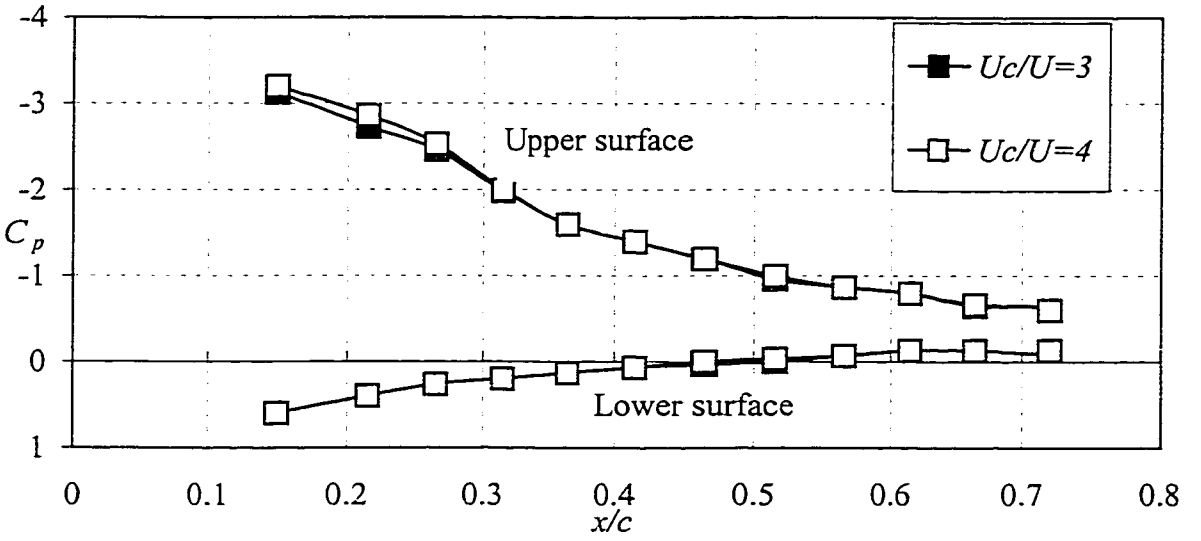

(b)

Figure 4.16 Effect of cylinder rotation on the surface pressure distribution for $\alpha = 20^{\circ}$ and $\delta = 10^{\circ}$: (a) low values of *Uc/U* (b) high values of *Uc/U*.

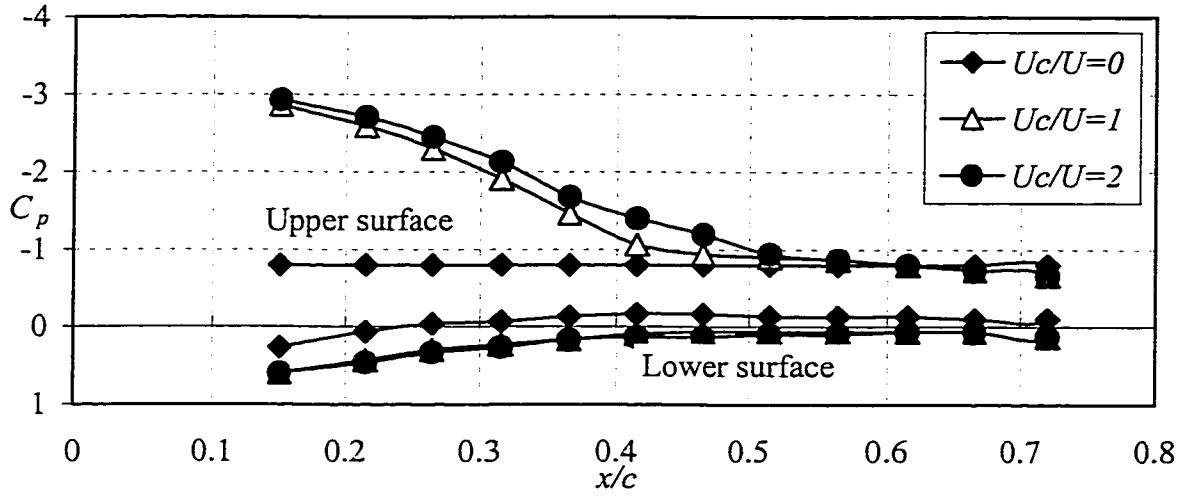

(a)

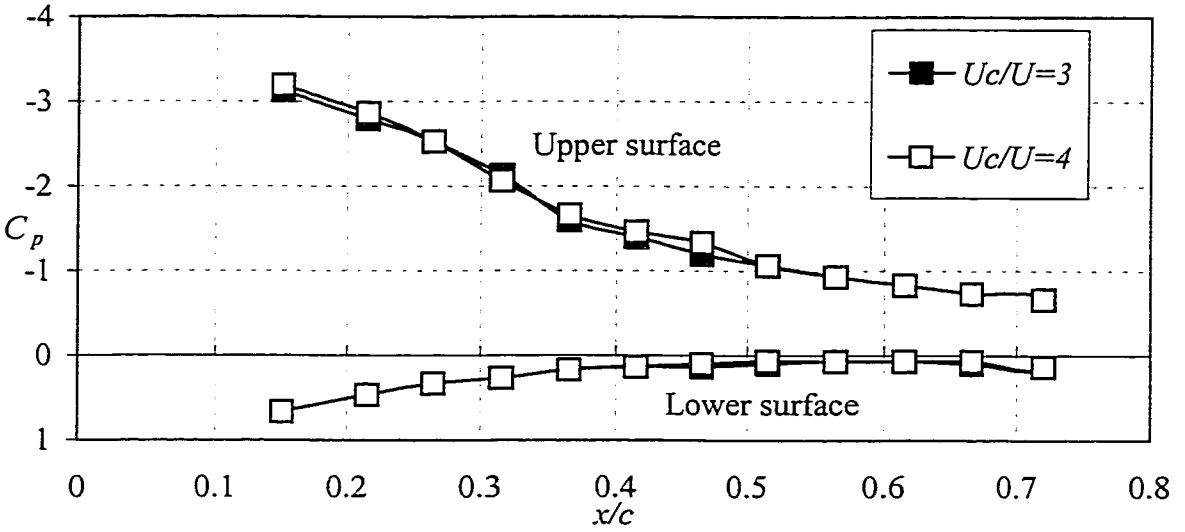

(b)

Figure 4.17 Effect of cylinder rotation on the surface pressure distribution for $\alpha = 20^{\circ}$ and $\delta = 20^{\circ}$: (a) low values of *Uc/U* (b) high values of *Uc/U*.

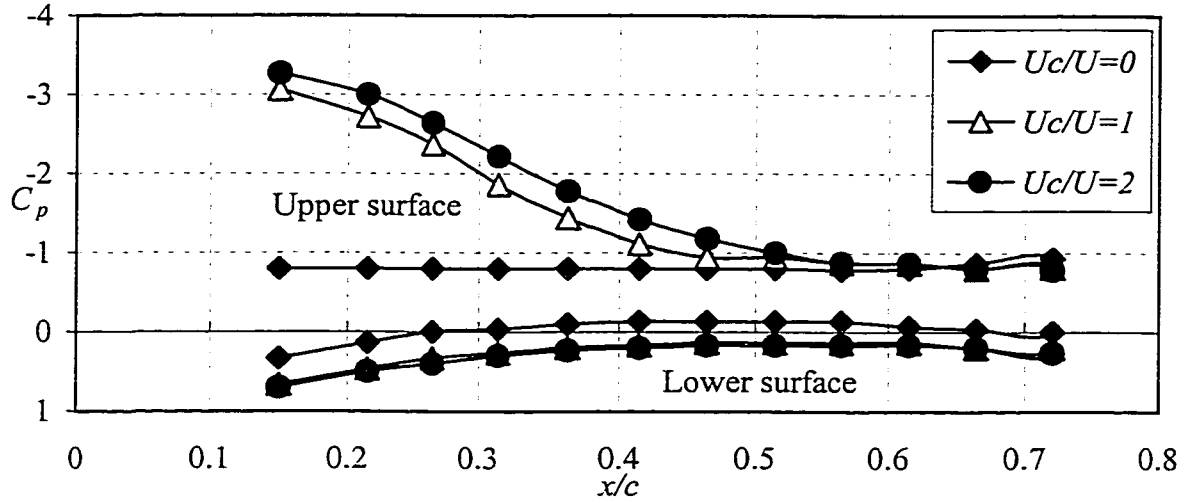

(a)

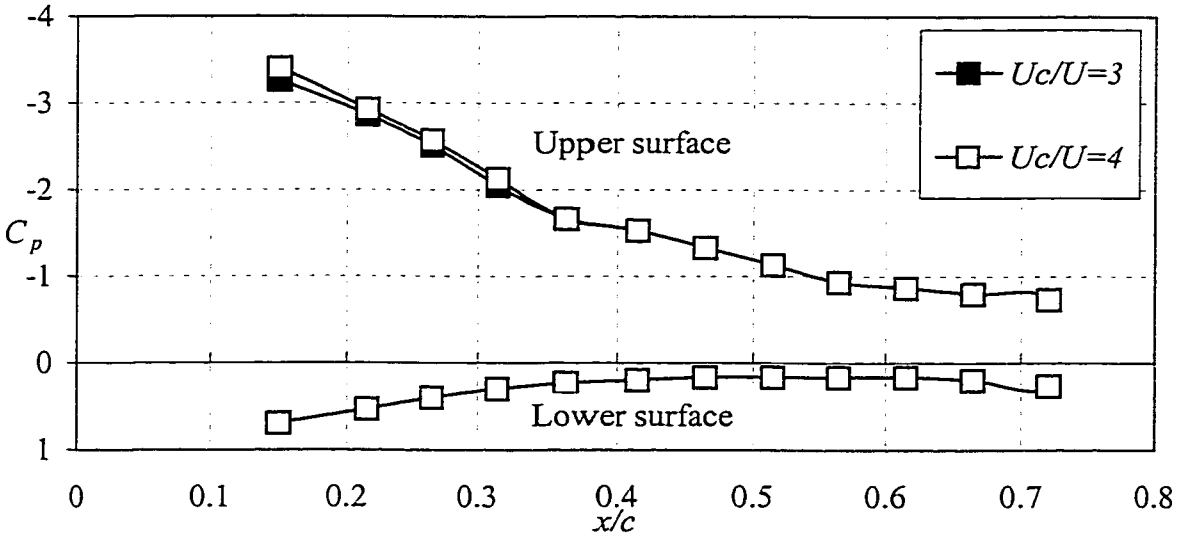

(b)

Figure 4.18 Effect of cylinder rotation on the surface pressure distribution for $\alpha = 20^{\circ}$ and $\delta = 30^{\circ}$: (a) low values of *Uc/U* (b) high values of *Uc/U*.

edge of the airfoil. In Fig. 4.18, the separation takes place at around $x/c \approx 45\%$ for the case of $U_c/U = 1$ and $x/c \approx 55\%$ for the case of $U_c/U = 2$. Deflecting the flap is seen to shift the separation point toward the leading edge. This observation is quite in agreement with the flow visualization picture shown in section 4.1. Again, the leading-edge rotating cylinder was very successful in increasing the negative peak pressure. Moreover, the increase in the negative peak pressure seem to increase in direct proportion to the increase in U_c/U. For example, at $\delta = 0°$ the negative peak pressure has been increased from –0.8 at $U_c/U = 0$ to around –3.1 at $U_c/U = 4$. The effect of the leading-edge rotating cylinder is seen very clearly at this angle of attack. One can see that the difference between the pressure distribution at $U_c/U = 3$ and $U_c/U = 4$ is almost negligible. This leads to a conclusion that at higher U_c/U the effect of the leading-edge rotating cylinder becomes less.

IV. At $\alpha = 30°$:

In Figs. 4.19 to 4.22, the airfoil is placed at, $\alpha = 30°$ and surface pressures were noted. It is apparent that the flow over the upper surface of the airfoil at cylinder rotations of $U_c/U = 0$ and 1 is under separation. This means that higher U_c/U is required to reattach the flow to the surface of the airfoil. Increasing $U_c/U = 2$ delays separation but does not bring complete re-attachment of the flow. Once the cylinder speed is set to $U_c/U = 4$, the separation on the upper surface of the airfoil is being delayed but not prevented. Deflecting the flap increases the

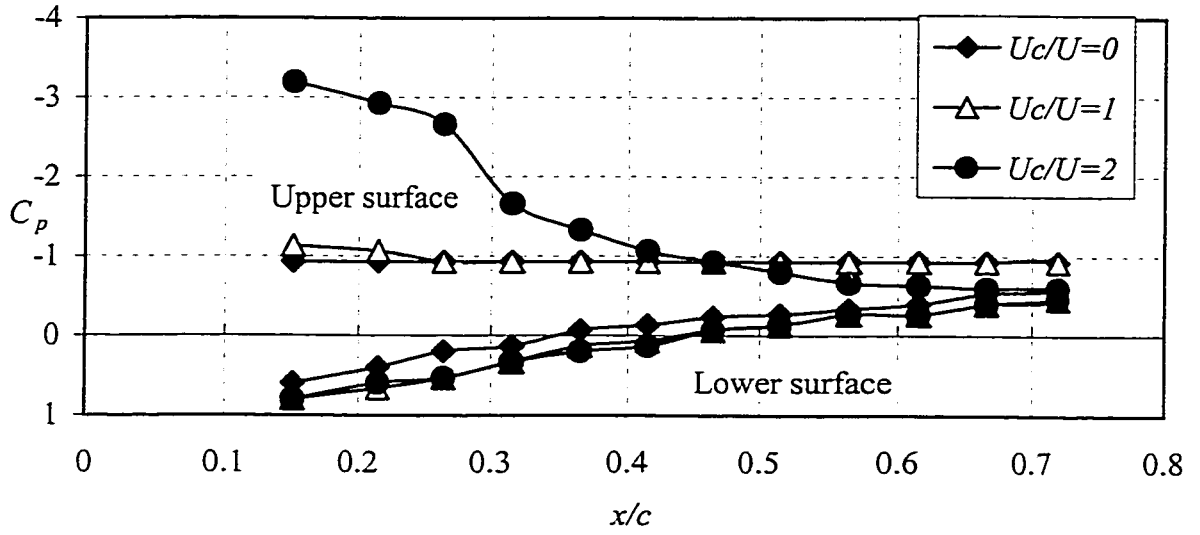

(a)

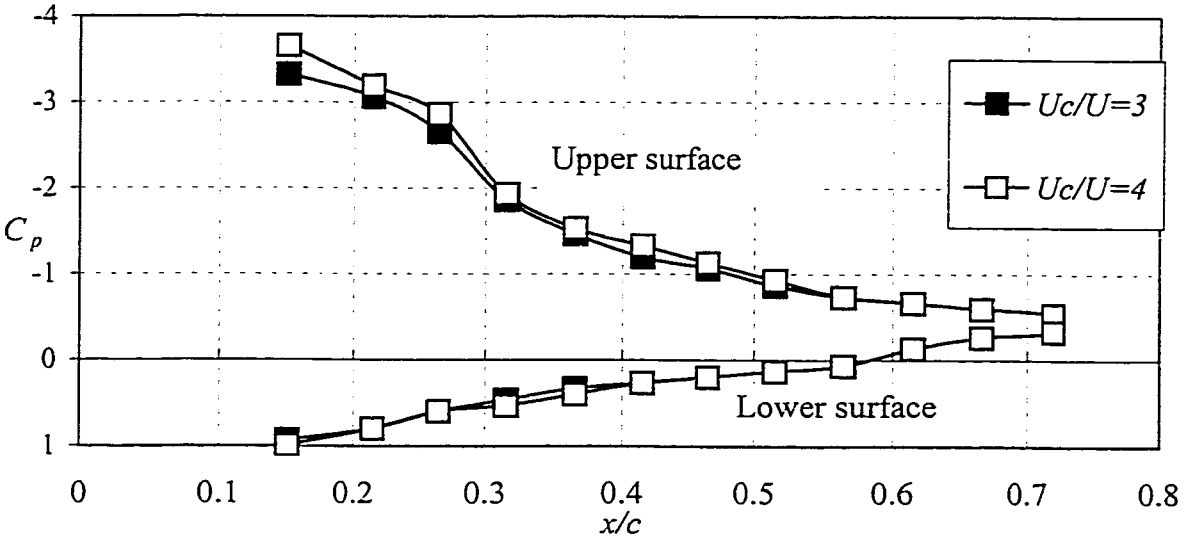

(b)

Figure 4.19 Effect of cylinder rotation on the surface pressure distribution for $\alpha = 30^{\circ}$ and $\delta = 0^{\circ}$: (a) low values of *Uc/U* (b) high values of *Uc/U*.

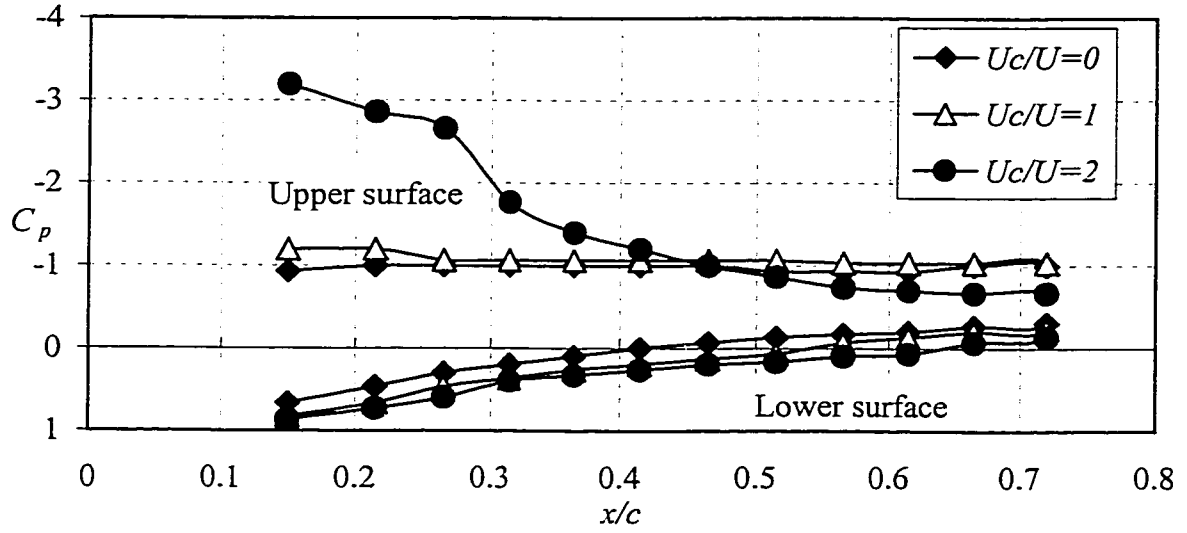

(a)

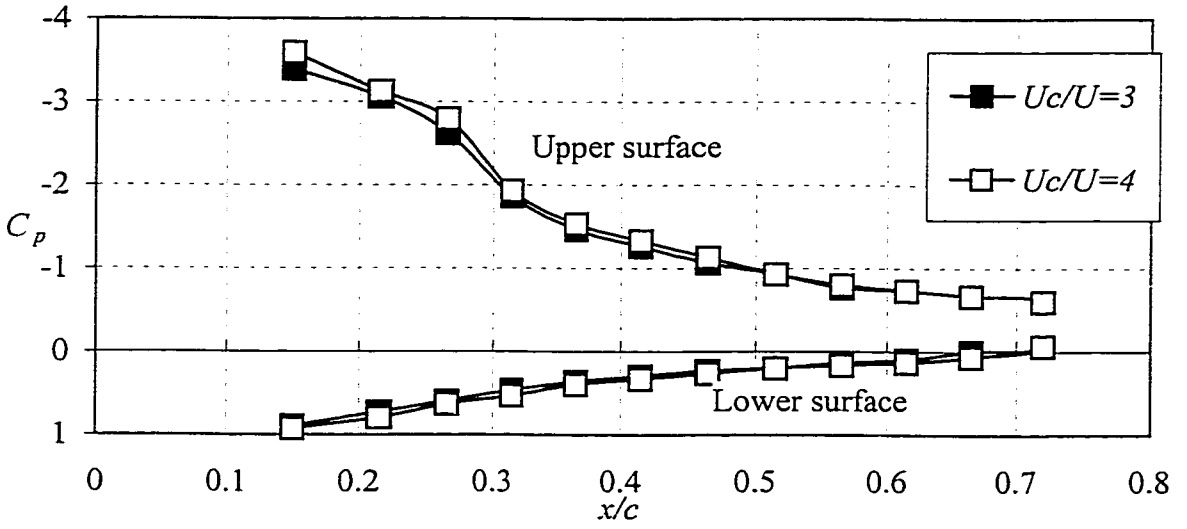

(b)

Figure 4.20 Effect of cylinder rotation on the surface pressure distribution for $\alpha = 30^{\circ}$ and $\delta = 10^{\circ}$: (a) low values of *Uc/U* (b) high values of *Uc/U*.

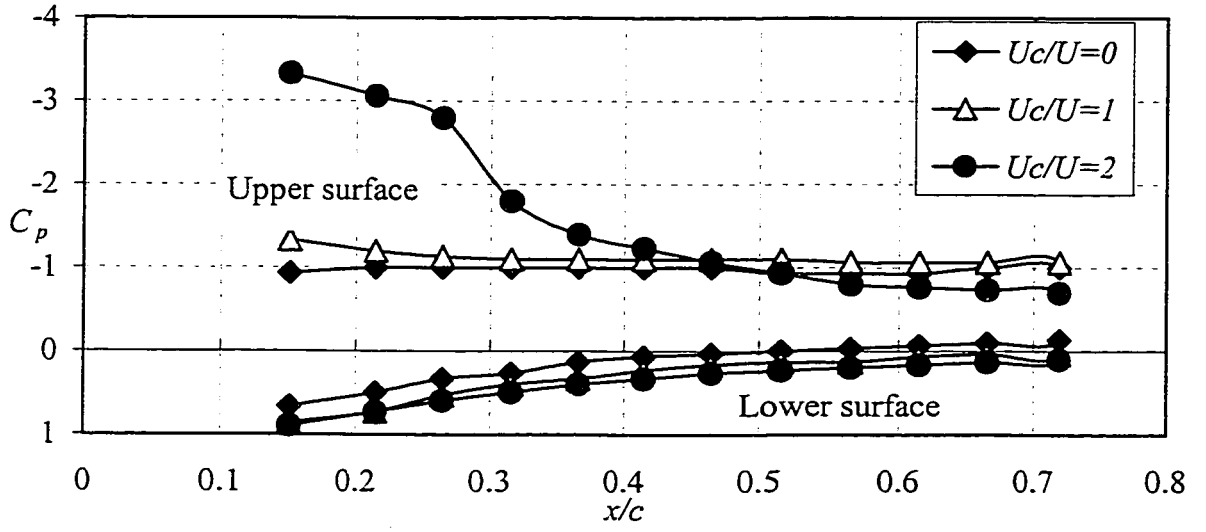

(a)

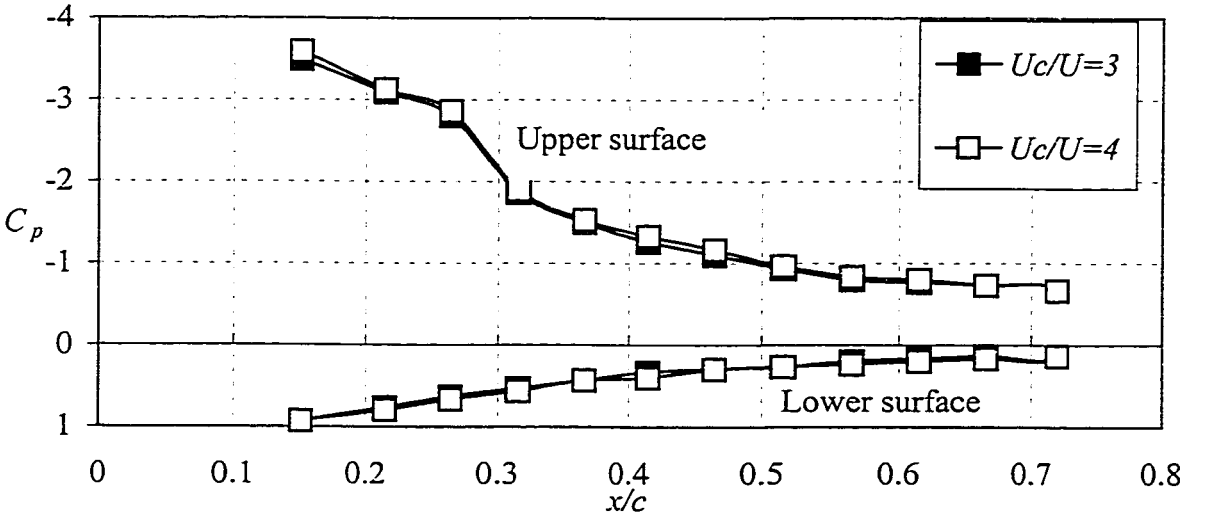

(b)

Figure 4.21 Effect of cylinder rotation on the surface pressure distribution for $\alpha = 30^{\circ}$ and $\delta = 20^{\circ}$: (a) low values of *Uc/U* (b) high values of *Uc/U*.

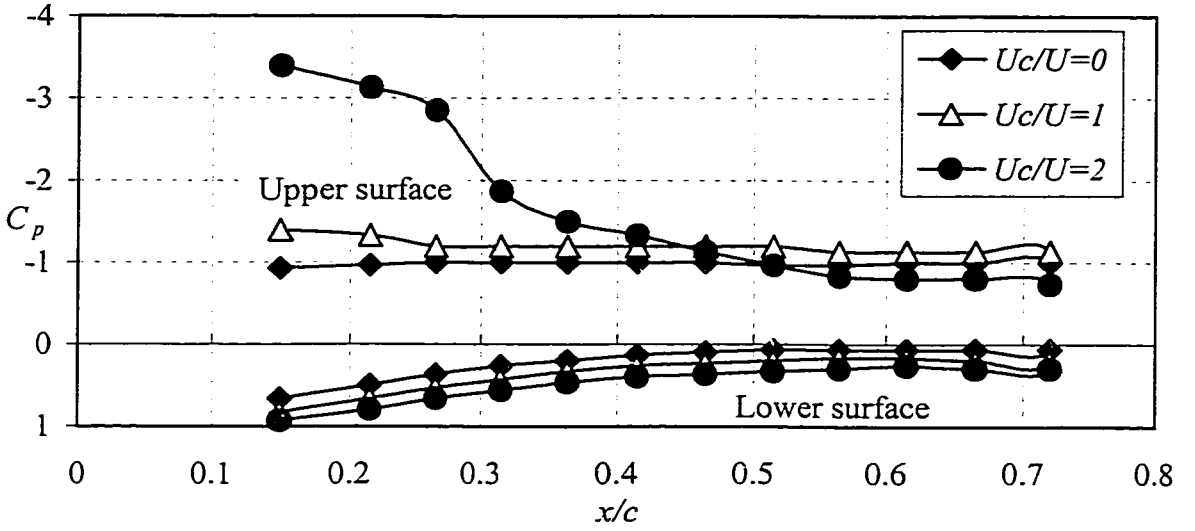

(a)

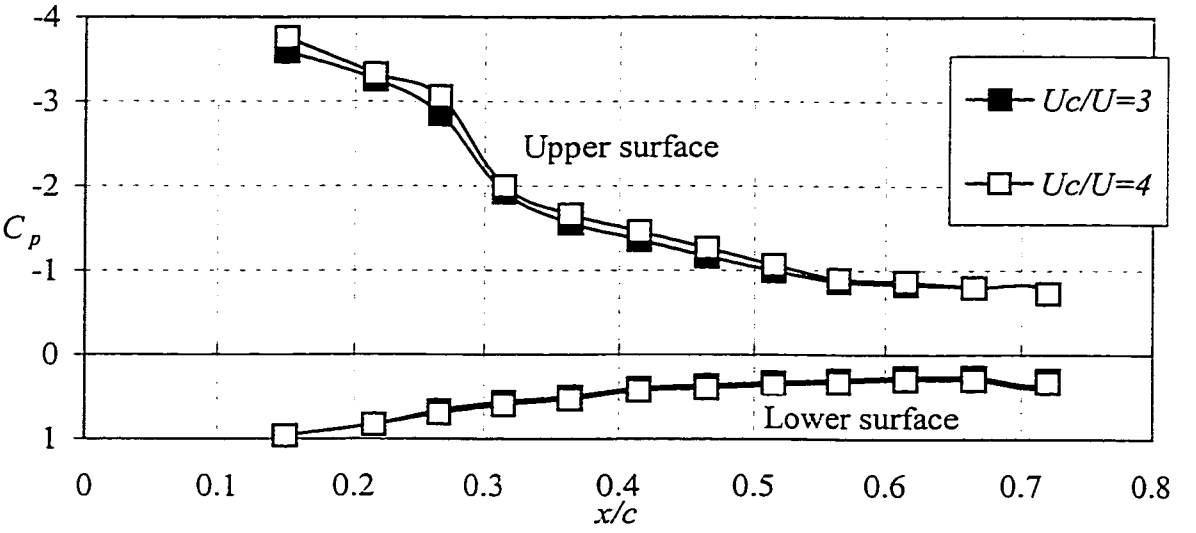

(b)

Figure 4.22 Effect of cylinder rotation on the surface pressure distribution for $\alpha = 30^{\circ}$ and $\delta = 30^{\circ}$: (a) low values of *Uc/U* (b) high values of *Uc/U*.

negative peak pressure without affecting the trend of the pressure distribution. At $\delta = 0°$, the negative peak pressure has increased from –0.95 at $U_c/U = 0$ to –3.5 at $U_c/U = 4$; with $\delta = 30°$, the peak negative pressure is about –3.8 at $U_c/U = 4$.

V. At $\alpha = 40°$:

Surface pressure distributions at high angle of attack such as 40° are shown in Fig. 4.23 to 4.26. In the case of $\delta = 0°$, the separation takes place at around x/c = 30% for the case of $U_c/U = 2$. However, with the cylinder rotating at $U_c/U = 4$, the separation has been delayed. Comparing the pressure distribution at $\alpha = 30°$ and 40° shows that the negative peak pressure and the pressure difference between the lower and upper surfaces are higher for $\alpha = 30°$. This means the airfoil is under stall at $\alpha = 40°$ even though the cylinder is rotating at $U_c/U = 4$. It should be noted that the complete reattachment of the boundary layer was not achieved for α = 40°.

It is noted that at higher angle of attack, the effect of the leading-edge rotating cylinder diminishes as we move downstream the leading edge of the airfoil which is expected because of the dissipation effect. Close to the trailing edge the flow is almost separated at even higher values of U_c/U. The difference between the pressure on the upper and lower surfaces is quite remarkable which leads to higher values of lift coefficient, as we will see shortly in the next section.

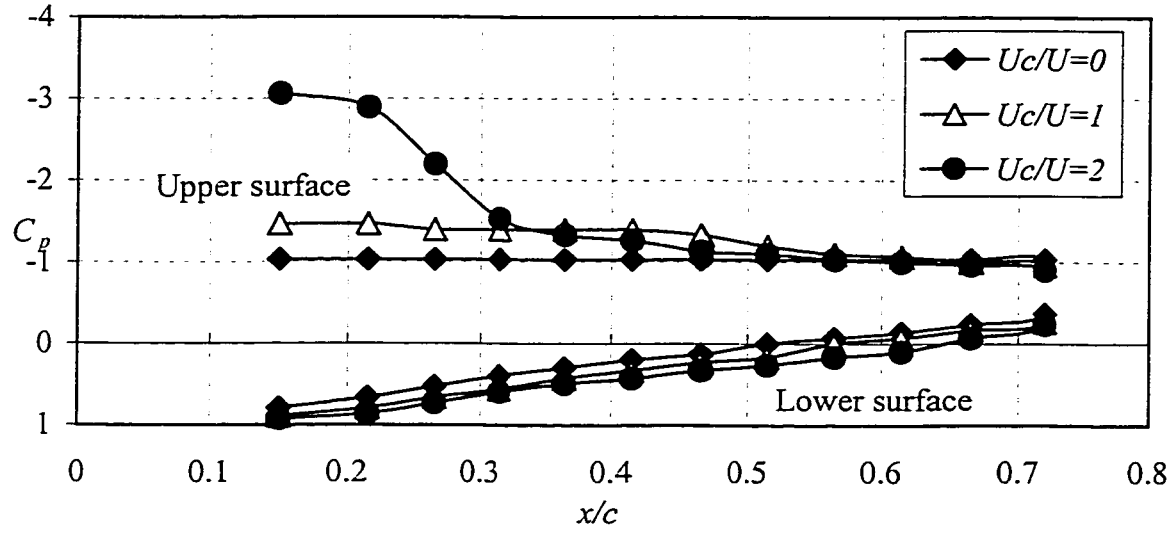

(a)

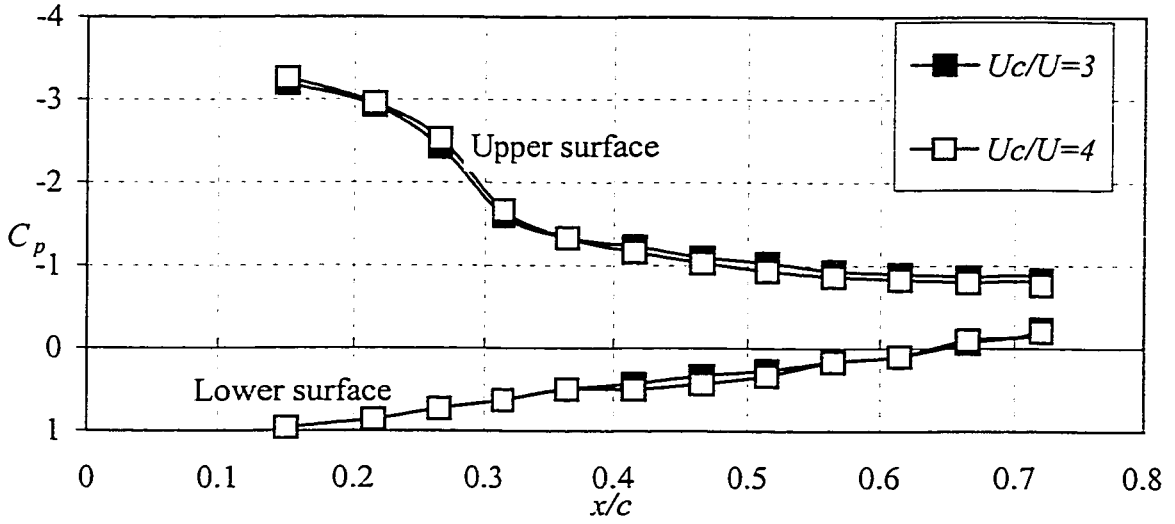

(b)

Figure 4.24 Effect of cylinder rotation on the surface pressure distribution for $\alpha = 40^{\circ}$ and $\delta = 0^{\circ}$: (a) low values of *Uc/U* (b) high values of *Uc/U*.

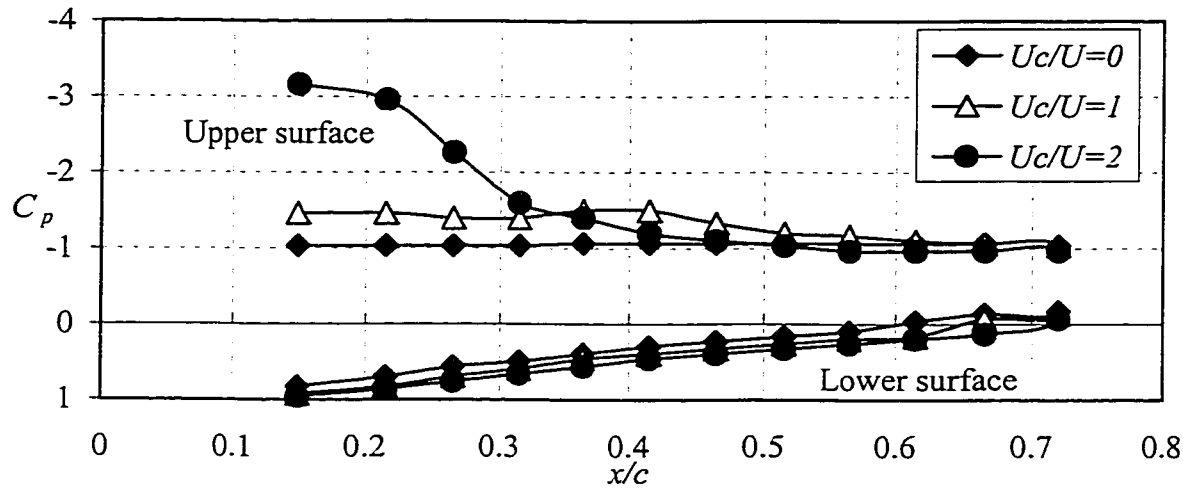

(a)

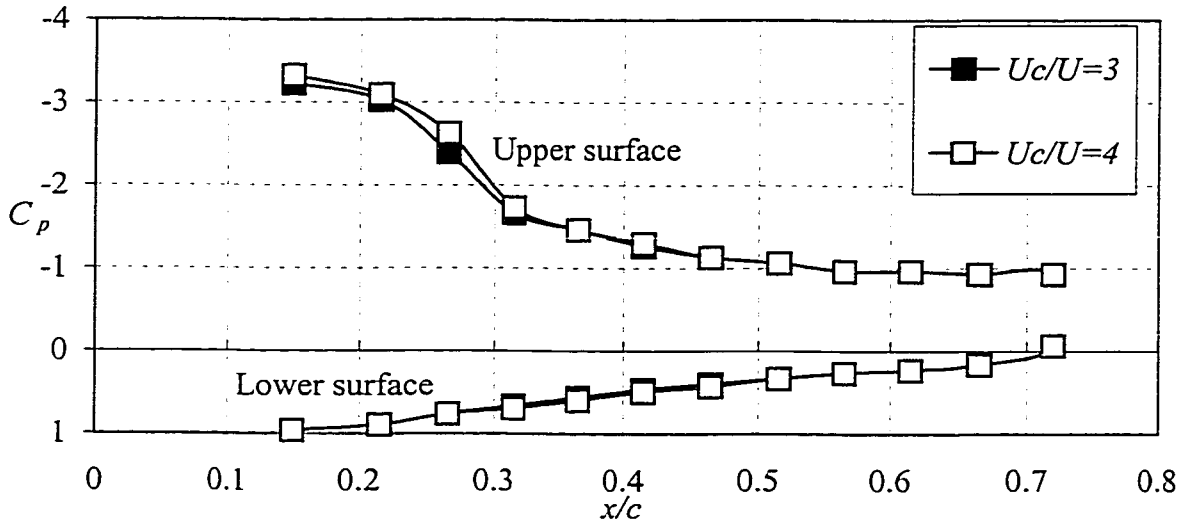

(b)

Figure 4.23 Effect of cylinder rotation on the surface pressure distribution for $\alpha = 40^{\circ}$ and $\delta = 10^{\circ}$: (a) low values of Uc/U (b) high values of Uc/U.

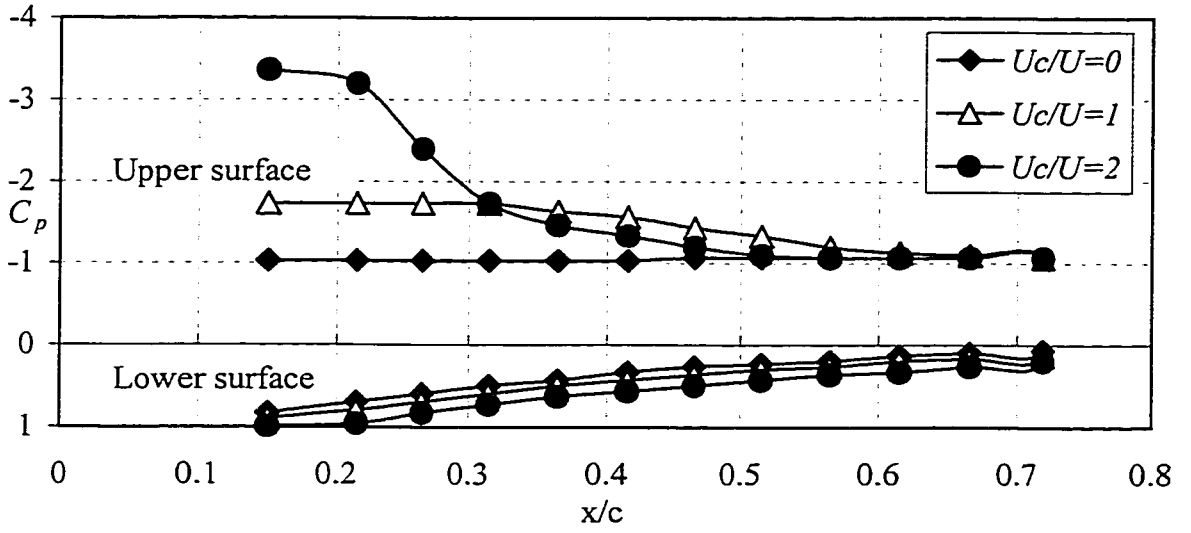

(a)

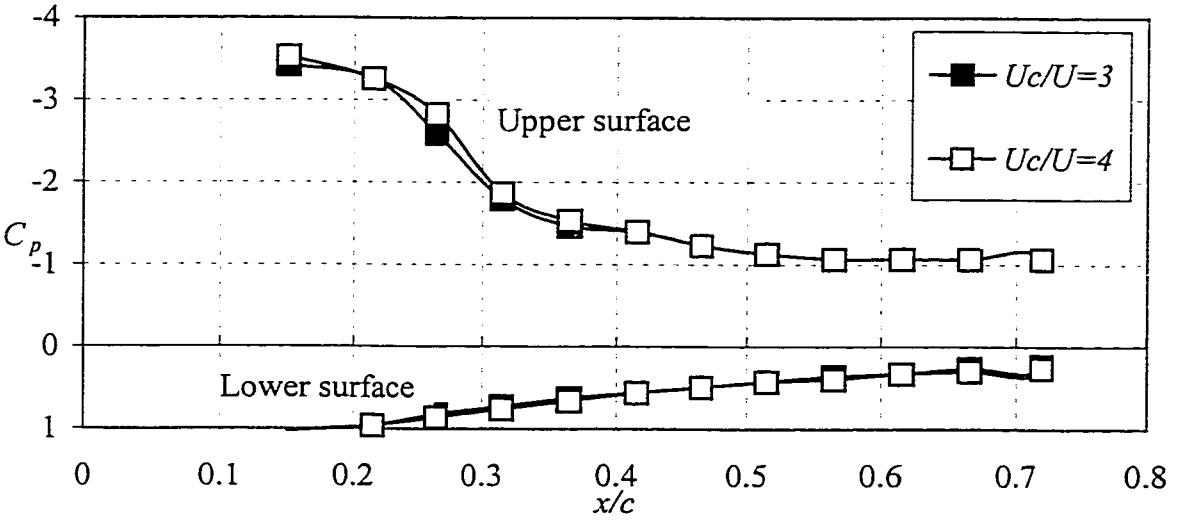

(b)

Figure 4.25 Effect of cylinder rotation on the surface pressure distribution for $\alpha = 40^{\circ}$ and $\delta = 20^{\circ}$: (a) low values of *Uc/U* (b) high values of *Uc/U*.

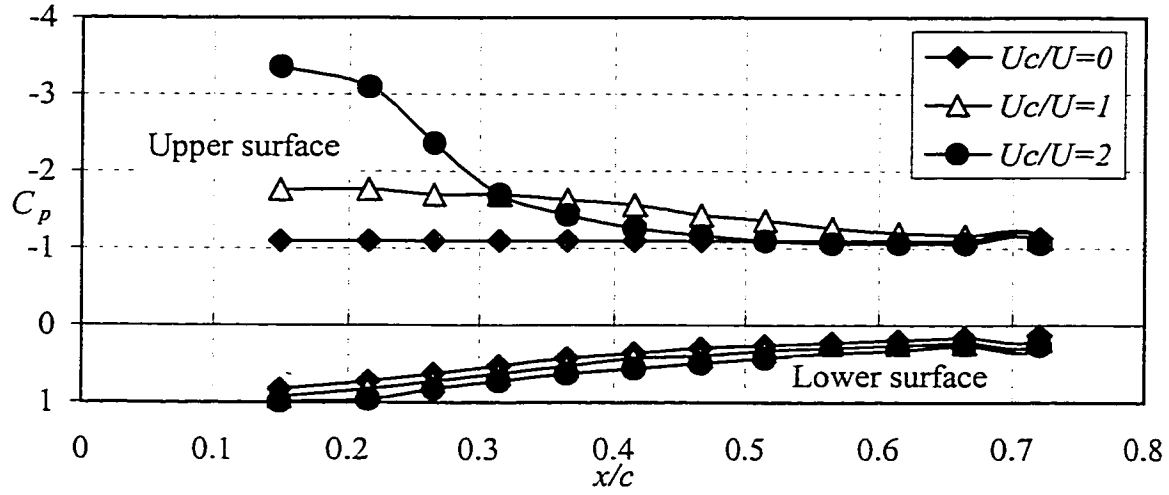

(a)

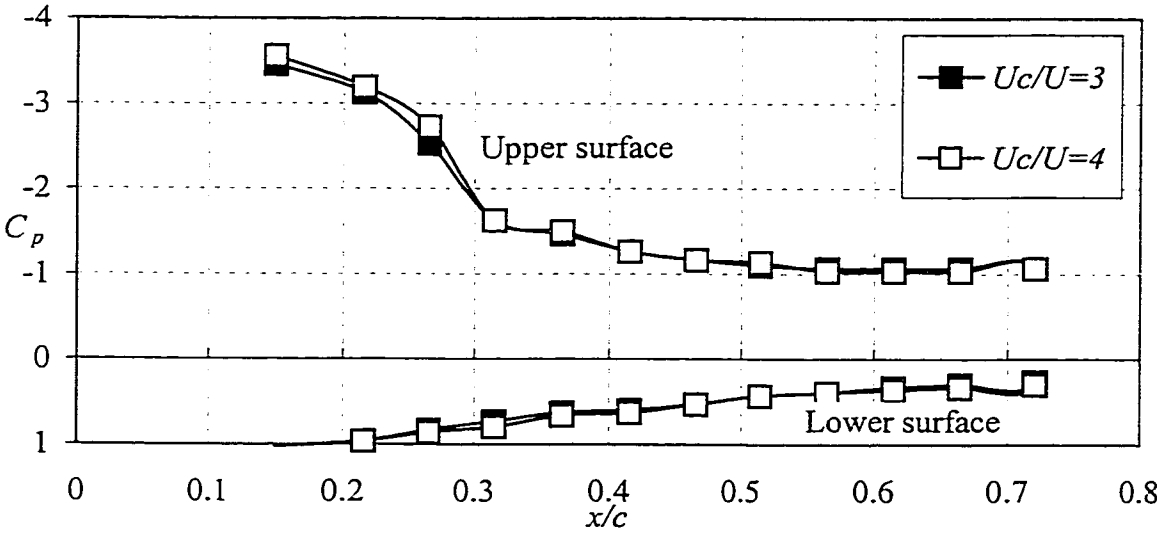

(b)

Figure 4.26 Effect of cylinder rotation on the surface pressure distribution for $\alpha = 40^{\circ}$ and $\delta = 30^{\circ}$: (a) low values of *Uc/U* (b) high values of *Uc/U*.

4.3 Lift and Drag Results

The pressure distributions were integrated, over the portion at which the pressure measurements were taken, using Eqs. 1.3 and 1.4 to obtain lift and drag forces acting on the airfoil.

4.3.1 Effect of the Leading-Edge Rotating Cylinder

Fig. 4.27 shows the lift coefficient, C_L, plotted against angle of attack for different cylinder rotations. It is clear that the lift coefficient increases as U_c/U increases. In the absence of any rotation, the maximum lift coefficient is about 0.85. However, with the cylinder rotating at U_c/U = 4, the maximum lift coefficient is about 1.63. This shows an increase in the lift coefficient by about 92 %. The slope of the lift curve remains unaffected.

The rotating cylinder increases the stalling angle of attack from around 10-15° at U_c/U = 0 to 30-35° at U_c/U= 4 which represents an increase of about 160%. One can observe that higher U_c/U produces gradual decrease in lift. At α = 40°, the lift coefficient is about 1.46 which is quite remarkable. This increase in the lift coefficient and stalling angle of attack would make an airplane fitted with such an

airfoil more maneuverable and improves the performance of the airplane in terms of a short takeoff and landing, and small stalling speeds.

The variation of drag coefficient, C_D, with the angle of attack for different cylinder rotations is illustrated in Fig. 4.28. As shown in the figure, the drag coefficient of the airfoil at $\alpha = 0°$ for different U_c/U is very small. At $\alpha = 40°$, the maximum C_D varies from about 0.82 for $U_c/U = 0$ to about 1.24 for $U_c/U = 4$. It is noted that increasing the cylinder rotation would increase the drag coefficient. This is because when the cylinder rotates, the pressure in the upper surface of the airfoil decreases while the pressure in the lower surface increases. As a result, the normal force acting perpendicular to the airfoil increases and since the drag force is proportional to the sine component of the normal force, i.e. $D \propto \sin \alpha$, the drag will increase.

Since the lift-to-drag ratio is a measure of the aerodynamic efficiency of an airfoil, it is shown in Fig. 4.29 versus the angle of attack for different U_c/U. Consequently, maximum lift-to-drag ratio should lead to minimum thrust required. Note that in the absence of any rotation, L/D ratio is almost zero at $\alpha = 0°$. However, increasing the cylinder rotation to $U_c/U = 4$ gave L/D ratio of around 20 for the same angle of attack. The maximum L/D was observed to be 20 at $\alpha = 0°$ and $U_c/U = 4$. It is interesting to recognize that the maximum L/D of the airfoil occurs at low angle of attack. Therefore, the leading-edge rotating cylinder reduces the need for higher angles of attack.

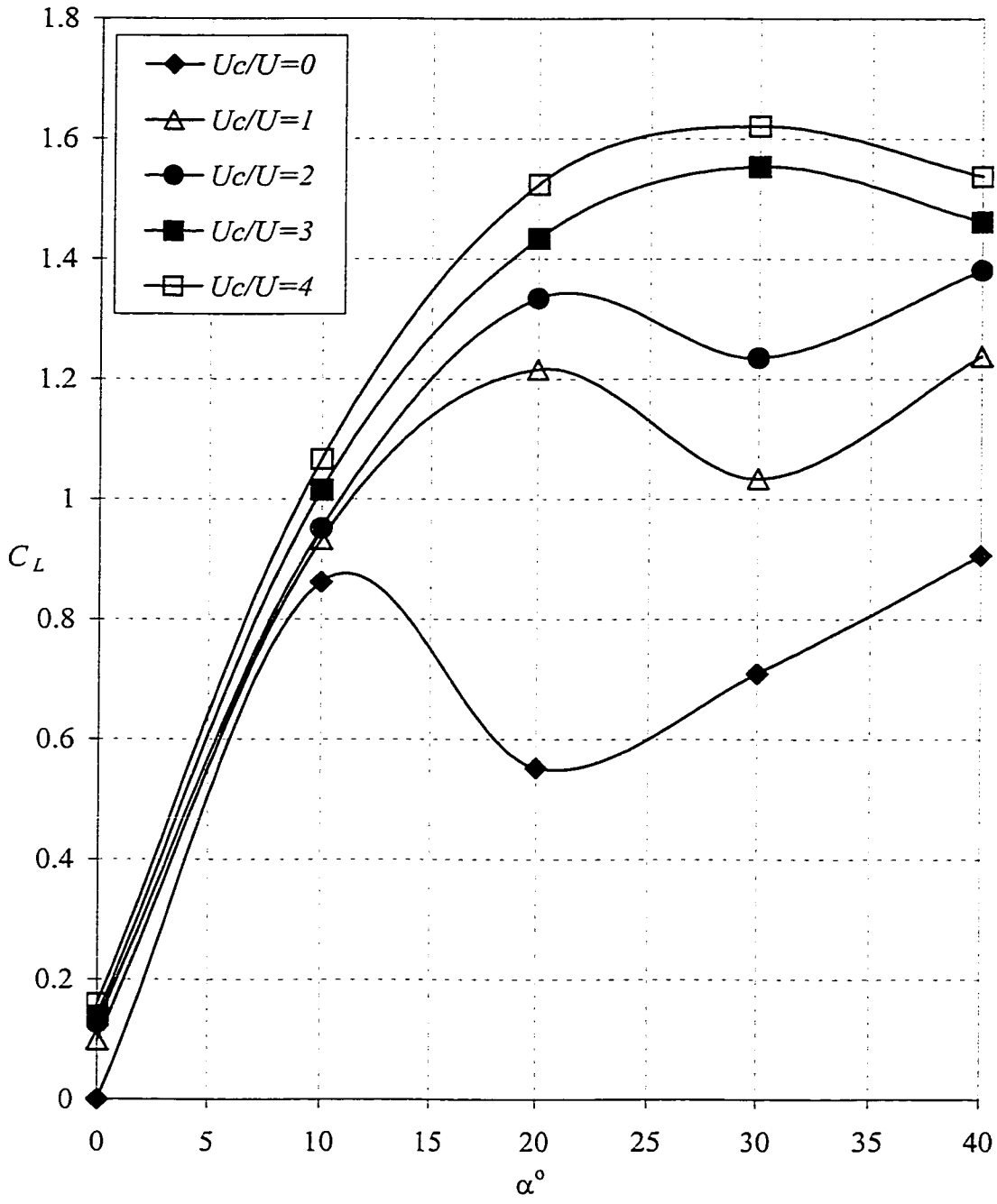

Figure 4.27 Effect of cylinder rotation on the lift and stall characteristics, $\delta = 0^{o}$.

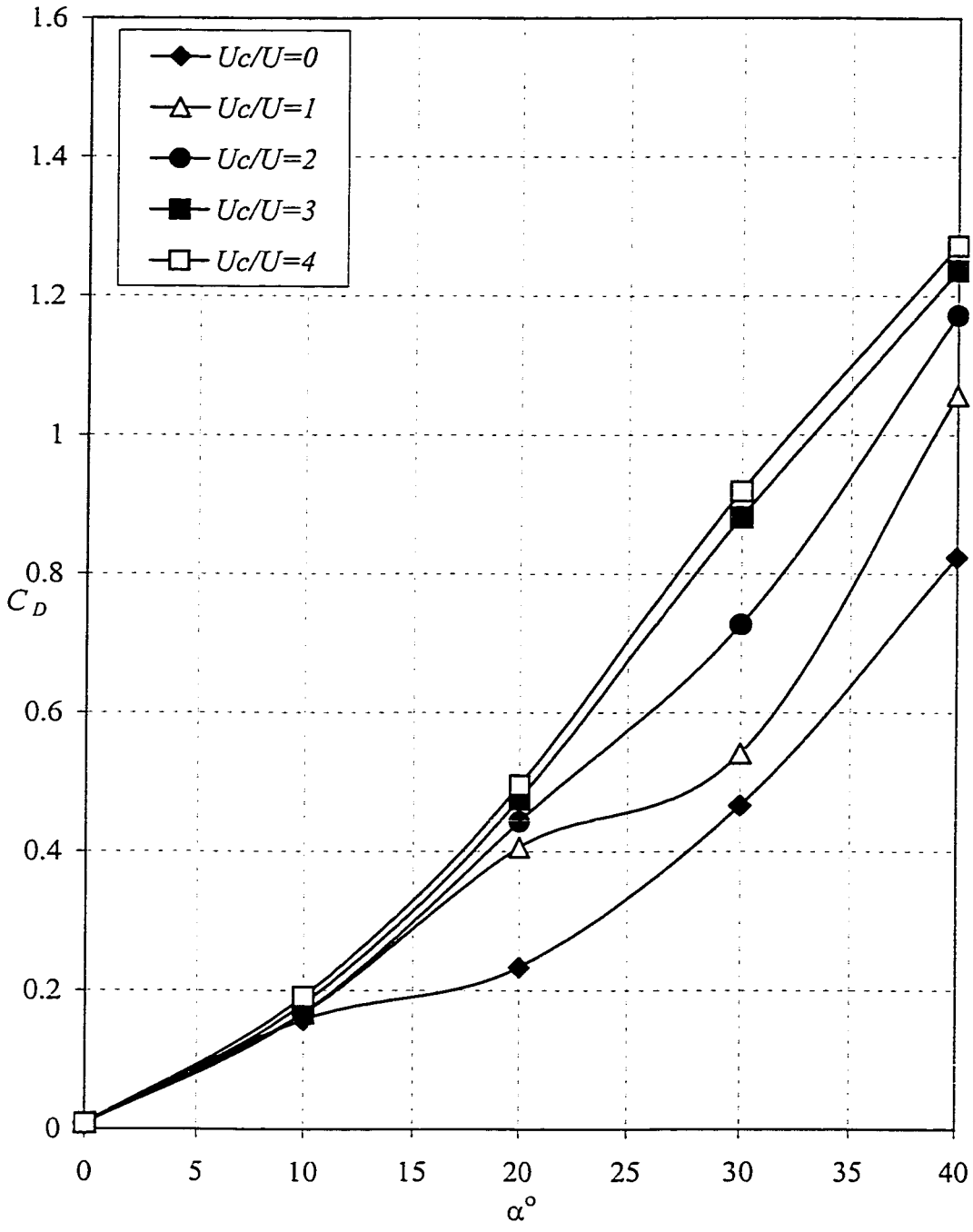

Figure 4.28 Effect of cylinder rotation on the drag coefficient, $\delta = 0^{\circ}$.

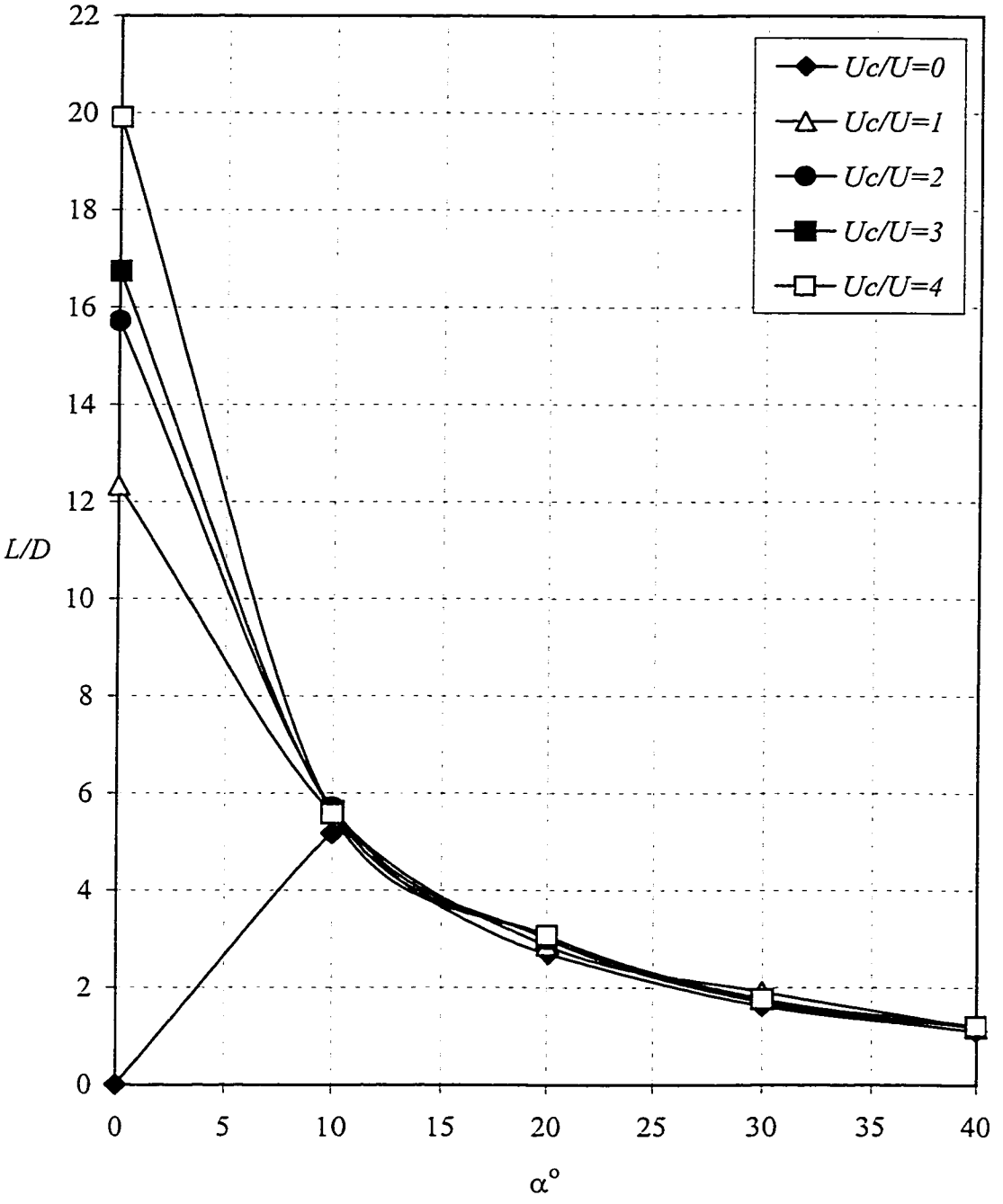

Figure 4.29 Effect of cylinder rotation on the lift-to-drag ratio, $\delta = 0^{\circ}$.

4.3.2 Effect of Plain Flap

The lifting properties of the airfoil with leading-edge rotating cylinder can be greatly enhanced by the use of high-lift devices such as flap. Figs. 4.30 to 4.38 summarize the effect of plain flap in the presence of cylinder rotation. Deflecting the flap is seen to shift the lift curve upward without affecting the slope. The highest sectional lift coefficient with the flap deflected to $\delta = 10°$ and the cylinder stationary (Fig. 4.30) is about 0.98; it is raised to 1.7 when the cylinder rotates at $U_c/U = 4$. This shows an increase in the maximum lift coefficient by about 73%.

Deflecting the flap to $\delta = 30°$ (Fig. 4.36) increases the maximum lift coefficient from about 1.24 for the case of $U_c/U = 0$ to 1.88 for the case of $U_c/U = 4$ which represents an increase of about 52%. It is apparent that the percentage increase in the presence of the flap is less than the percentage increase due to the rotating cylinder alone. However, the percentage increase due to the cylinder rotation at $U_c/U = 4$ and flap deflection to 30° is about 122%. Comparing Fig. 4.27 and Fig. 4.36 suggests that deflection of the flap decreases the stalling angle of attack from 32° at $\delta = 0°$ to 26° at $\delta = 30°$.

The effect of the leading-edge rotating cylinder on the drag coefficient in the presence of the flap is shown in Figs. 4.31, 4.34 and 4.37. As expected, the effect of the flap is to increase the drag coefficient. At $\alpha = 0°$, however, the effect

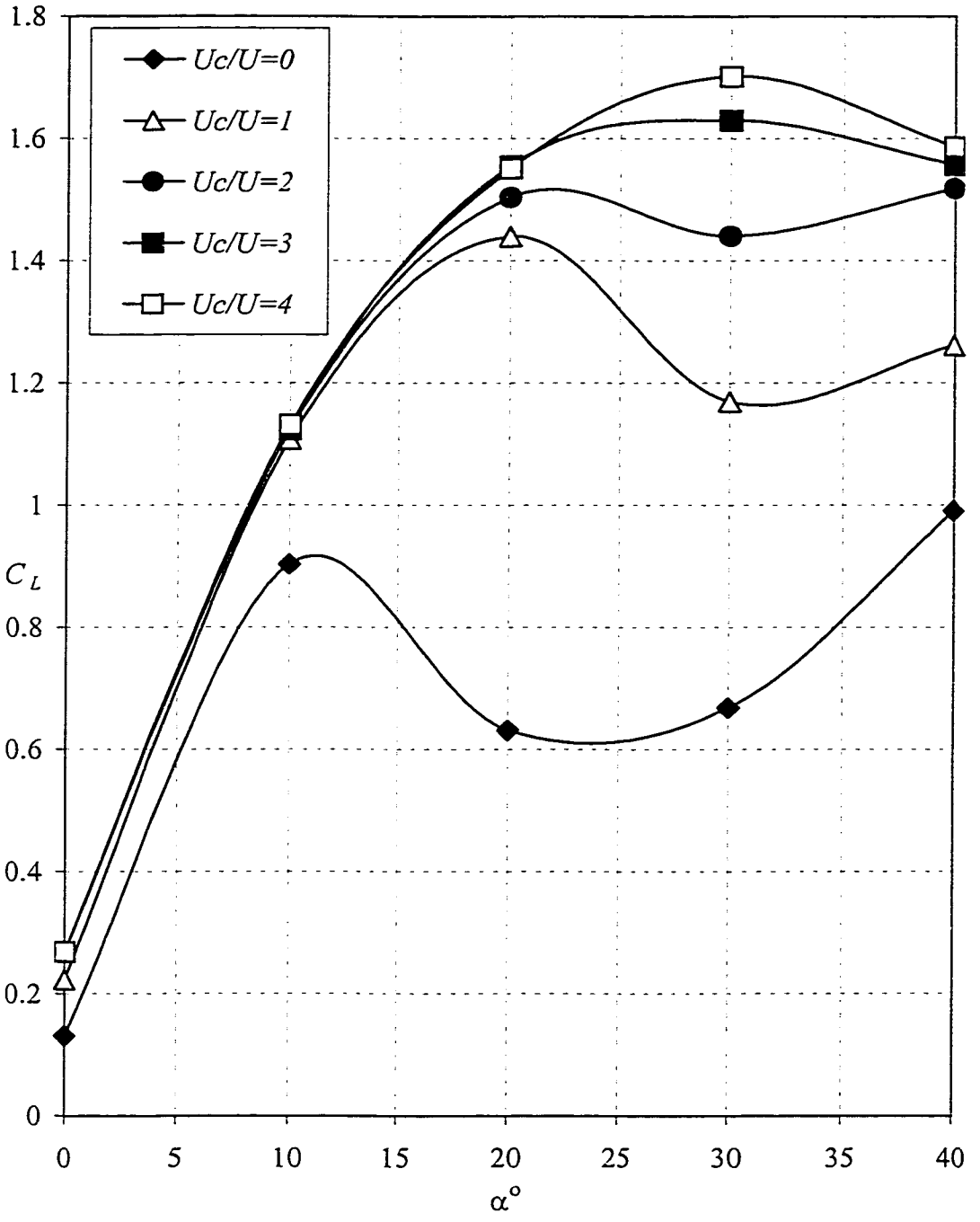

Figure 4.30 Effect of cylinder rotation on the lift and stall characteristics, δ = 10°.

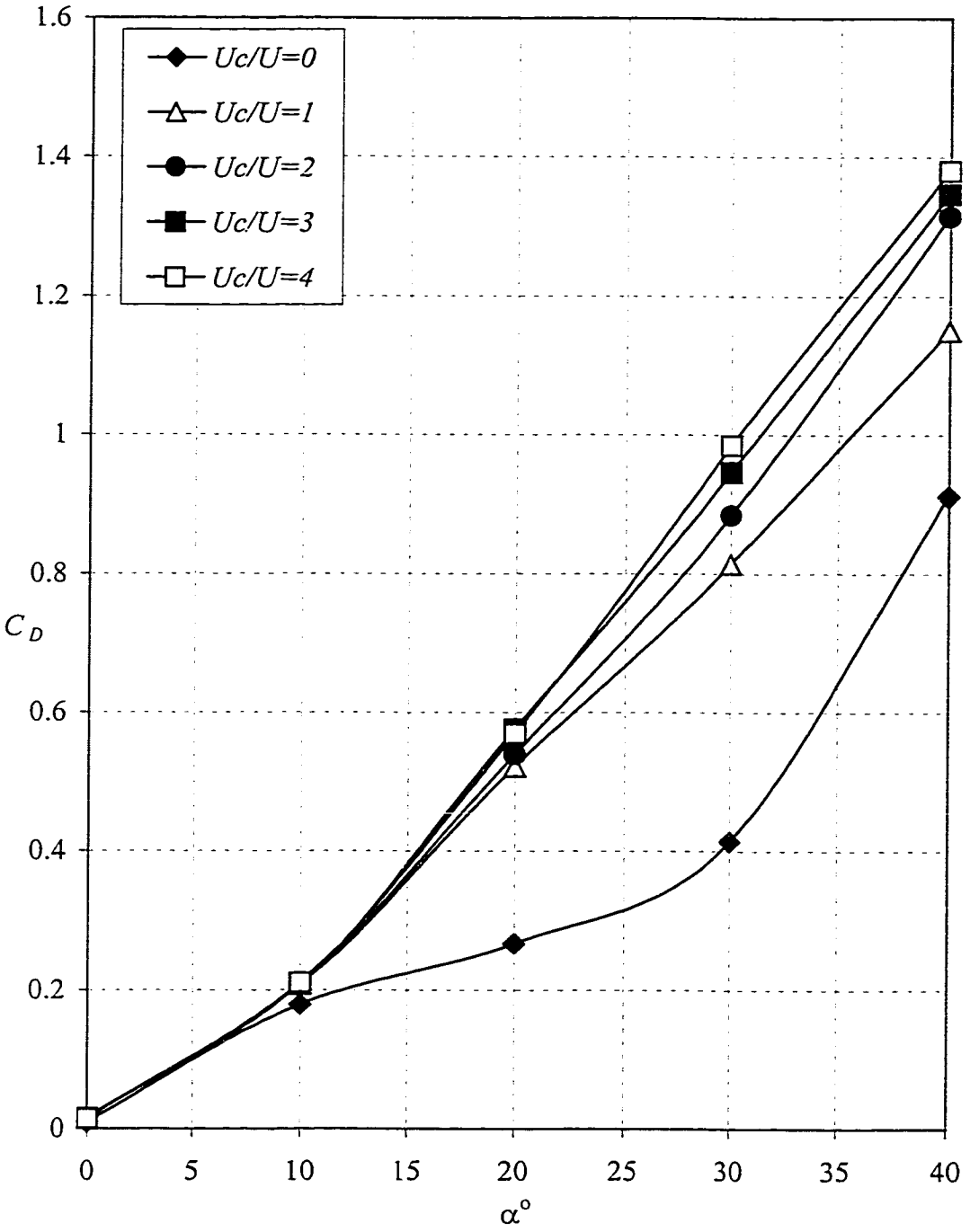

Figure 4.31 Effect of cylinder rotation on the drag coefficient, $\delta = 10°$.

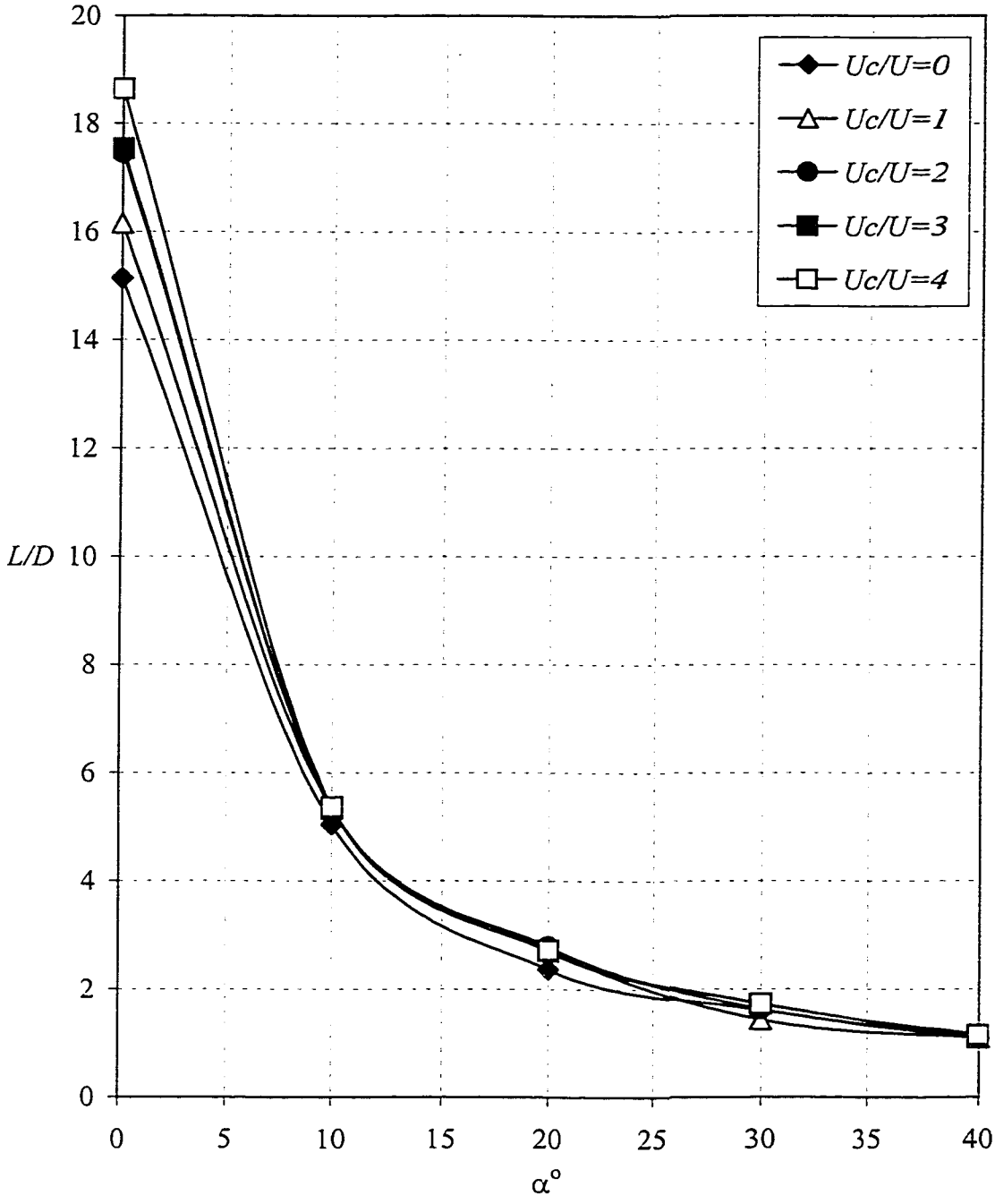

Figure 4.32 Effect of cylinder rotation on the lift-to-drag ratio, $\delta = 10^{\circ}$.

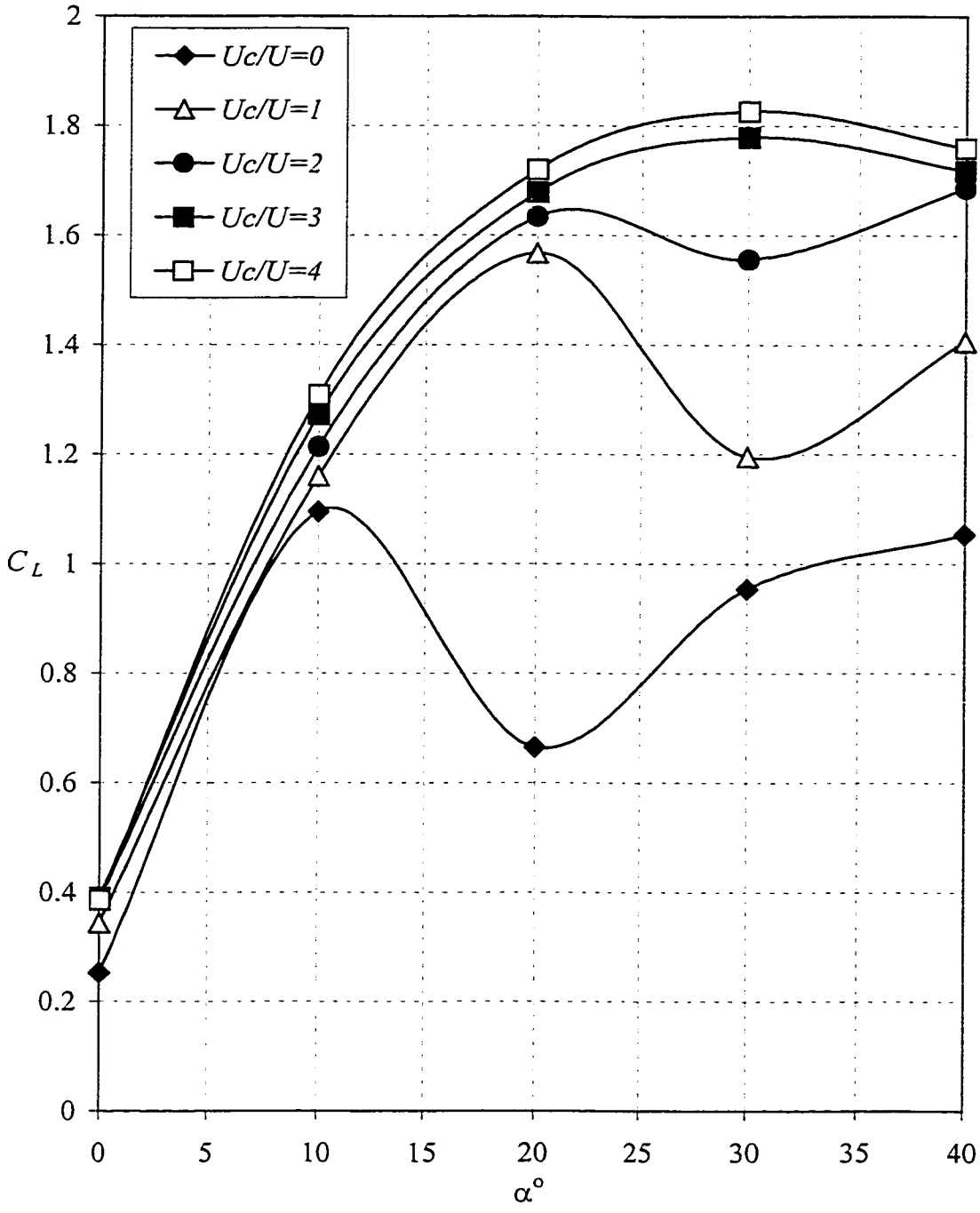

Figure 4.33 Effect of cylinder rotation on the lift and stall characteristics, $\delta = 20^{\circ}$.

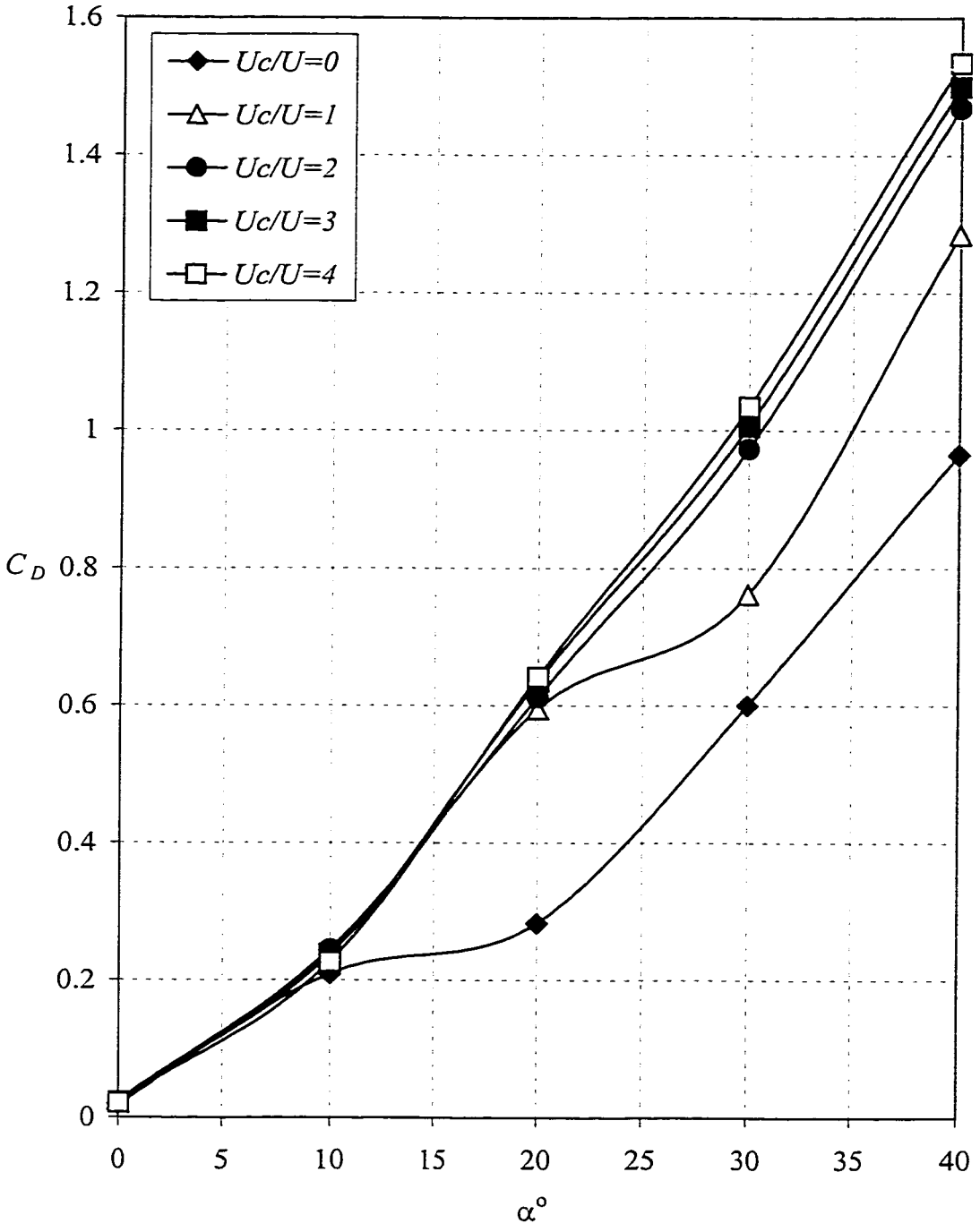

Figure 4.34 Effect of cylinder rotation on the drag coefficient, $\delta = 20^{\circ}$.

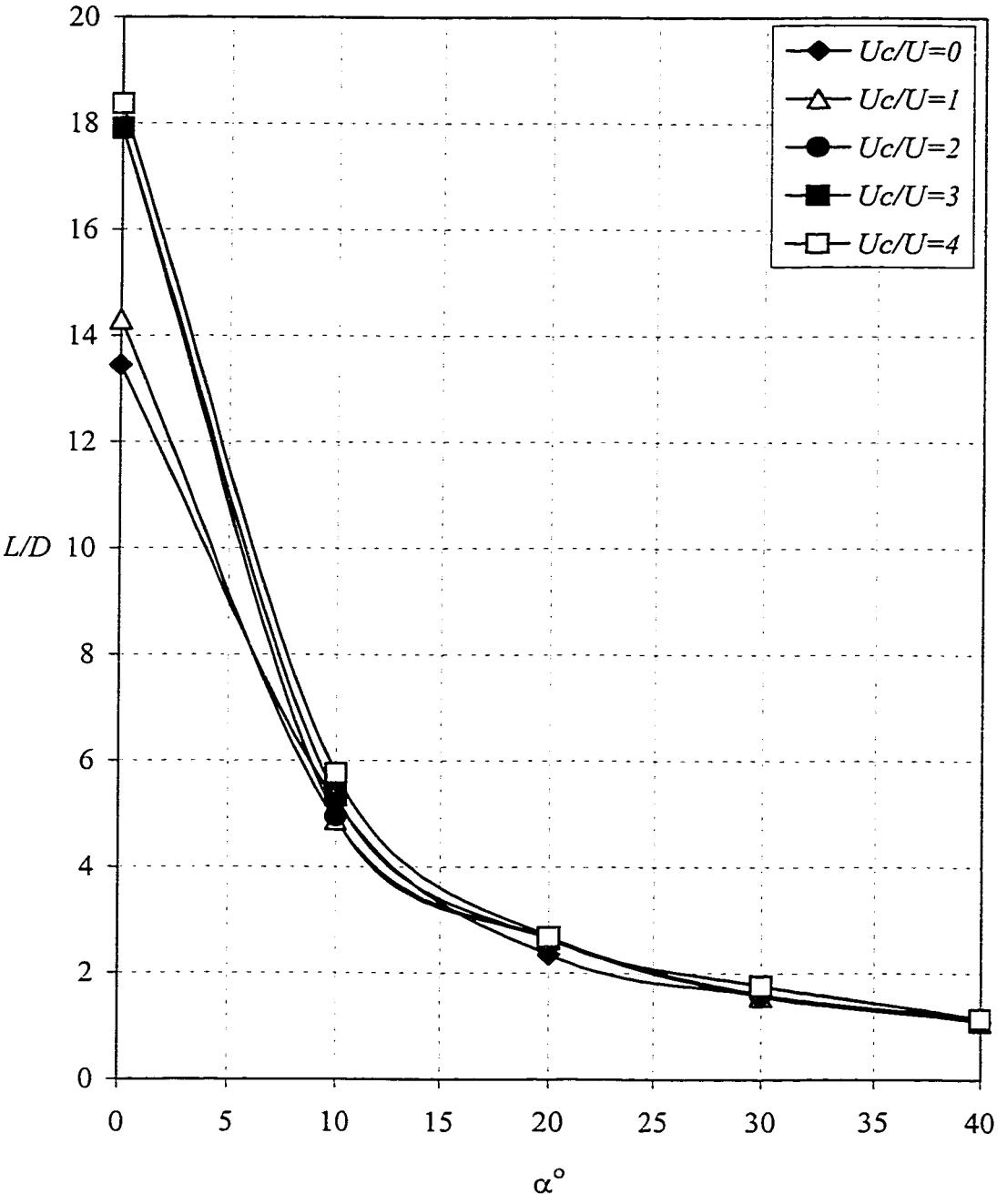

Figure 4.35 Effect of cylinder rotation on the lift-to-drag ratio, $\delta = 20^{\circ}$.

of the flap on the drag coefficient is seen to be small. For all cases, the drag coefficient varies almost linearly with the angle of attack. The maximum drag coefficient is found to be 1.54 at $U_e/U = 4$, $\alpha = 40°$ and $\delta = 30°$. On the other hand, the maximum drag coefficient is about 1.27 for the case of $U_e/U = 4$, $\alpha = 40°$ and $\delta = 0°$. Therefore, deflection of the flap increases the drag coefficient by about 25%.

Although the flap was successful in increasing the lift coefficient, it reduced the lift-to-drag ratio of the leading-edge rotating cylinder airfoil as it is shown in Figs. 4.32, 4.35 and 4.38. This is because the percentage increase in the drag was higher than that in the lift. The maximum L/D decreases from 20 for the case of $\alpha = 0°$, $\delta = 0°$ and $U_e/U = 4$ to 17.5 for the case of $\alpha = 0°$, $\delta = 30°$ and $U_e/U = 4$ which represents reduction of 12.5%.

4.4 Velocity Results

Miniature single hot-wire probe was used to survey the velocity fluctuations at different positions. The probe was placed at the midspan point and measurements were taken at $\alpha = 0°$ and 10° while $\delta = 0°$. Turbulence quantities were computed using TSI DAP software. The maximum statistical uncertainty, $1.96\,\sigma_u/\sqrt{N}$, with 95% confidence level for the mean velocity was about 0.5%.

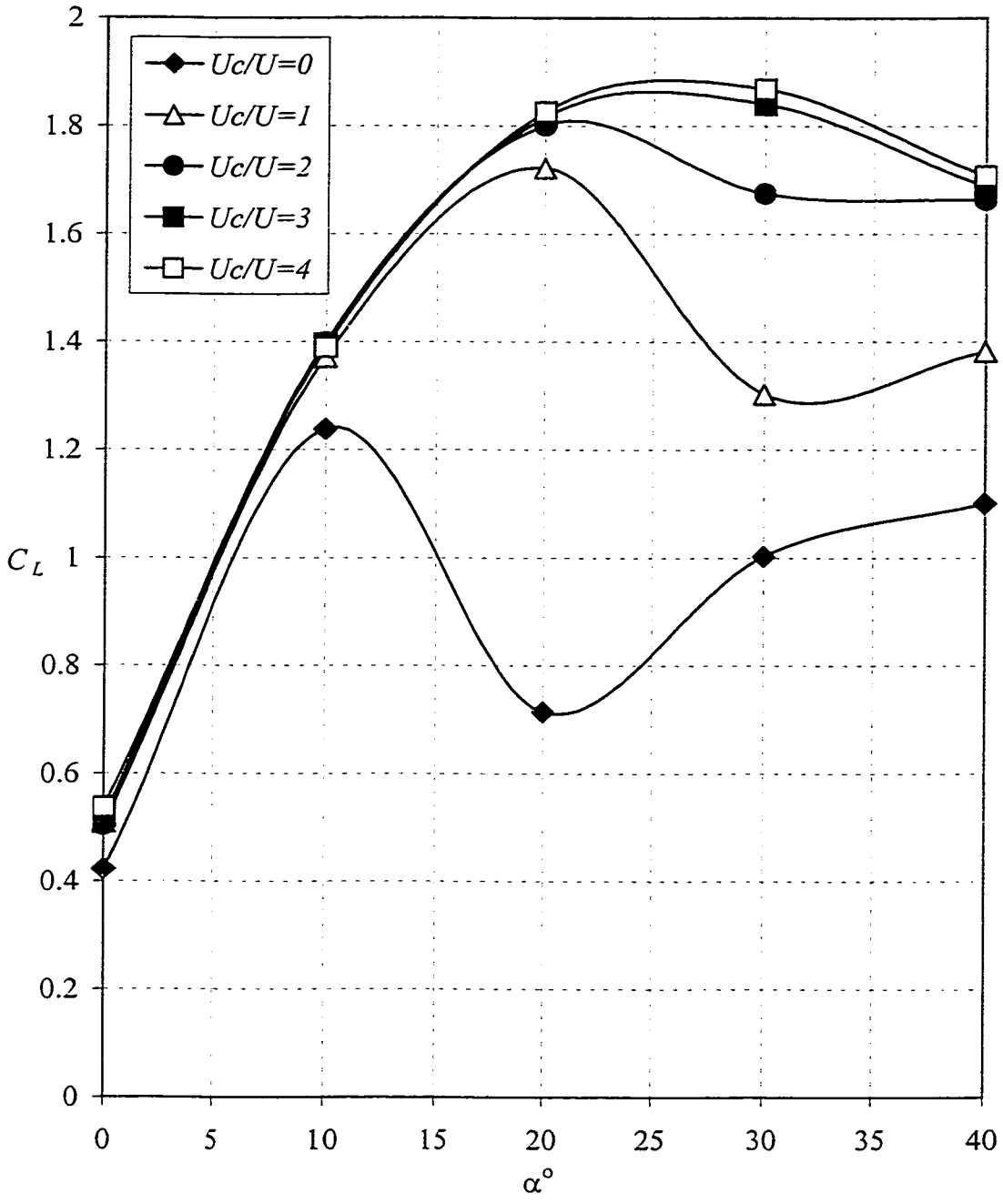

Figure 4.36 Effect of cylinder rotation on the lift and stall characteristics, δ = 30°.

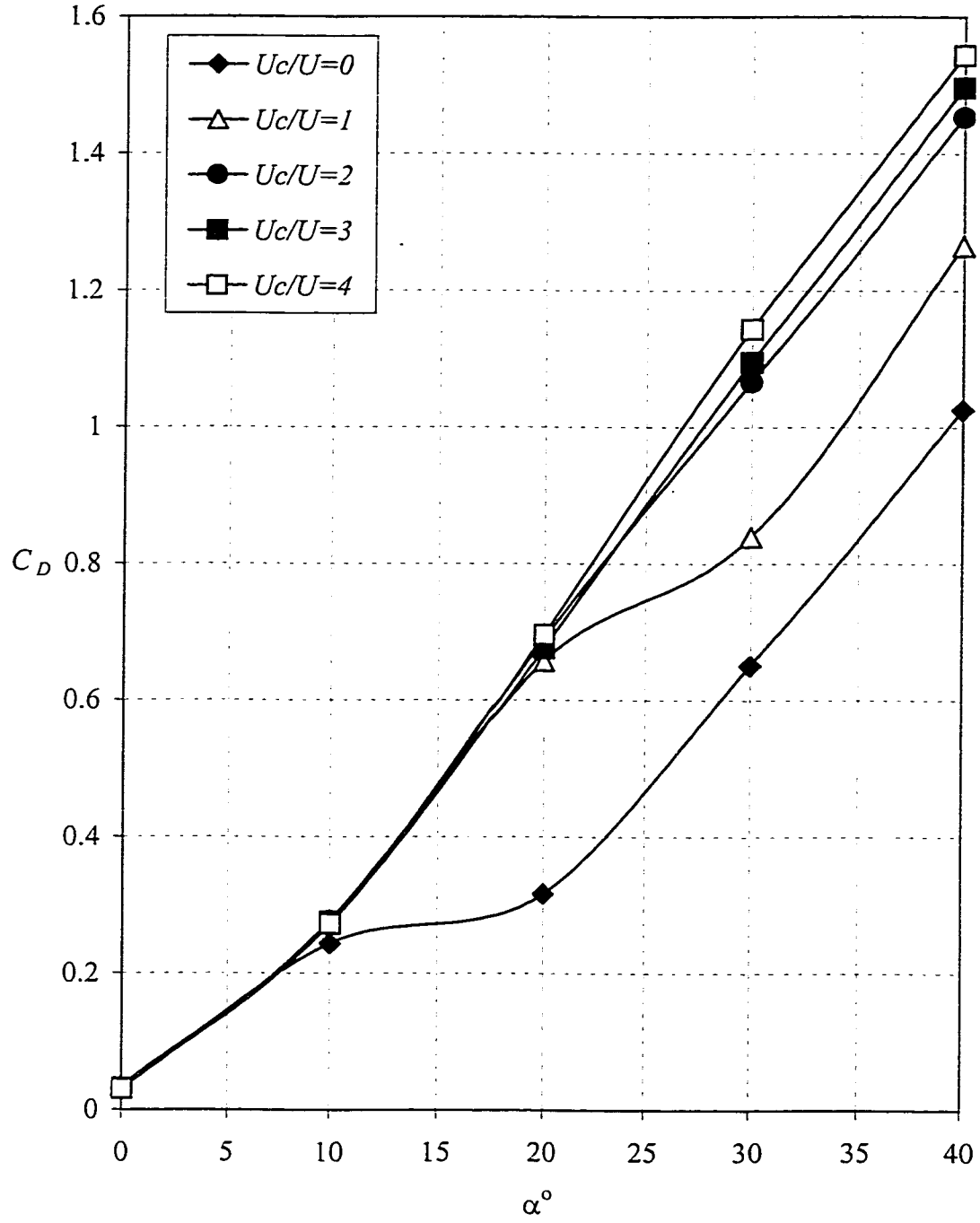

Figure 4.37 Effect of cylinder rotation on the drag coefficient, $\delta = 30^{\circ}$.

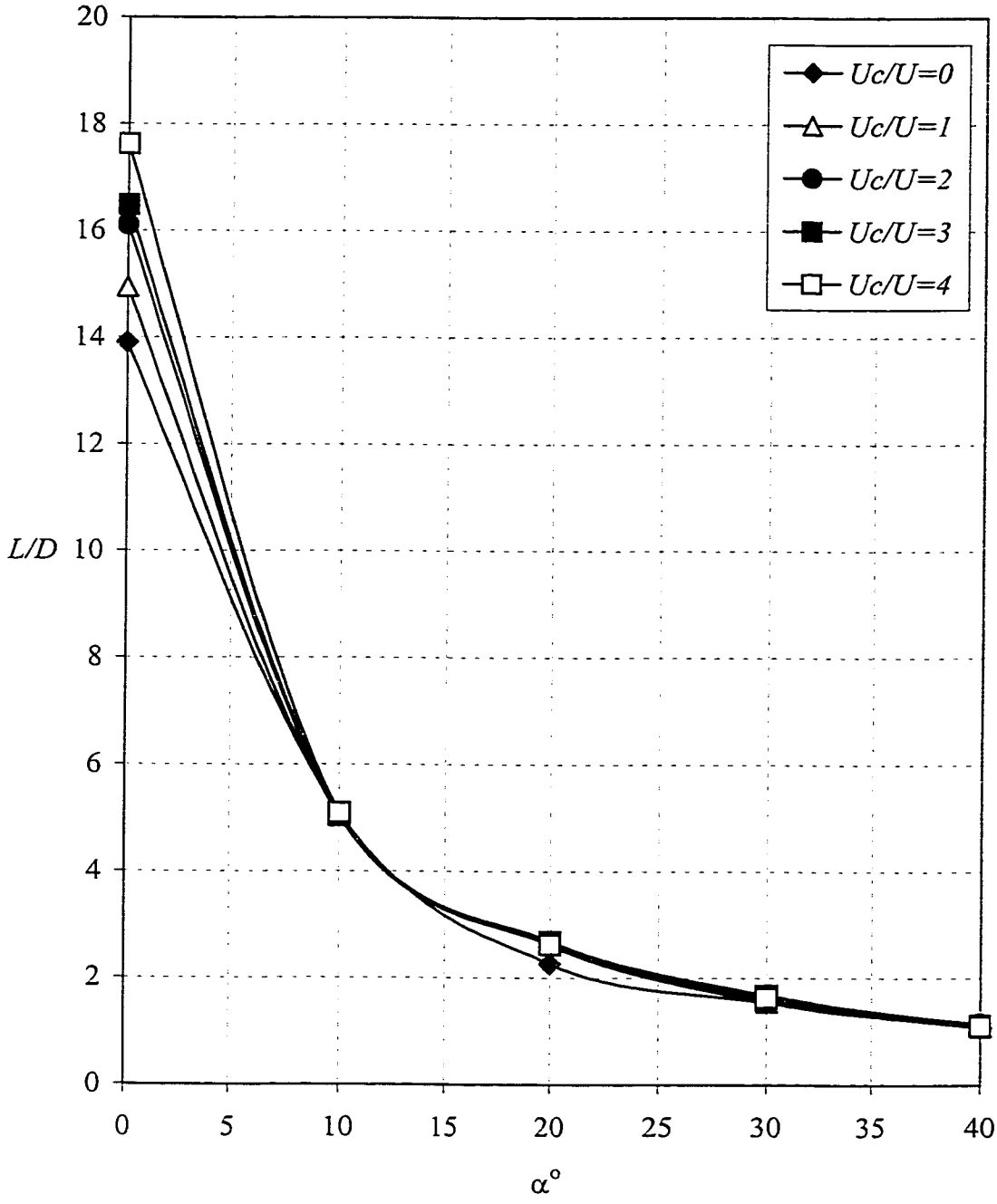

Figure 4.38 Effect of cylinder rotation on the lift-to-drag ratio, $\delta = 30^{\circ}$.

4.4.1 Mean Velocity Profiles

Fig. 4.39 illustrates the effect of the cylinder rotation on velocity profiles for $\alpha = 0°$ at five streamwise stations, $x/c = 0.2$, 0.4, 0.6, 0.8 and 1.0. For the sake of comparison, the velocity profiles for two cases, $U_c/U = 0$ and $U_c/U = 4$, are shown in one figure to give better insight into the phenomenon. Near the leading edge of the airfoil, $x/c = 0.2$, the velocity distribution is almost uniform. It is noted that the presence of cylinder rotation reduces the boundary layer thickness and causes the flow to adhere to the surface of the airfoil. The effect of the cylinder rotation is felt farther at the trailing edge of the airfoil. In the absence of any rotation, the boundary layer has a thickness of about 3 mm at $x/c = 0.4$ and grows to about 20 mm at $x/c = 1.0$. However, at $U_c/U = 4$ the boundary-layer thickness grows from 1.5 mm at $x/c = 0.4$ to 7 mm at $x/c = 1.0$ which is quite remarkable.

Fig. 4.40 summarizes the effect of the leading-edge rotating cylinder on velocity profiles at $\alpha = 10°$. Again, near the leading edge of the airfoil, $x/c = 0.2$, the velocity is almost uniform. Since the Reynolds number is low, the flow over the airfoil is laminar. Observing the changes in the velocity profiles in the figure suggests that in the absence of the cylinder rotation, the flow separates on the forward portion of the airfoil at around $x/c = 0.4$ due to adverse pressure gradient. However, it is followed by the reattachment of the turbulent boundary layer

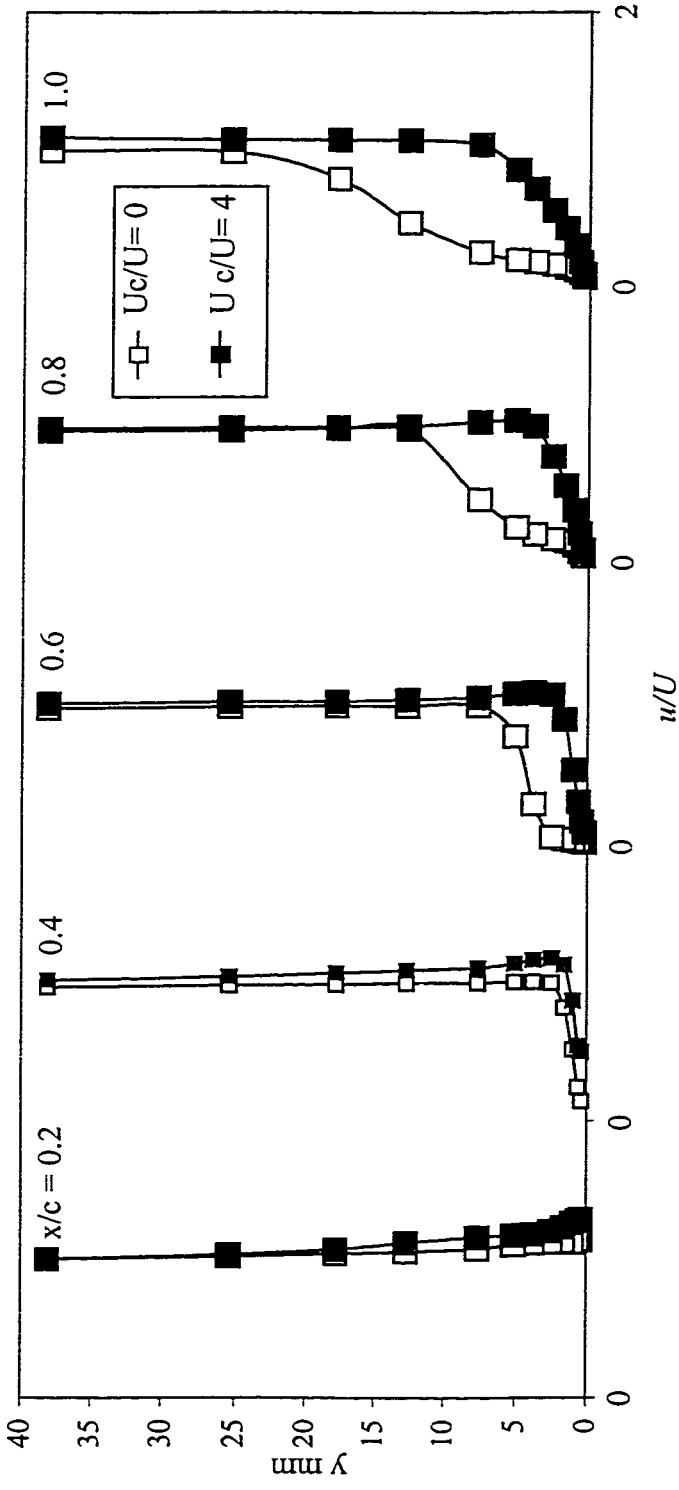

Figure 4.39 Effect of the leading-edge rotating cylinder on velocity profiles of the upper surface of the airfoil, $\alpha = 0^{o}$.

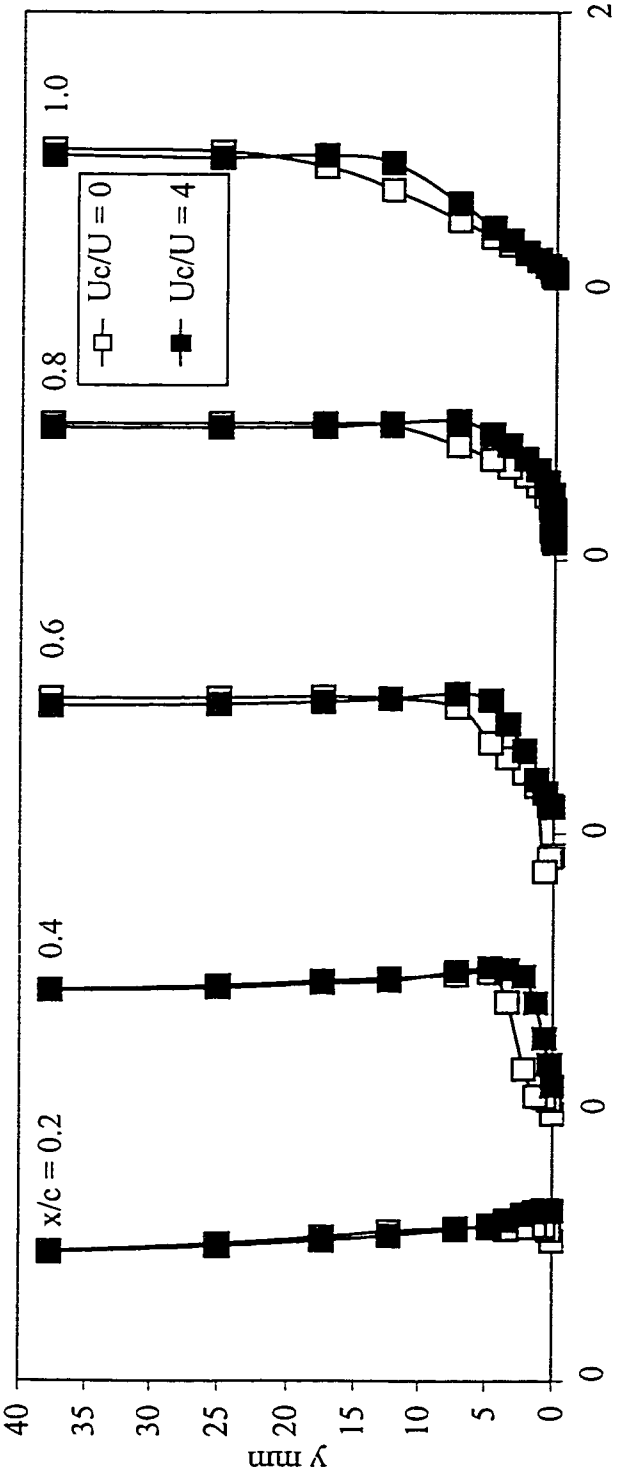

Figure 4.40 Effect of the leading-edge rotating cylinder on velocity profiles on the upper surface of the airfoil, α = 10°.

downstream at x/c = 0.8. Near the trailing edge at x/c = 1.0, the turbulent boundary layer tends to separate. With the cylinder rotation, the flow is energized and separation of the boundary layer was prevented. It is noted that near the trailing edge, the effect of the rotation is low. In the case of U_c/U = 0, the boundary layer thickness varies from about 5 mm at x/c = 0.4 to 25 mm at x/c = 1.0. On the other hand, at U_c/U = 4, the boundary layer thickness varies from 2.5 mm at x/c = 0.4 to 15 mm at x/c = 1.0.

4.4.2 Turbulence Intensity Profiles

The effects of the leading-edge rotating cylinder on the turbulence intensity at α = 0° and 10° are shown in Figs. 4.41 and 4.42, respectively. Since the flow is laminar near the leading edge of the airfoil and in the absence of any adverse pressure, it is noted that turbulence intensities near the leading edge for both cases, α = 0° and 10°, were small. At α = 0° (Fig. 4.41) and in the absence of cylinder rotation, the turbulent intensity has a maximum value of 21% at x/c = 1.0 while it is 15% for U_c/U = 4 at the same streamwise location. When the airfoil is placed at α = 10° (Fig. 4.42) and U_c/U = 0, the turbulence intensity has the maximum value of 20% at x/c = 0.6 and this is due the separation of the boundary layer. However, this value drops to 15% with the cylinder rotating at U_c/U = 4. Because of turbulent boundary layer attachment at x/c = 0.8, turbulence intensities

at x/c = 0.8 and 1.0 were less than that at x/c = 0.6. It is interesting to recognize that at $x/c \geq 0.6$ turbulence intensities were higher for the case of $U_c/U = 0$ than for the case of U_c/U = 4. This increase is likely to be due to the adverse pressure gradient to which the boundary layer for the case of $U_c/U = 0$ is subjected [28].

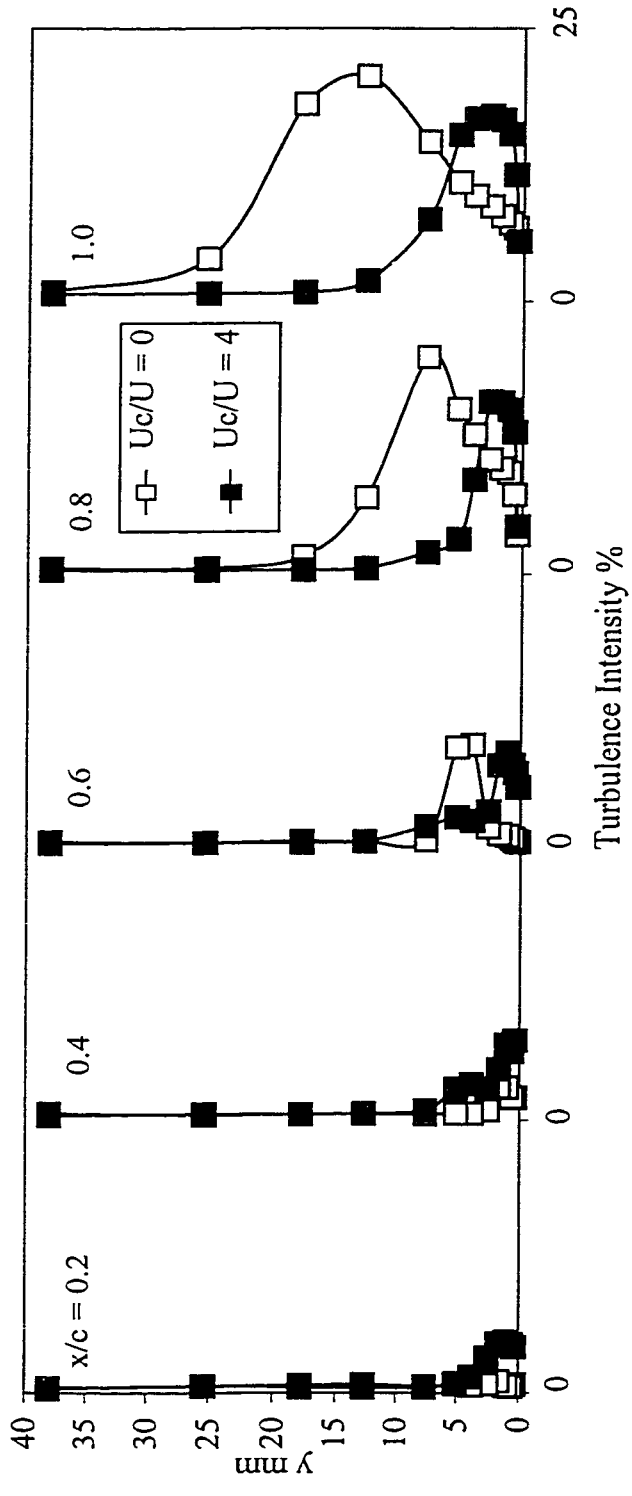

Figure 4.41 effect of the leading-edge rotating cylinder on turbulence intensity profiles of the upper surface of the airfoil, $\alpha = 0^{o}$.

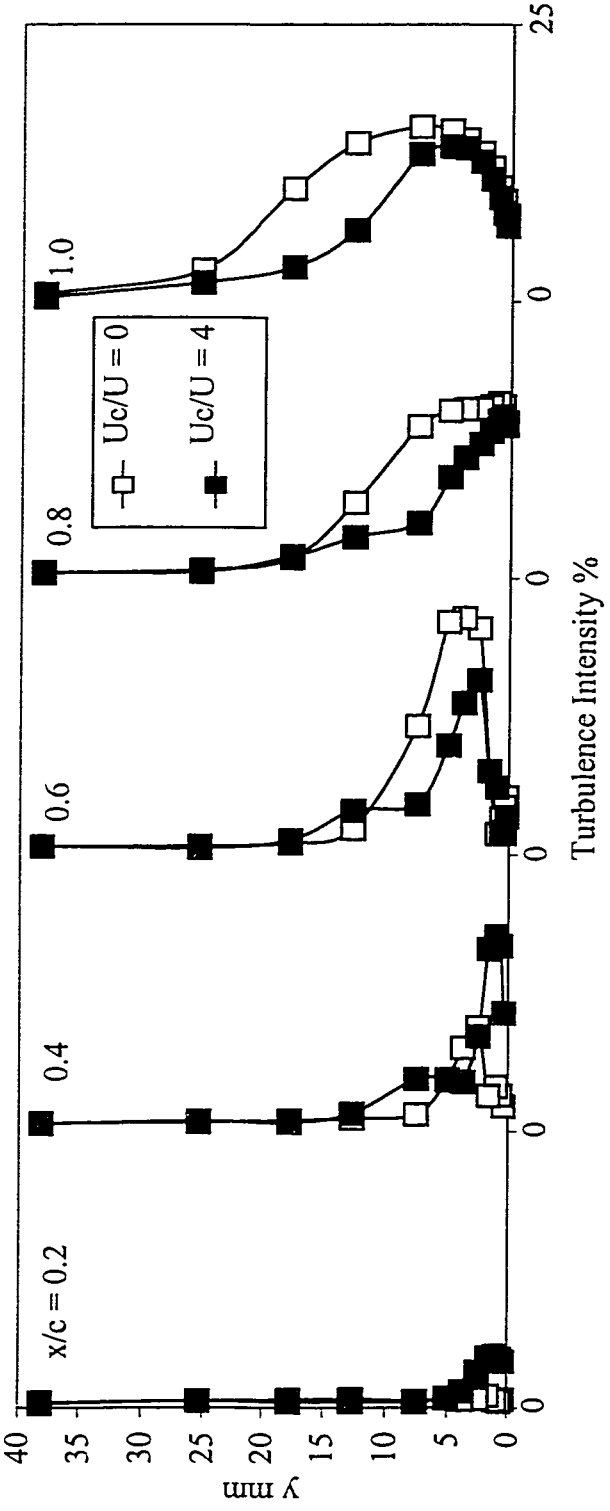

Figure 4.42 Effect of the leading-edge rotating cylinder on turbulence intensity profiles of the upper surface of the airfoil, $\alpha = 10^{o}$.

CHAPTER 5

CONCLUSIONS AND RECOMENDATIONS

5.1 Conclusions

An experimental investigation has been conducted to study the effect of the leading-edge rotating cylinder and the trailing-edge plain flap on :

1) pressure distributions over the upper and lower surfaces of the NACA 0024 airfoil,

2) the lift and drag coefficients and the stalling characteristics of the airfoil,

3) boundary layer growth and turbulence intensity on the upper surface of the airfoil, and

4) the size of the wake region.

The surface pressure measurements, taken at Reynolds number of 6.5×10^4 based on the model chord, showed that the leading-edge rotating cylinder is a successful device in increasing pressure differences between the upper and lower

surfaces of the airfoil. It also showed that the peak negative pressure increased with increasing U_c/U. The lift and drag were calculated by the integration of pressure measurements over the portion at which pressure measurements were taken.

In the absence of the flap, the increase in the lift coefficient and the delay in the stalling angle of attack were about 92% and 160%, at $\alpha = 30°$ and $U_c/U = 4$. The rotating cylinder increases the stalling angle of attack from 10-15°at $U_c/U = 0$ to about 30-35° at $U_c/U = 4$. Also, the decrease in the lift coefficient at higher rotations was gradual. The drag coefficient of the airfoil increases as the cylinder rotation increases. However, at low angles of attack, such as $\alpha = 0°$, the effect of the cylinder rotation is almost negligible.

In addition, results showed that lift-to-drag ratio has a maximum value of around 20 at $\alpha = 0°$and $U_c/U = 4$, hence reducing the need for higher angles of attack at take-off. This increase in the lift coefficient and stalling angle of attack would make an airplane fitted with such an airfoil highly maneuverable and improves the performance of the airplane in terms of a short takeoff and landing. Although the flap was successful in increasing the lift coefficient, it reduced the lift-to-drag ratio of the leading-edge rotating cylinder airfoil. The maximum *L/D* decreases from 20 to 17.5 when the flap is deflected to $\delta = 30°$, which represents a reduction of 12.5%.

Boundary layer measurements were taken at five streamwise stations, x/c = 0.2, 0.4, 0.6, 0.8 and 1.0 for the cases of $U_c/U = 0$ and 4 ($\alpha = 0°$ and 10° while $\delta = 0°$). Results of the boundary layer measurements showed that the leading-edge rotating cylinder reduced the boundary layer thickness and suppressed the effect of adverse pressure gradient. At $\alpha = 10°$ and in the absence of the cylinder rotation, the laminar boundary layer separated near the leading edge of the airfoil. This is followed by turbulent boundary layer reattachment near the trailing edge of the airfoil. When the cylinder rotated at $U_c/U = 4$, separation of the laminar boundary layer was prevented. It is noted that the turbulence intensity were less for the case of $U_c/U = 4$ than for the case of $U_c/U = 0$. This is likely due to the adverse pressure gradient to which the boundary layer, for the case of $U_c/U = 0$, is subjected.

The flow visualization results showed that an increase in the speed of the leading-edge rotating cylinder would delay the separation on the upper surface of the airfoil or perhaps re-attach the flow. At high angles of attack such as $\alpha = 40°$, reattachment of the flow could not be achieved but the separation was delayed. Considering the changes in the lift coefficient along with flow visualization results suggests that the effect of the leading-edge rotating cylinder becomes less at higher U_c/U.

5.2 Recommendations

1. the effect of the leading-edge rotating cylinder can be investigated at various Reynolds numbers to examine its effect.
2. The lift, drag, moment coefficients of the airfoil can be investigated by using strain gage balance.
3. The flow in the vicinity of the airfoil surface can be studied in a more careful way by using X hot-wire probe or Laser Doppler Anemometer (LDA).
4. Different methods of BLC such as suction and blowing can be applied to the airfoil and compare that with Leading-edge rotating cylinder effects.
5. The pressure holes on the surface of the airfoil can be used to study the effect of blowing and suction on the flow around the airfoil.
6. The influence of the gap between the leading-edge rotating cylinder and the fixed part of the airfoil.
7. Florescent paint could be used to measure pressure distribution on the surface of the rotating cylinder.
8. Surface flow visualization, by means of oil-flow or china-clay methods, can be used to observe the surface-flow pattern, which reveal a general picture of state of the boundary layer, location of separation and re-attachment points and location of vortices on the upper surface of the airfoil.

9. Mathematical modeling and numerical solutions could be investigated and compared to the available experimental data.

REFERENCES

[1] Chang, P. K., *Separation of Flow*, Pergamon Press, 1970.

[2] Schlichting, H., *Boundary Layer Theory*, McGraw-Hill, New York, 1968.

[3] Chang, P.K., *Control of Flow Separation*, McGraw-Hill, New York, 1976.

[4] Jonhson, W. S., Tennant, J. S. and Stamps, R. E., "Leading-Edge Rotating Cylinder for Boundary-Layer Control on Lifting Surfaces," *Journal of Hydronautics*, Vol. 9, No. 2, 1975, pp. 76-78.

[5] Sayers, A. T., "Lift Coefficient and Flow Visualization on Leading Edge Rotating Cylinder Rudder," *International Journal of Mechanical Engineering Education*, Vol. 7, No.2, 1979, pp. 75-79.

[6] Modi, V. J., Sun, J. L. C., Akutsu, T., Lake, P., McMillan, K., Swinton, P. G. and Mullins, D., "Moving-Surface Boundary-Layer Control for Aircraft Operation at High Incidence," *Journal of Aircraft*, Vol. 18, No.11, 1981, pp. 963-968.

[7] Hassan, A. A. and Sankar, L. N., "Separation Control using Moving Surface Effects: Numerical Simulation," *Journal of Aircraft*, Vol. 29, No.1, 1992, pp. 131-139.

[8] Modi, V. J., Mokhtarian, F., Fernando, M. S. U. K. and Yokomizo, T., "Moving Surface Boundary-Layer Control as Applied to Two-Dimensional Airfoils," *Journal of Aircraft*, Vol. 28, No.2, 1991, pp. 104-112.

[9] Tennant, J. S. and Yang, T., "Turbulent Boundary-Layer Flow from Stationary to Moving Surfaces," *AIAA Journal*, Vol. 11, No.8, 1973, pp. 1156-1160.

[10] Tennant, J. S., Jonhson, W. S. and Keaton, D. D., "Boundary-Layer Flows from Fixed to Moving Surfaces Including Gap Effects," *Journal of Hydronautics*, Vol. 12, No. 2, 1978, pp. 81-84.

[11] Modi, V. J., Fernando, M. S. U. K. and Yokomizo, T., "Moving Surface Boundary-Layer Control: Studied with Bluff Bodies and Application," *AIAA Journal*, Vol. 29, No.9, 1991, pp. 1400-1406.

[12] Mokhtarian, F. and Modi, V. J., "Fluid Dynamics of Airfoil with Moving Surface Boundary-Layer Control," *Journal of Aircraft*, Vol. 25, No.2, 1988, pp. 163-169.

[13] Kubo, Y., Modi, V. J., Yasuda, H. and Kato, K., "On the Suppression of Aerodynamic Instabilities Through the Moving Surface Boundary-Layer Control," *Journal of Wind Engineering and Industrial Aerodynamics*, 41-44, 1992, pp. 205-216.

[14] Tennant, J. S., Jonhson, W. S. and Krothapalli, A., "Rotating Cylinder for Circulation Control on an Airfoil," *Journal of Hydronautics*, Vol. 10, No. 3, 1976, pp. 102-105.

[15] Kubo, Y., Yasuda, H., Kotsubo, C. and Hirata, K., "Active Control of Super-Tall Structure Vibrations Under Wind Action by a Boundary-Layer Control

method," *Journal of Wind Engineering and Industrial Aerodynamics*, 50, 1993, pp. 361-372.

[16] Modi, V. J., Dobric, A. and Yokomizo, T., "Effect of Momentum Injection on the Fluid Dynamics of Bluff Bodies," *Proceedings of the Third International Offshore and Polar Engineering Conference*, Singapore, June1993, pp. 501-513.

[17] Mokhtarian, F., Modi, V. J., Yokomizo, T., "Rotating Air Scoop as Airfoil Boundary-Layer Control," *Journal of Aircraft*, Vol. 25, No.10, 1988, pp. 973-975.

[18] Kubo, Y., Modi, V. J., Kotsubo, C., Hayashida, K. and Kato, K., "Suppression of Wind-Induced of Tall Structures Through Moving Surface Boundary-Layer Control," *Journal of Wind Engineering and Industrial Aerodynamics*, 61, 1996, pp. 181-194.

[19] Modi, V. J., Ying, B. and Yokomizo, T., "Effect of Momentum Injection on the Aerodynamic of Several Bluff Bodies," *Journal of Wind Engineering and Industrial Aerodynamics*, 41-44, 1992, pp. 713-714.

[20] Modi, V. J., Munshi, S. R., Bandyopadhyay, G. and Yokomizo, T., "Multielement Systems with Moving Surface Boundary-Layer Control: Analysis and Validation," *Lecture Notes in Physics*, No. 453, 1995, pp. 490-495.

[21] Alvarez-Calderon, A. and Arnold, F. R., "A study of the Aerodynamic Characteristics of a High Lift Device Based on Rotating Cylinder Flap," Stanford Univ., Stanford, CA, TR RCF-1, 1961.

[22] Cook, W. L., Hickey, D. H. and Quigley, H. C., "Aerodynamics of Jet Flap and Rotating Cylinder Flap STOL Concepts," *AGARD Fluid Dynamics Panel on V/STOL Aerodynamics*, Delft, The Netherlands, Paper 10, April 1974.

[23] Cichy, D. R., Harris, J. W. and MacKay, J. K., "Flight Tests of a Rotating Cylinder Flap on a North American Rockwell YOV-10 Aircraft," *NASA CR-2135*, Nov. 1972.

[24] Modi, V. J., Munshi, S. R., Bandyopadhyay, G. and Yokomizo, T., "High-Performance Airfoil with Moving Surface Boundary-Layer Control," *Journal of Aircraft*, Vol. 35, No. 4, 1998, pp. 544-553.

[25] Tennant, J. S., "The Theory of Moving Wall Boundary Layer Control and its Experimental Application to Subsonic Diffusers," Ph.D. Dissertation, Clemson University, Clemson, S.C., May 1971.

[26] Rae, W. H. and Pope, A., *Low-Speed Wind Tunnel Testing*, Willy, 1984.

[27] Batill, S. M., and Mueller, T. J., "Visualization of Transition in the Flow Over an Airfoil Using the Smoke-Wire Technique," *AIAA Journal*, Vol. 19, No. 3, 1981, pp. 340-345.

[28] Fernholz, H. H., "*External Flows*," Turbulence, edited by P. Bradshaw, Springer-Verlag, Berlin, 1978.

Vita

- Al-Garni, Abdullah Mohammed.
- Born in Sabt Al-Alayiah, Saudi Arabia.
- Obtained a Bachelor's Degree with Honors in Mechanical Engineering from King Fahd University of Petroleum & Minerals, Dhahran, Saudi Arabia in July 1996.
- Completed Master's Degree requirements at King Fahd University of Petroleum & Minerals, Dhahran, Saudi Arabia in May, 1999.

IMAGE EVALUATION
TEST TARGET (QA-3)

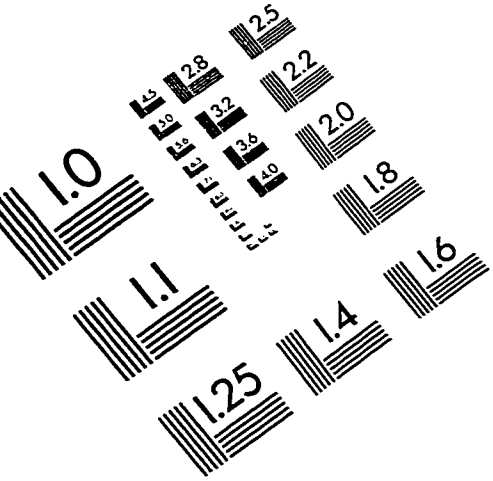

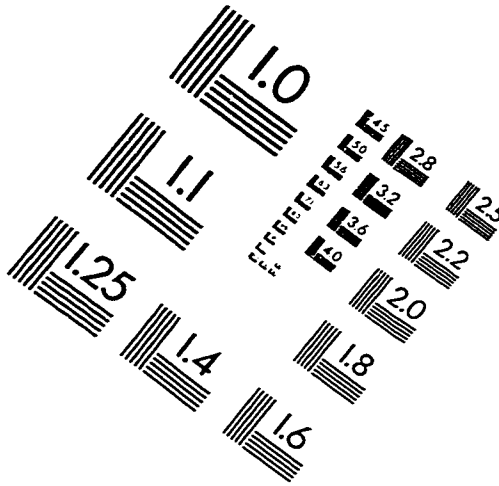

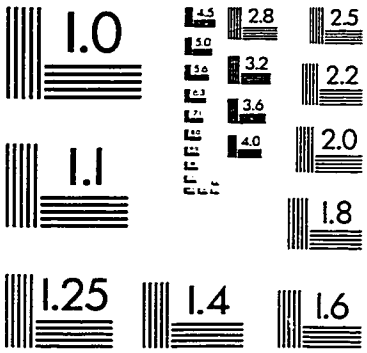

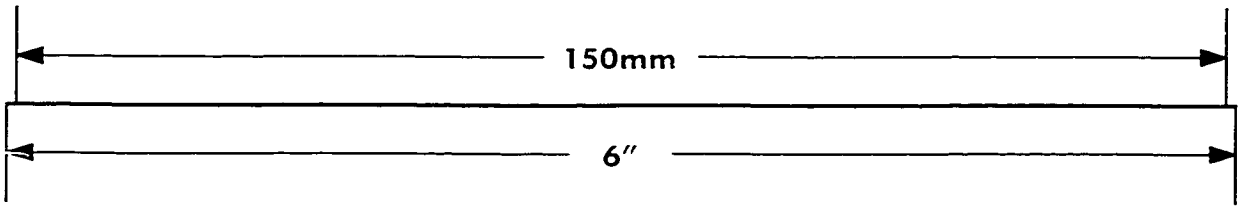

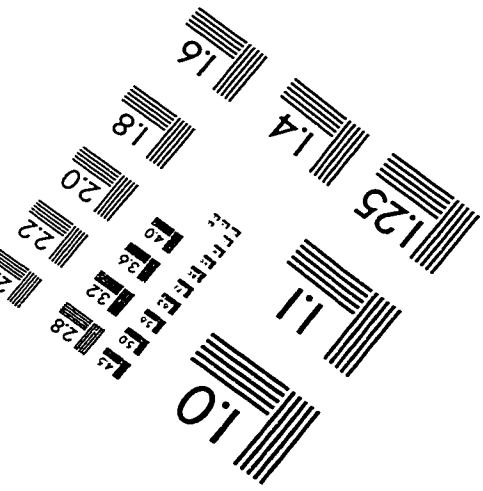

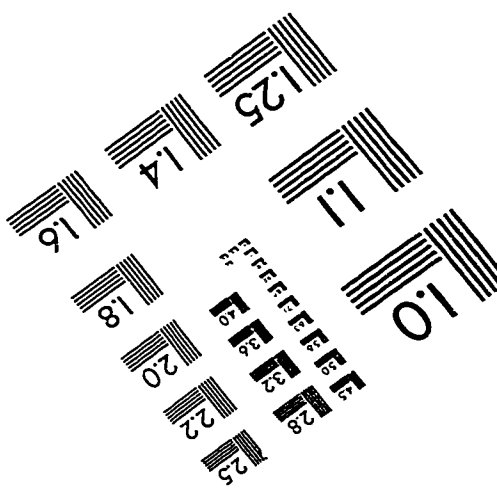

APPLIED IMAGE, Inc
1653 East Main Street
Rochester, NY 14609 USA
Phone: 716/482-0300
Fax: 716/288-5989